

Four dimensional supersymmetric Yang-Mills quantum mechanics with three colors

Zbigniew Ambroziński

Krakow, June 2014

PhD thesis at Jagiellonian University in Krakow

Supervisor: prof. Jacek Wosiek
Auxiliary supervisor: dr Piotr Korcyl

Abstract

The $D = 4$ supersymmetric Yang-Mills quantum mechanics with $SU(2)$ and $SU(3)$ gauge symmetry groups is studied. A numerical method to find finite matrix representation of the Hamiltonian is presented in detail. It is used to find spectrum of the theory. In the $SU(2)$ case there are bound states in all channels with definite total number of fermions and angular momentum. For 2,3,4 fermions continuous and discrete spectra coexist in the same range of energies. These results are confirmation of earlier studies. With $SU(3)$ gauge group, the continuous spectrum is moved to sectors with more fermions. Supersymmetry generators are used to identify supermultiplets and determine the level of restoration of supersymmetry for a finite cutoff. For both theories, with $SU(2)$ and $SU(3)$ symmetry, wavefunctions are studied and different behavior of bound and scattering states is observed.



To my wife.

Acknowledgements

I would like to express my gratitude to my supervisor prof. Jacek Wosiek for sharing his ideas and giving me inspiration. I am grateful for his assistance throughout my PhD studies and teaching me the physicist's point of view. Moreover, I thank for his thorough and critical reading of this thesis.

Secondly, I thank dr Piotr Korcyl for valuable discussions on SYMQM, his enthusiasm and friendship.

I am grateful to prof. Hermann Nicolai for hospitality during my visit in Max Planck Institute in Potsdam.

Finally, I would like to thank my wife Gosia for her patience and support.

This work was supported by Foundation for Polish Science MPD Programme co-financed by the European Regional Development Fund, agreement no. MPD/2009/6.

The research was carried out with the supercomputer „Deszno” purchased thanks to the financial support of the European Regional Development Fund in the framework of the Polish Innovation Economy Operational Program (contract no. POIG. 02.01.00-12-023/08).

Contents

Abstract	3
1 Introduction	9
2 The model	13
2.1 Symmetries	15
2.2 Matrix notation	16
3 The Cut Fock space method	19
3.1 The cut Fock space	20
3.2 Relations between bricks for $SU(3)$	21
3.3 The algorithm	22
3.3.1 Maximally annihilating form	23
3.3.2 Recursion	25
3.3.3 Diagonalization	27
3.4 Gauss elimination for bricks	28
3.5 Eigenvectors in terms of composite bricks	30
3.6 Additional variational parameter	31
3.7 Modifications for $SU(2)$	34
3.8 Summary	34
4 Number of gauge invariant states	37
4.1 The character method	37
4.2 Calculation of the generating function	40
4.3 Comparison with the numerical approach	41
5 The spectrum	45
5.1 SYMQM with $SU(2)$ gauge group	45
5.1.1 Review of other approaches	45
5.1.2 Spectra in sectors with given number of fermions	46
5.1.3 Scaling relations	47
5.2 The spectrum for the $SU(3)$ gauge group	50
6 Supersymmetry multiplets	57
6.1 Supersymmetry multiplets in the continuum limit	57
6.2 Supersymmetry fractions	59
6.3 Finite cutoff effects	61
6.4 Detailed analysis of supersymmetry fractions	63

6.5	Summary	64
7	Wavefunctions	71
7.1	Structure of fermionic wavefunctions	72
7.2	Probability density from fermionic wavefunctions	74
7.3	Wavefunctions for $SU(2)$ gauge group	75
7.3.1	Invariants	75
7.3.2	Bound and scattering states – models and expectations	76
7.3.3	Interacting case – results	78
7.4	Wavefunctions for $SU(3)$ gauge group	80
7.4.1	Fixing the gauge	80
7.4.2	Flat and steep directions	81
7.4.3	Analysis of wavefunctions	83
8	Summary	87
A	Symmetries	93
A.1	Number of fermions	93
A.2	Parity	94
A.3	Particle – hole symmetry	95
A.4	Conservation of supercharge	96
B	Absence of vector states in the bosonic sector for $SU(2)$	97
C	Finiteness of the recursive algorithm	99
D	Construction of zero angular momentum functions	101
E	Gauge fixing for $SU(3)$	107

Chapter 1

Introduction

The widely accepted model which describes physics in microscale is the Standard Model. Recent experiments (in particular at LHC) show an astonishing agreement with the Standard Model (SM). Nevertheless, it leaves some fundamental problems unresolved. This leads to the belief that the Standard Model is only an effective theory and needs to be extended. An example of such issue is the hierarchy problem [1]. A possible solution proposed in [2] is extending SM to a Minimal Supersymmetric Standard Model (MSSM). Another motivation for MSSM is that it ensures that the coupling constants of strong, electromagnetic and weak interactions meet at one point at the energy scale of grand unification [3]. Finally, the Standard Model does not provide a good candidate for dark matter. On the other hand, certain models propose the lightest supersymmetric particle (LSP) as a possible constituent of the cold dark matter [4]. Although there are certain theoretical motivations for the supersymmetry to be a true symmetry of nature, no evidence for it was yet found in experiment. Instead, it starts to be more constrained and pushed away to higher energies. Nevertheless, supersymmetry remains at the center of interest of theoretical physics. One of the supersymmetric models is the supersymmetric Yang-Mills gauge theory [5, 6].

The supersymmetric Yang-Mills gauge theory was studied in [6]. It was found that it can be supersymmetric only in certain dimensions, namely $D = 2, 4, 6, 10$. The gauge theory can be used to construct supersymmetric Yang-Mills quantum mechanics (SYMQM). By definition, D -dimensional SYMQM is obtained from the $\mathcal{N} = 1$ supersymmetric Yang-Mills field theory in $D = d + 1$ dimensions by reducing the whole space to a single point. The number of supersymmetry generators in the resulting quantum mechanics is $\mathcal{N} = 2, 4, 8, 16$ respectively for the given dimensions. In [7] the authors gave complete solution for the case of $D = 2$ and $SU(2)$ gauge group. Their result was then generalized and vacuum wavefunctions were found for arbitrary $SU(N)$ [8].

Dimensional reduction is not only a simplification of the field theory, but SYMQM has its own motivations. In [9] the purely bosonic part of SYMQM was proposed as a regularized description of a membrane. More precisely, coordinates of a membrane are first expanded in terms of an orthogonal set of functions Y^a on the membrane. Then, a cutoff to the expansion is introduced. Finally, it was shown that for each $N \in \mathbb{N}$ the algebra of the first $N^2 - 1$ functions Y^a is closed and isomorphic to $su(N)$. A membrane is represented by an $N \times N$ matrix in the fundamental representation of $SU(N)$. These matrices are the bosonic degrees of freedom of the Yang-Mills theory. The parameter N is a regulator and the continuum limit is recovered for $N \rightarrow \infty$. This correspondence can be extended to the full SYMQM describing the dynamics of supermembranes [10, 11].

It was later shown in [12] that the spectrum of SYMQM is continuous and thus the supermembrane is unstable. This gave rise to the interpretation that a theory quantum supermembranes is second-quantized from the very beginning [13].

In [14] an M-theory compactified on a circle is considered in an infinite momentum frame [15]. It is argued that the dynamics of the M-theory are given by D0 branes. Those are described precisely by the large N limit of SYMQM in $D = 10$. This is called the BFSS conjecture (named after Banks, Fischler, Shenker and Susskind) and is perhaps the most remarkable application of SYMQM. The continuous spectrum of SYMQM turned to be a virtue and corresponds to scattering states in the M-theory. A necessary condition for the BFSS hypothesis to be true is the existence of a normalizable massless state in SYMQM. It would correspond to the graviton one the side of M-theory. It was shown that such state cannot exist in dimension lower than $D = 10$ [16]. Other papers suggest that there may be such state for $D = 10$ [17, 18]. More details can be found e.g. in a review article [19]. The BFSS conjecture aroused a large interest in this model [20, 21, 19]. Asymptotic ground states for the $SU(2)$ case were found in [22, 23]. The lattice methods were applied in [24, 25]. SYMQM was also studied with a hybrid Monte Carlo approach [26, 27, 28].

A different motivation for the Yang-Mills quantum mechanics is given in [29]. It was advocated that the dynamics of a QCD gauge field can be understood by analyzing the theory in a small volume, of order 10^{-14} cm. An approximate description is then given by constant fields. These are described by the dimensionally reduced theory, i.e. the purely bosonic part of four dimensional SYMQM.

A more complete study was proposed in [30] where a small volume (or equivalently weak coupling) expansion is considered. The zeroth order approximation is the Yang-Mills quantum mechanics. In [30, 31, 32] this system was studied for $SU(2)$ and $SU(3)$ gauge groups with a numerical Rayleigh-Ritz technique. In [33] also higher groups, up to $SU(6)$ were considered. Further analysis, in medium volume was performed in [34, 35].

A program to study the whole family of SYMQM with various dimensions and gauge groups was proposed in [36]. The cut Fock space method, which will be our tool was used in a set of papers. In [37, 38] the four dimensional model with $SU(2)$ symmetry group was addressed. The $D = 2$ case was studied and eventually a complete solution for $SU(N)$ gauge group was found in [39, 40, 41]. There was yet another study based on the Schrödinger equation [42, 43, 44]. With this method the energies and eigenstates in 0-angular momentum sector of $D = 4$ model with $SU(2)$ gauge group were found with great precision.

This thesis is a continuation of the program. The primary goal is to analyze the supersymmetric Yang-Mills quantum mechanics in four dimensions with $SU(3)$ gauge group. Analysis of this model is based on numerical results obtained using the cut Fock space. The main result is the spectrum of the theory. It is calculated in channels with definite number of fermions and spin. Eigenstates of the Hamiltonian with equal energies form supermultiplets. A way to identify members of these supermultiplets is given. An important part of this thesis is devoted to studying wavefunctions of the bound states and scattering states. Analysis of the wavefunctions delivers important information, in particular how the wavefunctions penetrate valleys of the potential. All results are given for $SU(2)$ as well as for $SU(3)$ gauge group. Construction of wavefunctions for this class of systems is a novelty. It was addressed before in [42, 43] but only for vanishing angular momentum and only for $SU(2)$. The method presented in this thesis applies to all angular momenta and in principle to all gauge groups.

Outline of the dissertation is following.

In Chapter 2 we provide an introduction to SYMQM with $D = 4$ and $SU(N)$ gauge group symmetry. The dimensional reduction of the quantum field theory is performed. The Majorana condition is imposed so that the model is supersymmetric. Next, the symmetries of the Hamiltonian are identified. The two basic properties are conservation of the total angular momentum and number of fermions. It is also invariant under the particle–hole transformation. Thanks to the last symmetry, there is degeneracy between channels with n_F and $n'_F = 2(N^2 - 1) - n_F$ fermions and therefore only half of the sectors with given number of fermions need to be analyzed. Finally, the model is supersymmetric. The matrix notation is introduced. It is a common tool for simplifying the notation and plays an important role in the algorithm for constructing matrices of physical observables.

In Chapter 3 the cut Fock space method is presented. The idea of this approach is to represent the Hamiltonian as an infinite matrix and to introduce a cutoff. Here, as in many other cases, it is most useful to use the Fock basis. The cutoff limits the total occupation number of bosons. The maximal number of fermions is $2(N^2 - 1)$ because of the Pauli exclusion principle, so there is no need to limit the number of fermions. The basis of the gauge invariant space is generated by bricks which are traces of products of creation operators. Thanks to conservation of number of fermions, the Hamiltonian can be constructed in each fermionic sector separately. Matrix of the Hamiltonian could be constructed independently also in channels with definite angular momentum, as in [38]. However, this procedure would involve constructing bricks with definite angular momentum which is inefficient for the $SU(3)$ gauge group. Instead, bricks with definite 3 bosonic and 2 fermionic occupation numbers (corresponding to three spatial and two spinor indices) are used. Construction of the matrix is performed using a recursive algorithm. This is the most numerically involved part of calculations. Once the matrix is created, it is diagonalized to obtain its eigenvectors and eigenvalues.

In Chapter 4 we present a method based on group theory to obtain dimensions of all sectors with definite set of quantum numbers of the cut Fock space. It was first introduced in [45] to calculate dimensions of spaces with definite fermionic and bosonic occupation numbers n_F and n_B and also with definite angular momentum j . It is modified in order to calculate dimensions of spaces with more occupation numbers specified, i.e. n_F^+ , n_F^- , n_B^x , n_B^y and n_B^z . Dimensions of such subspaces can be also obtained numerically from the rank of Gramm matrix for the overcomplete set of basis vectors. At the end of the chapter a cross–check of both approaches is provided. The knowledge of dimensions of certain subspaces is also useful for constructing matrix elements of the Hamiltonian.

In Chapter 5 results for eigenenergies of the system are given. They are obtained in channels with definite number of fermions and angular momentum. An important question is to distinguish the discrete spectrum from the continuous one. This analysis is based on dependence of energies on the cutoff. Thanks to the particle–hole symmetry, only sectors with $n_F \leq N^2 - 1$ need to be examined in the theory with $SU(N)$ gauge group. It turns out that the spectrum in the few lowest fermionic channels is discrete, while the continuum spectrum appears for many fermions. Because of the supersymmetry, energies from neighboring fermionic sectors are degenerate. For this reason, for some n_F there are discrete energy levels immersed in the continuous spectrum. It was found for the case of $SU(2)$ and is now confirmed also for $SU(3)$. We present results for both, $SU(2)$ and $SU(3)$ cases for comparison with each other and with earlier papers.

In Chapter 6 the supersymmetry multiplets are identified and discussed. Supermultiplets contain $SO(3)$ multiplets of states with equal energies and different numbers of

fermions and angular momentum. Existence of supersymmetric multiplets is a direct consequence of the fact that supercharges conserve energy. On the other hand, the supercharge operators do not conserve bosonic (and fermionic) occupation number. Therefore, supersymmetry is broken for finite cutoff. In order to identify states which form multiplets in the continuous limit, we define so called supersymmetry fractions. They measure how supercharges map one energy states into other. Values of supersymmetry fractions in the continuum limit are known. Therefore, they are useful to analyze the degree of breaking of supersymmetry. Moreover, they help to identify SUSY partners.

In Chapter 7 we present a method to construct wavefunctions of energy eigenstates. These distributions are used to directly illustrate the effect of nonabelian interactions. First, given an angular momentum multiplet of states in the Fock space a single rotationally invariant function is introduced. It is an analogue of square of radial part of the wavefunction in the case of an ordinary three dimensional problem. Then, the structure of the configuration space in both cases, $SU(2)$ and $SU(3)$ is investigated. The flat valleys of the potential and directions in which the potential grows fastest are identified. They are essential in distinguishing between behavior of bound and scattering states. Finally, behavior of wavefunctions of several energy eigenstates along the flat valleys and steep directions is studied.

Finally, in Chapter 8 a summary of our results is given.

Some less significant and lengthy calculations are put in appendices. In Appendix A symmetries of the SYMQM Hamiltonian are discussed. In B we prove after [31] that there are no $SU(2)$ -invariant bosonic vector states. Appendix C contains a proof that the recursive algorithm for constructing matrix elements introduced in Chapter 3 is finite. Finally, Appendices D and E are related to Chapter 7.

Chapter 2

The model

The Yang Mills quantum mechanics is obtained by dimensional reduction [7] of a four dimensional gauge theory given by the action

$$S = \int d^4x \mathcal{L} = \int d^4x \left(-\frac{1}{4} F_{\mu\nu}^a F^{\mu\nu a} + \frac{i}{2} \bar{\psi}^a \gamma^\mu D_\mu \psi^a \right) \quad (2.1)$$

The gauge group is $SU(N)$ and a is the group index in the adjoint representation. The strength tensor and covariant derivative are given by

$$\begin{aligned} F_{\mu\nu}^a &= \partial_\mu A_\nu^a - \partial_\nu A_\mu^a + g f^{abc} A_\mu^b A_\nu^c, \\ D_\mu \psi^a &= \partial_\mu \psi^a - g f^{abc} A_\mu^c \psi^b, \end{aligned} \quad (2.2)$$

where f^{abc} are the structure constants of $SU(N)$.

The Lagrangian contains no time derivative of the field A_0^a . Therefore, A_0^a is not a dynamical field and the Euler–Lagrange equations for A_0^a are constraints of the system:

$$G^a \equiv \frac{\delta \mathcal{L}}{\delta A_0^a} - \partial_i \frac{\delta \mathcal{L}}{\delta (\partial_i A_0^a)} = 0. \quad (2.3)$$

G^a is generator of the gauge symmetry and (2.3) is the Gauss law. As A_0^a is not dynamical, it can have an arbitrary value. One can use the gauge freedom to eliminate it. In the following, we work in the temporal gauge, with $A_0^a = 0$. In the quantized theory, the Gauss law [29] is imposed on the states of the Hilbert space. That is, the physical Hilbert space is composed of states annihilated by G^a .

In the dimensional reduction procedure one removes dependence of fields on spatial coordinates, so that $A_i^a(t, \vec{x}) = A_i^a(t)$. In the following we will adopt the notation of quantum mechanics $A_i^a \rightarrow x_i^a$. The resulting dimensionally reduced Lagrangian reads

$$\mathcal{L} = \frac{1}{2} (\dot{x}_i^a)^2 + \frac{1}{2} \bar{\psi}^a \gamma^0 \partial_0 \psi^a - \frac{g^2}{4} (f^{abc} x_i^b x_j^c)^2 - \frac{i}{2} g f^{abc} \bar{\psi}^a \gamma^k x_k^c \psi^b. \quad (2.4)$$

The corresponding Hamiltonian is [7]

$$\begin{aligned} H &= H_K + g^2 H_V + g H_F, \\ H_K &= \frac{1}{2} p_i^a p_i^a, \\ H_V &= \frac{1}{4} f^{abc} f^{ade} x_i^b x_j^c x_i^d x_j^e, \\ H_F &= \frac{i}{2} f^{abc} \psi^{a\dagger} \Gamma_k \psi^b x_k^c. \end{aligned} \quad (2.5)$$

Γ_k are the alpha matrices, i.e. $\Gamma_k = \gamma^0 \gamma^k$ where γ^μ are Dirac matrices. H_K , H_V and H_F are kinetic, potential and fermionic parts of the Hamiltonian respectively. Spatial indices i, j, k take values 1, 2, 3 and color indices a, b, \dots range from 1 to $N^2 - 1$. Therefore there are 24 bosonic degrees of freedom in model for the $SU(3)$ group.

Once spatial dependence of A_i^a is removed, the gauge group generator G^a has particularly simple form

$$G^a \equiv f^{abc} (x_i^b p_i^c - \frac{i}{2} \psi_\alpha^{b\dagger} \psi_\alpha^c). \quad (2.6)$$

This is nothing but the total angular momentum in the color space.

In what follows in all explicit calculations the Weyl representation of Dirac matrices from [46] will be used. The Dirac matrices are

$$\gamma^0 = \begin{pmatrix} 0 & \mathbb{1} \\ \mathbb{1} & 0 \end{pmatrix}, \quad \gamma^k = \begin{pmatrix} 0 & \sigma_k \\ -\sigma_k & 0 \end{pmatrix}, \quad \gamma^5 = \begin{pmatrix} -\mathbb{1} & 0 \\ 0 & \mathbb{1} \end{pmatrix}. \quad (2.7)$$

This theory is not yet supersymmetric. Indeed, in SUSY models the number of bosonic and fermionic degrees of freedom must match. If ψ is a Dirac fermion, then there are $4(N^2 - 1)$ fermionic d.o.f. On the other hand, the number of bosonic d.o.f. is reduced by the Gauss law from $3(N^2 - 1)$ to $2(N^2 - 1)$. The supersymmetry can be achieved by imposing Weyl or Majorana condition on the spinor ψ . In what follows we choose the Majorana condition. Then, ψ must satisfy $\psi_C = \psi$ where for the charge conjugation we use the phase convention

$$\psi_C^a = -iC(\bar{\psi}^a)^T, \quad (2.8)$$

$$C = \begin{pmatrix} -i\sigma_2 & 0 \\ 0 & i\sigma_2 \end{pmatrix}. \quad (2.9)$$

Finally, we proceed to quantizing the system. The quantization procedure gives algebra of operators

$$[x_i^a, p_j^b] = \delta^{ab} \delta_{ij}, \quad (2.10)$$

$$\{\psi_\alpha^a, \psi_\beta^{b\dagger}\} = \delta^{ab} \delta_{\alpha\beta}. \quad (2.11)$$

Because of the Majorana condition, components ψ_α^a cannot be independent. Instead, ψ can be constructed from a two-component Weyl spinor f_α^a ($\alpha = 1, 2$). By definition, the Weyl spinor satisfies anticommutation relations

$$\{f_\alpha^a, f_\beta^{b\dagger}\} = \delta^{ab} \delta_{\alpha\beta}. \quad (2.12)$$

The Weyl spinor can be written in a four component notation

$$\psi_W^a = -e^{i\pi/4} \begin{pmatrix} f_1^a \\ f_2^a \\ 0 \\ 0 \end{pmatrix}. \quad (2.13)$$

ψ_W satisfies $\gamma^5 \psi_W = -\psi_W$, so it is indeed a left-handed spinor. The phase in front is chosen such that all components of spinor in the next formula (2.14) have common phase.

The Majorana spinor is then constructed from the Weyl spinor and its charge conjugate [47]:

$$\psi^a = \psi_W^a + (\psi_W)_C^a = e^{i\pi/4} \begin{pmatrix} -f_1^a \\ -f_2^a \\ f_2^{a\dagger} \\ -f_1^{a\dagger} \end{pmatrix}. \quad (2.14)$$

The spinor ψ^a automatically satisfies the Majorana condition because charge conjugation is an involution, i.e. for any χ there is $(\chi_C)_C = \chi$.

2.1 Symmetries

Now we come to discussion of symmetries of the Hamiltonian. An extension of this paragraph can be found in Appendix A. In particular, Appendix A contains proofs that generators of the symmetries commute with the Hamiltonian.

The supercharges arising from invariance under the supersymmetry transformation are

$$Q_\alpha = (\Gamma_k \psi^a)_\alpha p_k^a + ig f^{abc} (\Sigma_{jk} \psi^a)_\alpha x_j^b x_k^c, \quad (2.15)$$

where $\Sigma_{jk} = -\frac{i}{4}[\Gamma_j, \Gamma_k]$. They obey anticommutation relations

$$\{Q_\alpha, Q_\beta^\dagger\} = 2\delta_{\alpha\beta} H + g \Gamma_{k\alpha\beta} x_k^a G^a. \quad (2.16)$$

In the space of physical states, i.e. when G_a vanishes, the anticommutator $\{Q_\alpha, Q_\beta^\dagger\}$ is proportional to the Hamiltonian. By acting with Q_α and Q_α^\dagger on eigenstates of the Hamiltonian one generates a supersymmetry multiplet. The supercharge operator Q_α commutes with the Hamiltonian, so all states in the supermultiplet have identical energy. Structure of these multiplets is analyzed in detail in Chapter 6.

In the dimensional reduction procedure the full configuration space is reduced to a single point. Still, the resulting Hamiltonian exhibits an inherited rotational symmetry. The angular momentum operators are

$$J_i = L_i + S_i = \epsilon_{ijk} \left(x_j^a p_k^a + \frac{1}{4} \psi^{a\dagger} \Sigma_{jk} \psi^a \right). \quad (2.17)$$

Commutators of H and J_i vanish and thus the angular momentum is conserved.

A remarkable feature of the four-dimensional theory is conservation of the total number of fermions $n_F = \sum_{a\alpha} f_\alpha^a f_\alpha^{a\dagger}$. It is not true e.g. in 10 dimensions which is interesting due to the BFSS conjecture.

Furthermore, there is a particle-hole symmetry:

$$\begin{aligned} f_1^a &\rightarrow -f_2^{a\dagger}, & f_1^{a\dagger} &\rightarrow -f_2^a, \\ f_2^a &\rightarrow f_1^{a\dagger}, & f_2^{a\dagger} &\rightarrow f_1^a, \\ x_i^a &\rightarrow -x_i^a, & p_i^a &\rightarrow -p_i^a. \end{aligned} \quad (2.18)$$

A natural consequence of this symmetry is that one can find eigenstates of the Hamiltonian which are even or odd under (2.18). However, conservation of n_F is a stronger

symmetry. It implies that the full Hilbert space splits into independent sectors with definite number of fermions. The particle–hole symmetry relates these sectors. For each state with n_F fermions there is a state with $2(N^2 - 1) - n_F$ fermions and the same energy. Construction of the other state is given explicitly so all its properties can be easily inferred. In particular, the particle–hole transformation preserves the total angular momentum.

Moreover, the Hamiltonian has a scaling property

$$\begin{aligned} x_i^a &\rightarrow g^{-1/3} x_i^a, \\ p_i^a &\rightarrow g^{1/3} p_i^a, \\ f_\alpha^a &\rightarrow f_\alpha^a, \\ H = H_K + g^2 H_V + g H_F &\rightarrow g^{2/3} (H_K + H_V + H_K). \end{aligned} \tag{2.19}$$

In what follows g will be set to 1. For any other finite g the spectrum is merely scaled by $g^{2/3}$. Eigenstates are stretched by $g^{-1/3}$ and all their quantum numbers do not change.

Finally, consider parity. The operators transform under parity in the following way:

$$\begin{aligned} p_i^a &\rightarrow -p_i^a, \\ x_i^a &\rightarrow -x_i^a, \\ \psi_\alpha^a &\rightarrow (\psi_P)_\alpha^a \equiv \gamma_{\alpha\beta}^0 \psi_\beta^a. \end{aligned} \tag{2.20}$$

One can check that the Hamiltonian is invariant under the transformation (2.20). However, the spinor ψ_P does not satisfy the Majorana condition. It follows that states generated by ψ_P are not invariant under the charge conjugation. Therefore, the Hilbert space breaks the parity symmetry. A more detailed discussion of parity breaking can be found in Appendix A.

2.2 Matrix notation

It is convenient to use the so called matrix notation. Let T^a be the $N^2 - 1$ generators of $SU(N)$ in the fundamental representation. They are hermitean traceless $N \times N$ matrices and satisfy multiplication law

$$T^a T^b = \frac{1}{2N} \delta^{ab} \mathbb{1}_N + \frac{1}{2} (i f^{abc} + d^{abc}) T^c, \tag{2.21}$$

where f^{abc} and d^{abc} are antisymmetric and symmetric $SU(N)$ group structure constants respectively. For $N = 2$ the generators are simply Pauli matrices $T^a = \frac{1}{2} \sigma^a$, $a = 1, 2, 3$. The antisymmetric structure constant is $f^{abc} = \epsilon^{abc}$ and the symmetric d^{abc} vanishes. For

$N = 3$ the generators are Gell–Mann matrices

$$\begin{aligned}
 T^1 &= \frac{1}{2} \begin{pmatrix} 0 & 1 & 0 \\ 1 & 0 & 0 \\ 0 & 0 & 0 \end{pmatrix}, & T^2 &= \frac{1}{2} \begin{pmatrix} 0 & -i & 0 \\ i & 0 & 0 \\ 0 & 0 & 0 \end{pmatrix}, \\
 T^3 &= \frac{1}{2} \begin{pmatrix} 1 & 0 & 0 \\ 0 & -1 & 0 \\ 0 & 0 & 0 \end{pmatrix}, & T^4 &= \frac{1}{2} \begin{pmatrix} 0 & 0 & 1 \\ 0 & 0 & 0 \\ 1 & 0 & 0 \end{pmatrix}, \\
 T^5 &= \frac{1}{2} \begin{pmatrix} 0 & 0 & -i \\ 0 & 0 & 0 \\ i & 0 & 0 \end{pmatrix}, & T^6 &= \frac{1}{2} \begin{pmatrix} 0 & 0 & 0 \\ 0 & 0 & 1 \\ 0 & 1 & 0 \end{pmatrix}, \\
 T^7 &= \frac{1}{2} \begin{pmatrix} 0 & 0 & 0 \\ 0 & 0 & -i \\ 0 & i & 0 \end{pmatrix}, & T^8 &= \frac{1}{2\sqrt{3}} \begin{pmatrix} 1 & 0 & 0 \\ 0 & 1 & 0 \\ 0 & 0 & -2 \end{pmatrix}. \tag{2.22}
 \end{aligned}$$

Consider an operator with an adjoint color index A^a . Then $A = A^a T^a$ is a $N \times N$ matrix with operator–valued matrix elements. In this notation $x_i = x_i^a T^a$, $p_i = p_i^a T^a$, $\psi_\alpha = \psi_\alpha^a T^a$, etc. In the matrix notation the Hamiltonian, angular momentum and supersymmetry generators are

$$\begin{aligned}
 H_K &= \text{Tr}(p_i p_i), \\
 H_V &= - \sum_{i < j} \text{Tr}([x_i, x_j]^2), \\
 H_F &= \sum_{k\alpha\beta} \Gamma_{k\alpha\beta} \text{Tr}(\psi_\alpha^\dagger [\psi_\beta, x^k]), \\
 J_i &= \epsilon_{ijk} \left(2\text{Tr}(x_j p_k) + \frac{1}{2} (\Sigma_{jk})_{\alpha\beta} \text{Tr}(\psi_\alpha^\dagger \psi_\beta) \right), \\
 Q_\alpha &= 2\Gamma_{k\alpha\beta} \text{Tr}(\psi_\beta p_k) + \frac{i}{4} \Sigma_{jk\alpha\beta} \text{Tr}(\psi_\beta x_j x_k), \\
 G &= -i[x_i, p_i] - \frac{1}{2} \{\psi_\alpha^\dagger, \psi_\alpha\} + (1 + 3i) \frac{N^2 - 1}{2N} \mathbb{1}_N. \tag{2.23}
 \end{aligned}$$

The first five operators in (2.23) are color singlets and are given in terms of traces. G^a which is a vector in the color space is represented by a matrix. The last term in G may look strange, since G must be traceless. However, one has to remember that the two operators $[x_i, p_i]$, $\{\psi_\alpha^\dagger, \psi_\alpha\}$ have non–vanishing trace. The whole expression is indeed traceless.

The matrix notation is only a way to rewrite the same operators. However, it is much more convenient to manipulate with traces of matrix operators rather than to keep the color indices explicit.

Chapter 3

The Cut Fock space method

In this chapter we discuss a numerical technique, called cut Fock space method, which is used to solve our model. It originates from the variational Tamm–Dancoff method [48] where one uses a small set of trial states to construct an approximate ground state of a theory. Quality of the variational approach relies on how many parameters one uses to approximate the ground state and how clever one is in choosing these parameters. The ground state energy is always approximated from above.

The idea of this method is to first choose a basis in the Hilbert space and then to introduce a cutoff. The cutoff has to be such that dimension of the cut space is finite. Then one constructs and diagonalizes matrix of the Hamiltonian in the cut space. The lowest eigenvalue is an approximation to the ground state energy. It is the energy obtained with variational technique where all basis states in the cut space are trial states. It is usually most convenient to work in the Fock space (hence the name) with the standard occupation number basis. The cutoff is then the maximal occupation number N_B . As the cutoff increases, energies converge to their exact values.

One of the virtues of this approach is that one can construct not only Hamiltonian, but also other observables. Having computed eigenvectors of the Hamiltonian, one can easily obtain expectation value of other observable in these states. Another asset is that one has a direct access to wavefunctions of energy eigenstates. They will be studied in following chapters.

Wavefunctions $\langle x|n\rangle$ of basis states in the configuration space are simply Hermite functions. It is known that $\langle x|n\rangle$ in practice have finite support, i.e. they are exponentially suppressed for $|x| \gtrsim \sqrt{2n+1}$. That is, for a finite cutoff $n \leq N_B$ all states are localized inside a finite box of size $L = \sqrt{2N_B+1}$. Wavefunctions in the momentum space $\langle p|n\rangle$ share the same behavior and thus the momenta are also limited. One can then take a point of view that the cut Fock space is a regularized Hilbert space. The cutoff N_B plays a role of both, IR and UV cutoffs which are approximately $(2N_B)^{-1/2}$ and $(2N_B)^{1/2}$.

The cut Fock space method was already applied with success to other simpler models. Properties of the cut Fock space were studied for one dimensional quantum mechanics [49]. The technique was used for computations with high precision for the double well potential [50] and multiple wells with periodic boundary conditions [51]. Then it was also applied to SYMQM in two dimensions [39, 40, 41] and finally to four dimensional theory with $SU(2)$ gauge group [37, 38].

3.1 The cut Fock space

In order to construct the Fock space we introduce creation and annihilation operators, which satisfy the usual commutation rules

$$a_i^a = \frac{1}{\sqrt{2}}(x_i^a + ip_i^a), \quad a_i^{a\dagger} = \frac{1}{\sqrt{2}}(x_i^a - ip_i^a), \quad (3.1)$$

$$[a_i^a, a_j^{b\dagger}] = \delta^{ab}\delta_{ij}. \quad (3.2)$$

Fermionic creation and annihilation operators $f_\alpha^{a\dagger}$ and f_α^a were already introduced in (2.12). The Fock vacuum is defined as usual by

$$a_i^a |0\rangle = 0, \quad f_\alpha^a |0\rangle = 0. \quad (3.3)$$

All other states are generated by acting with bosonic and fermionic creation operators on $|0\rangle$.

Since we would like to construct a Hilbert space consisting only of gauge invariant states, we use only specific combinations of creation operators. Take a set of matrix operators A_1, \dots, A_n where $A_k = A_k^a T^a$. For each k operators A_k^a are in adjoint $SU(N)$ representation. The lower index k is not related to any symmetry and A_k can be any operators. In the following the object

$$(A_1 \cdots A_n) \equiv Tr(A_1 \cdots A_n) = A_1^{a_1} \cdots A_n^{a_n} Tr(T^{a_1} \cdots T^{a_n}) \quad (3.4)$$

is called a *trace operator*. If all operators A_k are bosonic or fermionic creation operators then $(A_1 \cdots A_n)$ is called a *brick*. For the rest of the thesis the round bracket (\cdot) is used for a short notation of the trace. It was shown [52] that the space of gauge invariant states is spanned by states obtained by repeatedly acting with bricks on the Fock vacuum. A product of bricks is called a *composite brick*. A state generated by a composite brick has a definite number of bosons n_B and fermions n_F

$$n_B = \sum a_i^{a\dagger} a_i^a, \quad n_F = \sum f_\alpha^{a\dagger} f_\alpha^a. \quad (3.5)$$

There are only $2(N^2 - 1)$ fermionic creator operators $f_\alpha^{a\dagger}$, so the Pauli exclusion principle implies $n_F \leq 2(N^2 - 1)$.

Because the Hamiltonian conserves the fermion number n_F , it is convenient to work with subspaces with fixed number of fermions \mathcal{H}_{n_F} . For each n_F we introduce a different cutoff N_B . The cut Fock space \mathcal{H}_{n_F, N_B} is then the space of all states which contain precisely n_F fermions and at most N_B bosons.

The cut Fock space method will be used to construct matrices for several operators. The angular momentum operators conserve n_F and n_B , so the cut matrices of these operators are $(J_i)_{n_F, N_B} : \mathcal{H}_{n_F, N_B} \rightarrow \mathcal{H}_{n_F, N_B}$. Eigenvalues of these matrices are exact eigenvalues of J_i . Therefore, we may use eigenvectors of $(J^2)_{n_F, N_B}$ and $(J_3)_{n_F, N_B}$ to construct Hilbert spaces $\mathcal{H}_{n_F, N_B, j, m}$ with definite quantum numbers j and m .

The Hamiltonian conserves n_F but not n_B . The matrix $H_{n_F, N_B} : \mathcal{H}_{n_F, N_B} \rightarrow \mathcal{H}_{n_F, N_B}$ has eigenvalues which approximate energy levels of the Hamiltonian in the $N_B \rightarrow \infty$ limit. In principle, one can construct H directly on subspaces $\mathcal{H}_{n_F, N_B, j, m}$. This procedure would generate smaller matrices which are easier to diagonalize. However, then one needs to use bricks with definite angular momentum. The computational cost of this procedure would exceed the gain from smaller matrices.

Finally, matrices of Q_α will be constructed. Supercharges do not conserve n_F . In Chapter 6 we introduce operators \mathcal{Q}_\pm which are closely related to the supercharges Q_α and play exactly the same role. \mathcal{Q}_\pm do not conserve n_F . Instead, they decrease the number of fermions by 1. Therefore, We generate matrices $(\mathcal{Q}_\pm)_{n_F, N_B, N'_B} : \mathcal{H}_{n_F, N_B} \rightarrow \mathcal{H}_{n_F-1, N'_B}$. In practice the two cutoffs N_B and N'_B are always different.

3.2 Relations between bricks for $SU(3)$

The full Fock space of gauge invariant states is spanned by all possible composite brick acting on the Fock vacuum. However, these states are not linearly independent. For optimization reasons it is necessary to have as few states as possible. Therefore, we try to identify and remove those bricks which can be expressed in terms of other bricks. The more complicated case of $SU(3)$ gauge group is addressed in this subchapter.

The Cayley Hamilton theorem states that a matrix is a root of its characteristic polynomial. Let M be a square traceless matrix of size 3. Then, the theorem implies that

$$M^3 = (M)M^2 + \frac{1}{2}((M^2) - (M)^2)M + \frac{1}{6}((M)^3 - 3(M^2)(M) + 2(M^3))\mathbf{1}_3. \quad (3.6)$$

Recall that (\cdot) is a short notation for a trace. This theorem holds if the matrix is operator-valued, i.e. its matrix elements are operators, as long as the matrix elements commute. Multiply the above equation by another operator-valued matrix O and take a trace. Then,

$$\begin{aligned} (M^3O) &= (M)(M^2O) + \frac{1}{2}((M^2) - (M)^2)(MO) \\ &\quad + \frac{1}{6}((M)^3 - 3(M^2)(M) + 2(M^3))(O). \end{aligned} \quad (3.7)$$

It follows that if a brick contains an expression which is repeated three times and at least one more operator, then it can be written in terms of shorter bricks, e.g. for $M = a_1^\dagger a_2^\dagger$ and $O = f_1^\dagger a_1^\dagger$ there is

$$\begin{aligned} (a_1^\dagger a_2^\dagger a_1^\dagger a_2^\dagger a_1^\dagger a_2^\dagger f_1^\dagger a_1^\dagger) &= (a_1^\dagger a_2^\dagger)(a_1^\dagger a_2^\dagger a_1^\dagger a_2^\dagger f_1^\dagger a_1^\dagger) + \frac{1}{2}(a_1^\dagger a_2^\dagger a_1^\dagger a_2^\dagger)(a_1^\dagger a_2^\dagger f_1^\dagger a_1^\dagger) \\ &\quad - \frac{1}{2}(a_1^\dagger a_2^\dagger)^2(a_1^\dagger a_2^\dagger f_1^\dagger a_1^\dagger) + \frac{1}{6}(a_1^\dagger a_2^\dagger)^3(f_1^\dagger a_1^\dagger) \\ &\quad - \frac{1}{2}(a_1^\dagger a_2^\dagger a_1^\dagger a_2^\dagger)(a_1^\dagger a_2^\dagger)(f_1^\dagger a_1^\dagger) + \frac{1}{3}(a_1^\dagger a_2^\dagger a_1^\dagger a_2^\dagger a_1^\dagger a_2^\dagger)(f_1^\dagger a_1^\dagger). \end{aligned} \quad (3.8)$$

Because the trace of a single matrix operator is zero, i.e. $(a_i^\dagger) = (f_a^\dagger) = 0$, this formula simplifies if M or O in (3.7) are single creation operators. For $M = a_1^\dagger$ and $O = f_1^\dagger a_3^\dagger$ it reads

$$(a_1^\dagger a_1^\dagger a_1^\dagger f_1^\dagger a_3^\dagger) = \frac{1}{2}(a_1^\dagger a_1^\dagger)(a_1^\dagger f_1^\dagger a_3^\dagger) + \frac{1}{3}(a_1^\dagger a_1^\dagger a_1^\dagger)(f_1^\dagger a_3^\dagger). \quad (3.9)$$

There are other relations for fermionic operators. The simplest example is vanishing of a square of single fermionic creation operator.

$$(f_1^\dagger f_1^\dagger) = f_1^{a_1^\dagger} f_1^{a_2^\dagger} (T^{a_1} T^{a_2}) = -f_1^{a_2^\dagger} f_1^{a_1^\dagger} (T^{a_2} T^{a_1}) = -(f_1^\dagger f_1^\dagger), \quad (3.10)$$

so $(f_1^\dagger f_1^\dagger) = 0$. This can be easily generalized. Let M be a operator valued matrix with anticommuting matrix elements. Then,

$$(M^2) = (M^4) = 0, \quad M^6 = 0. \quad (3.11)$$

The proof of the first two relations is analogous to (3.10). The last equality can be easily shown by plugging M^2 into (3.6) and using the first two identities from (3.11). There is also a Cayley–Hamilton relation for matrix with anticommuting matrix elements:

$$M^5 = \frac{1}{3}(M^3)M^2 + \frac{1}{3}(M^5). \quad (3.12)$$

It can be proven by a direct calculation. In order to use it for eliminating bricks, one has to multiply (3.12) by an arbitrary operator O and take a trace. Then,

$$(M^5 O) = \frac{1}{3}(M^3)(M^2 O) + \frac{1}{3}(M^5)(O). \quad (3.13)$$

The Cayley–Hamilton relation for Grassmann–valued matrices can be also extended to any $SU(N)$ group [53]. For an $N \times N$ matrix M whose entries anticommute it reads

$$M^{2N-1} = \frac{1}{N}(M^{2N-1}) + \frac{1}{N} \sum_{i=1}^{N-1} M^{2i}(M^{2N-2i-1}). \quad (3.14)$$

There is one more identity for $SU(3)$ which is used in eliminating bricks, namely [54]

$$T^{\{a}T^bT^c\} = \frac{1}{4}\delta^{\{ab}T^c\} + \frac{1}{3}(T^{\{a}T^bT^c\})\mathbf{1}_3. \quad (3.15)$$

Curly brackets denote symmetrization without additional coefficient $\frac{1}{3!}$. Formulas presented earlier (3.6) – (3.12) allow to discard some bricks because they are expressed by shorter bricks. (3.15) is different, because it relates bricks of the same length. For any six bricks that differ by permutations of three operators then one of them can be eliminated.

Finally, the procedure of eliminating dependent bricks is the following. For each n_B and n_F generate all possible bricks with appropriate occupation numbers. Then, eliminate as many bricks as possible using relations (3.7), (3.12), (3.11) and (3.15). All composite bricks with fermionic and bosonic occupation numbers n_F and n_B form an overcomplete basis in sector (n_F, n_B) . This overcompleteness cannot be eliminated entirely and is taken into account in the program for generating matrices.

There is yet another way to eliminate superfluous bricks. It involves objects introduced below and will be presented in 3.4.

3.3 The algorithm

In this part we present the algorithm for constructing matrix elements of interesting operators. The same algorithm is used for both cases, SYMQM with $SU(2)$ and $SU(3)$ group, so it is presented in a general form for a group $SU(N)$.

First we introduce the notion of a trace operator. Take n operators A_k^a , $k = 1, \dots, m$, where a is the color index. Each A_k^a is a fermionic or bosonic creation or annihilation operator. Then, $(A_1 \cdots A_m)$ given by the formula

$$(A_1 \cdots A_m) \equiv A_1^{a_1} \cdots A_m^{a_m} (T^{a_1} \cdots T^{a_m}) \quad (3.16)$$

will be called a *trace operator*. The number m of operators inside the trace (3.16) is called the *length* of the trace. In particular, identity is a trace operator of length 0, i.e. $id = \frac{1}{N}Tr(\mathbf{1}_N)$. A product of trace operators is called a *composite trace*. Length of a composite trace is the total of all lengths of single traces in the product. All operators of our interest, i.e. angular momentum, Hamiltonian and supercharges can be expressed by traces of creation and annihilation operators. The angular momentum has a particularly simple form

$$\begin{aligned} J_1 &= 2i(a_3^\dagger a_2) - 2i(a_2^\dagger a_3) + (f_1^\dagger f_2) + (f_2^\dagger f_1), \\ J_2 &= 2i(a_1^\dagger a_3) - 2i(a_3^\dagger a_1) - i(f_1^\dagger f_2) + i(f_2^\dagger f_1), \\ J_3 &= 2i(a_2^\dagger a_1) - 2i(a_1^\dagger a_2) + (f_1^\dagger f_1) - (f_2^\dagger f_2). \end{aligned} \quad (3.17)$$

The explicit expression for Hamiltonian is much more complex and is not given here.

The cut Fock space can be decomposed into subspaces with definite occupation numbers

$$\mathcal{H}_{n_F, N_B} = \bigoplus_{\mathbf{n}} \mathcal{H}_{\mathbf{n}}, \quad (3.18)$$

where the sum runs over $\mathbf{n} = (n_F^1, n_F^2, n_B^1, n_B^2, n_B^3) \geq 0$ which satisfy $\sum_{\alpha} n_F^{\alpha} = n_F$ and $\sum_i n_B^i \leq N_B$.

Given a composite brick \mathcal{P} one can associate the occupation labels \mathbf{n} with \mathcal{P} . Each component of \mathbf{n} is the total number of corresponding creation operators in \mathcal{P} . A subspace $\mathcal{H}_{\mathbf{n}}$ is spanned by all composite bricks \mathcal{P} with occupation labels \mathbf{n} acting on the Fock vacuum.

3.3.1 Maximally annihilating form

The maximally annihilating form is an analog of the Wick's expansion. Consider an operator $(a_i a_j^\dagger)$. The Wick's expansion is

$$(a_i a_j^\dagger) = a_i^a a_j^{b\dagger} (T^a T^b) = [a_j^{b\dagger} a_i^a + \delta_{ij}^{ab}] (T^a T^b) = (a_j^\dagger a_i) + \frac{1}{2} \delta_{ij}. \quad (3.19)$$

The operator on the right is normal ordered and each term is a trace operator. However, not always all operators in the Wick's expansion are trace operators. For example, in the Wick expansion of $(a_i a_j^\dagger a_k a_l^\dagger)$ there is a term $a_j^{b\dagger} a_l^{d\dagger} a_i^a a_k^c (T^a T^b T^c T^d)$. Note that the order of color indices is different for creation/annihilation operators and $SU(N)$ generators. We would like to use the matrix notation introduced in Chapter 2, so the trace-operator structure has to be preserved. The maximally annihilating form is defined in a way that all operators are trace operators and it is as close to the Wick's expansion as possible.

Consider a trace operator $A = (A_1 \cdots A_m)$ with $m \geq 1$. With operator A we associate *annihilation rank* $\boldsymbol{\nu} = (\nu_F^1, \nu_F^2, \nu_B^1, \nu_B^2, \nu_B^3)$. It is defined in the following way. Let μ_i be the number of operators f_1 minus the number of operators f_1^\dagger in the set $\{A_{i+1}, \dots, A_m\}$ for $i = 0, \dots, m$. Then ν_F^1 is defined as the maximum of all μ_i 's. That means that if a state has quantum numbers \mathbf{n} and $n_F^1 < \nu_F^1$, then it is annihilated by A . The other components of $\boldsymbol{\nu}$ are defined in analogous way. Note that different operators with the same quantum numbers can have different annihilation ranks. For instance, a trace operator $(a_1^\dagger a_1)$ has annihilation rank $\boldsymbol{\nu} = (0, 0, 1, 0, 0)$ while the operator $(a_1 a_1^\dagger)$ has $\boldsymbol{\nu} = (0, 0, 0, 0, 0)$.

A cyclic permutation of operator A is understood as $(A_i \dots A_m A_1 \dots A_{i-1})$. Consider now the set \mathcal{N} of annihilation ranks ν_i of all cyclic permutations of A and annihilation ranks $\bar{\nu}_i$ of cyclic permutations of $A^\dagger = (A_m^\dagger \dots A_1^\dagger)$. We say that $(A_i \dots A_m A_1 \dots A_{i-1})$ is maximally annihilating rotation of A if ν_i or $\bar{\nu}_i$ maximizes \mathcal{N} (in lexicographical order). The crucial observation is that either ν_i or $\bar{\nu}_i$ is nonzero for the maximally annihilation rotation. For instance, the maximally annihilating rotation of $(a_1 a_1^\dagger a_2)$ is $(a_1^\dagger a_2 a_1)$.

Let \tilde{A} be the maximally annihilating rotation of A . We now show how to transform A into the following expression:

$$A = \tilde{A} + \mathcal{R}, \quad (3.20)$$

where \mathcal{R} is a linear combination of products of trace operators. Each product of trace operators in \mathcal{R} has total length smaller than m . Operator A can be written in the following way:

$$\begin{aligned} (A_1 \dots A_m) &= A_1^{a_1} \dots A_m^{a_m} (T^{a_1} \dots T^{a_m}) \\ &= A_2^{a_2} \dots A_m^{a_m} A_1^{a_1} (T^{a_2} \dots T^{a_m} T^{a_1}) + \mathcal{R} \\ &= (A_2 \dots A_m A_1) + \mathcal{R}. \end{aligned} \quad (3.21)$$

The remainder \mathcal{R} is

$$\mathcal{R} = \sum_i \epsilon_i A_2^{a_2} \dots A_{i-1}^{a_{i-1}} [A_1^{a_1}, A_i^{a_i}]_{\pm} A_{i+1}^{a_{i+1}} \dots A_m^{a_m} (T^{a_1} \dots T^{a_m}), \quad (3.22)$$

where $[\cdot, \cdot]_{\pm}$ is a commutator or anticommutator, depending on whether both, $A_1^{a_1}$ and $A_i^{a_i}$ are fermionic or not. Coefficients ϵ_i are $(-1)^k$ where k is the number of $j \in \{1, \dots, i-1\}$ for which $[A_1^{a_1}, A_j^{a_j}]_{\pm}$ is an anticommutator. Because all operators A_i^a are creation or annihilation operators, each (anti)commutator $[A_1^{a_1}, A_i^{a_i}]_{\pm}$ is zero or $\pm \delta^{a_1, a_i}$. We take the sign into account by changing ϵ_i , which now can be ± 1 or 0. Now,

$$\mathcal{R} = \sum_{i=2}^m \epsilon_i \delta^{a_1 a_i} A_2^{a_2} \dots A_{i-1}^{a_{i-1}} A_{i+1}^{a_{i+1}} \dots A_m^{a_m} (T^{a_1} \dots T^{a_m}). \quad (3.23)$$

In order to perform sum over a_1 we use the identity $T_{ij}^a T_{kl}^a = \frac{1}{2} \delta_{il} \delta_{kj} - \frac{1}{2N} \delta_{ij} \delta_{kl}$. This is in fact the only place where the value of N is used. For $i = 3, \dots, m-1$ the trace in formula (3.23) is

$$\delta^{a_1 a_i} (T^{a_1} \dots T^{a_m}) = \frac{1}{2} (T^{a_2} \dots T^{a_{i-1}}) (T^{a_{i+1}} \dots T^{a_m}) - \frac{1}{2N} (T^{a_2} \dots T^{a_{i-1}} T^{a_{i+1}} \dots T^{a_m}). \quad (3.24)$$

For $i = 2, m$ it is

$$\begin{aligned} \delta^{a_1 a_2} (T^{a_1} \dots T^{a_m}) &= \frac{N^2 - 1}{2N} (T^{a_3} \dots T^{a_m}), \quad m > 2, \\ \delta^{a_1 a_m} (T^{a_1} \dots T^{a_m}) &= \frac{N^2 - 1}{2N} (T^{a_2} \dots T^{a_{m-1}}), \quad m > 2, \\ \delta^{a_1 a_2} (T^{a_1} T^{a_2}) &= \frac{N^2 - 1}{2}. \end{aligned} \quad (3.25)$$

In each case \mathcal{R} can be written in terms of products of traces. The total length of traces in each product is equal to $m-2$. Up to this point A was rotated by one position and an

additional remainder was produced. This procedure is continued until A is turned into its maximally annihilating rotation. Then it is applied to each trace operator in \mathcal{R} to turn it into its maximally annihilating rotation.

Now, take a composite trace operator $B = B_1 \cdots B_p$ where each B_j is in its maximally annihilating rotation. We associate annihilation rank ν with B in the following way. Let μ_i be the difference of numbers of operators f_1 and f_1^\dagger in trace operators $B_{i+1} \cdots B_p$. Then ν_F^1 is maximum of all μ_i . Let now \mathcal{N} be the set of all annihilation ranks ν_σ and $\bar{\nu}_\sigma$ which correspond to permutations $B_{\sigma(1)} \cdots B_{\sigma(p)}$ and their conjugates $B_{\sigma(p)}^\dagger \cdots B_{\sigma(1)}^\dagger$. We say that B is in the most annihilating permutation if its annihilation rank or annihilation rank of its hermitean conjugate maximizes \mathcal{N} (in lexicographical order). The maximally annihilating form of B will be denoted by \tilde{B} .

We now commute trace operators in B in such way that it transforms into maximally annihilating permutation. Commuting trace operators reduces to commuting creating and annihilation operators between different traces. This gives contractions of color indices between traces. Such contractions are eliminated by the following relation:

$$\begin{aligned} \delta^{a_i b_j} (T^{a_1} \dots T^{a_m}) (T^{b_1} \dots T^{b_k}) &= \frac{1}{2} (T^{a_1} \dots T^{a_{i-1}} T^{b_{j+1}} \dots T^{b_k} T^{b_1} \dots T^{b_{j-1}} T^{a_{i+1}} \dots T^{a_m}) \\ &\quad - \frac{1}{2N} (T^{a_1} \dots T^{a_{i-1}} T^{a_{i+1}} \dots T^{a_m}) (T^{b_1} \dots T^{b_{j-1}} T^{b_{j+1}} \dots T^{b_k}). \end{aligned} \quad (3.26)$$

Finally, commuting traces produces only more products of trace operators. Therefore, B can be written as

$$B = \tilde{B} + \mathcal{R}, \quad (3.27)$$

where \mathcal{R} is a combination of products of trace operators. Length of each composite trace in \mathcal{R} is smaller than length of B . Next, we turn all trace operators in \mathcal{R} into their maximally annihilating rotations and all composite traces into their maximally annihilating permutations.

Finally, take an arbitrary linear combination of products of trace operators C . Transform all trace operators in C into their maximally annihilating rotations and all products of these into their maximally annihilating permutations. The result of this procedure is called *maximally annihilating form* of C . What is important, all trace operators and thus also products of these have positive annihilation rank ν (or $\bar{\nu}$) in the sense that it has a nonzero component and the first nonzero component is positive. The only exception is the identity for which $\nu = \bar{\nu} = 0$.

3.3.2 Recursion

We now present the algorithm of computing the matrix of a given operator A . Assume that A is given by sum of composite traces: $A = \sum_i \alpha_i \prod_j O_{ij}$ where O_{ij} are trace operators and α_i are constants. Assume that each O_{ij} is given in maximally annihilating form.

Recall that the full Hilbert space is decomposed into orthogonal subspaces (3.18) and each subspace $\mathcal{H}_{\mathbf{n}}$ is spanned by all composite bricks with occupation numbers \mathbf{n} acting on the Fock vacuum. The matrix of operator A can be written in a block form with blocks $A|_{\mathbf{n}'\mathbf{n}} : \mathcal{H}_{\mathbf{n}} \rightarrow \mathcal{H}_{\mathbf{n}'}$. Dimension $D_{\mathbf{n}}$ of $\mathcal{H}_{\mathbf{n}}$ is finite for each \mathbf{n} . It can be determined numerically as it will be shown below or calculated from the character method which is

presented in Chapter 4. Clearly, each block $A|_{\mathbf{n}'\mathbf{n}}$ can be expressed as a combination of products of block of components of A : $O_{ij}|_{\mathbf{n}''\mathbf{n}'''}$. Therefore, we assume that A is a trace operator itself: $A = (A_1 \dots A_m)$.

Let \hat{n}_F^α be the number of creation operators f_α^\dagger in A minus the number of annihilation operators f_α . Let \hat{n}_B^i be defined in analogous way. Then $\hat{\mathbf{n}} = (\hat{n}_F^1, \hat{n}_F^2, \hat{n}_B^1, \hat{n}_B^2, \hat{n}_B^3)$ is called *creation labels* for A .

The block $A|_{\mathbf{n}'\mathbf{n}}$ is known a priori in several cases. If A is an identity operator then $A|_{\mathbf{n}'\mathbf{n}}$ is an identity matrix for $\mathbf{n} = \mathbf{n}'$ and vanished otherwise. The block vanishes for any A if $\mathbf{n}' \neq \mathbf{n} + \hat{\mathbf{n}}$. It is also true when the annihilation rank ν of A is greater than \mathbf{n} for at least one of five components. Similarly, the block vanishes when annihilation rank $\bar{\nu}$ of A^\dagger is greater than \mathbf{n}' for at least one component. From now on we assume that none of these is true. Moreover, if ν is greater than $\bar{\nu}$ then we calculate $A^\dagger|_{\mathbf{m}\mathbf{m}'}$ and write $A|_{\mathbf{n}'\mathbf{n}} = (A^\dagger|_{\mathbf{m}\mathbf{m}'})^\dagger$.

Let $\{\mathcal{B}_i\}$ be the set of all bricks that contain at least one creation operator corresponding to the first not vanishing component of \mathbf{n} (e.g. if $n_F^1 \neq 0$ it is f_1^\dagger and if $n_F^1 = 0 \neq n_F^2$ then it is f_2^\dagger , etc.). Next, remove all bricks for which $\mathcal{H}_{\mathbf{n}_i}$, where $\mathbf{n}_i = \mathbf{n} - \hat{\mathbf{n}}_i$, is empty. In particular, all bricks for which at least one component of \mathbf{n}_i is negative have to be removed. $\mathcal{H}_{\mathbf{n}_i}$ is then spanned by composite bricks acting on Fock vacuum, each containing at least one brick from the set $\{\mathcal{B}_i\}$. Now, take an orthonormal basis $|e_j^{\mathbf{n}_i}\rangle$ in the sector $\mathcal{H}_{\mathbf{n}_i}$. Then, vectors $|v_k\rangle = \mathcal{B}_i|e_j^{\mathbf{n}_i}\rangle$ span $\mathcal{H}_{\mathbf{n}}$. The index k enumerates all pairs (i, j) on the right hand side. Vectors $|v_k\rangle$ may be not orthogonal and the number of them can be larger than the dimension $D_{\mathbf{n}}$ of $\mathcal{H}_{\mathbf{n}}$. This will be taken into account by orthogonalization matrix.

The block element of A is constructed in two steps. First, a block in the overcomplete basis is built:

$$(\bar{A}|_{\mathbf{n}'\mathbf{n}})_{lk} = \langle e_l^{\mathbf{n}'} | A | v_k \rangle = \langle e_l^{\mathbf{n}'} | A \mathcal{B}_i | e_j^{\mathbf{n}_i} \rangle. \quad (3.28)$$

It can be written in a block form:

$$\bar{A}|_{\mathbf{n}'\mathbf{n}} = \begin{pmatrix} (A\mathcal{B}_1)|_{\mathbf{n}'\mathbf{n}_1} \\ \vdots \\ (A\mathcal{B}_q)|_{\mathbf{n}'\mathbf{n}_q} \end{pmatrix}. \quad (3.29)$$

For each block, one finds first the maximally annihilating form of $A\mathcal{B}_i$ and then constructs $(A\mathcal{B}_i)|_{\mathbf{n}'\mathbf{n}_i}$. After the whole block $\bar{A}|_{\mathbf{n}'\mathbf{n}}$ is constructed, we orthogonalize basis of $\mathcal{H}_{\mathbf{n}}$. Let $S_{\mathbf{n}}$ be the Gramm matrix in the sector $\mathcal{H}_{\mathbf{n}}$:

$$S_{\mathbf{n}} = \begin{pmatrix} (\mathcal{B}_1^\dagger \mathcal{B}_1)|_{\mathbf{n}_1\mathbf{n}_1} & \dots & (\mathcal{B}_1^\dagger \mathcal{B}_q)|_{\mathbf{n}_1\mathbf{n}_q} \\ \vdots & \ddots & \vdots \\ (\mathcal{B}_q^\dagger \mathcal{B}_1)|_{\mathbf{n}_q\mathbf{n}_1} & \dots & (\mathcal{B}_q^\dagger \mathcal{B}_q)|_{\mathbf{n}_q\mathbf{n}_q} \end{pmatrix}. \quad (3.30)$$

Matrix $S_{\mathbf{n}}$ has exactly $D_{\mathbf{n}}$ nonzero eigenvalues λ_l . Eigenvectors w_k^l of $S_{\mathbf{n}}$ which correspond to nonzero eigenvalues are used to construct basis of $\mathcal{H}_{\mathbf{n}}$. More precisely, the orthonormal basis is given by

$$|e_l^{\mathbf{n}}\rangle = \frac{1}{\sqrt{\lambda_l}} \sum_k w_k^l |v_k\rangle. \quad (3.31)$$

These states are indeed orthonormal:

$$\begin{aligned}\langle e_m^{\mathbf{n}} | e_l^{\mathbf{n}} \rangle &= \frac{1}{\sqrt{\lambda_m \lambda_l}} \sum_{kj} w_j^{m*} w_k^l \langle v_j | v_k \rangle = \frac{1}{\sqrt{\lambda_m \lambda_l}} \sum_{kj} w_j^{m*} w_k^l (S_{\mathbf{n}})^j_k \\ &= \frac{1}{\sqrt{\lambda_m \lambda_l}} \sum_j \lambda_l w_j^{m*} w_j^l = \delta_{ml}.\end{aligned}\tag{3.32}$$

Finally, we construct the orthogonalization matrix $R_{\mathbf{n}}$ by setting its matrix elements to $(R_{\mathbf{n}})_{kl} = \frac{1}{\sqrt{\lambda_l}} w_k^l$. Then, $A|_{\mathbf{n}'\mathbf{n}}$ is the product of the block in overcomplete basis and the orthogonalization matrix:

$$(\bar{A}|_{\mathbf{n}'\mathbf{n}} R_{\mathbf{n}})_{ij} = \sum_k (\bar{A}|_{\mathbf{n}'\mathbf{n}})_{ik} (R_{\mathbf{n}})_{kj} = \sum_k \langle e_i^{\mathbf{n}'} | A | v_k \rangle \frac{1}{\sqrt{\lambda_j}} w_k^j = \langle e_i^{\mathbf{n}'} | A | e_j^{\mathbf{n}} \rangle.\tag{3.33}$$

The block $A|_{\mathbf{n}'\mathbf{n}}$ is constructed. We give now summary of the algorithm.

1. Find all bricks \mathcal{B}_i with creation labels $\hat{\mathbf{n}}_i$ such that the first nonzero component of $\hat{\mathbf{n}}_i$ is at the same position as for \mathbf{n} and $\mathbf{n}_i = \mathbf{n} - \hat{\mathbf{n}}_i$ is non negative.
2. For each brick \mathcal{B}_i write the operator $A\mathcal{B}_i$ in its maximally annihilating form.
3. Find all blocks $(A\mathcal{B}_i)|_{\mathbf{n}'\mathbf{n}_i}$ and use them to construct $\bar{A}|_{\mathbf{n}'\mathbf{n}}$.
4. Write all operators $\mathcal{B}_i^\dagger \mathcal{B}_j$ in maximally annihilating form.
5. Find all blocks $(\mathcal{B}_i^\dagger \mathcal{B}_j)|_{\mathbf{n}_i, \mathbf{n}_j}$ and construct Gramm matrix $S_{\mathbf{n}}$.
6. Diagonalize $S_{\mathbf{n}}$ and construct the orthogonalization matrix $R_{\mathbf{n}}$.
7. The matrix block of A is $A|_{\mathbf{n}'\mathbf{n}} = \bar{A}|_{\mathbf{n}'\mathbf{n}} R_{\mathbf{n}}$.

The algorithm is recursive, so it requires a proof that it is finite. The proof is given in Appendix C.

3.3.3 Diagonalization

Some remarks concerning diagonalization of matrices are in place. Assume that we constructed matrices of the Hamiltonian H , square of total angular momentum J^2 and the third component of angular momentum J_3 in a sector with n_F fermions and at most N_B bosons. In order to obtain energies one can diagonalize H and then eventually act with J^2 and J_3 on eigenvectors to check what are their quantum numbers. This procedure is however ineffective.

Recall that J^2 and J_3 conserve the number of bosons n_B (c.f. 3.17) while H does not. Therefore, matrices of angular momentum decompose into smaller matrices on subspaces with fixed n_B :

$$J_{N_B}^2 = \begin{pmatrix} J_{n_B=1}^2 & & & 0 \\ & J_{n_B=2}^2 & & \\ & 0 & \ddots & \\ & & & J_{n_B=N_B}^2 \end{pmatrix} \quad (3.34)$$

$$J_{3,N_B} = \begin{pmatrix} J_{3,n_B=1} & & & 0 \\ & J_{3,n_B=2} & & \\ & 0 & \ddots & \\ & & & J_{3,n_B=N_B} \end{pmatrix} \quad (3.35)$$

We diagonalize $J_{n_B}^2$ for each n_B . Since these matrices are smaller, it is much faster to diagonalize them. For each value of angular momentum j we construct a projection matrix $P_j^{n_B}$. It maps the sector \mathcal{H}_{n_B} onto a subspace $\mathcal{H}_{n_B,j}$ corresponding to given j . The projection matrix is composed of eigenvectors of J^2 . Then J_3 on these small subspaces are

$$J_{3,n_B,j} = P_{n_B j}^\dagger J_{3,n_B} P_{n_B j}. \quad (3.36)$$

These matrices are yet smaller and can be diagonalized for each n_B and j separately. The projection matrices $P_{n_B,j,m}$ from $\mathcal{H}_{n_B,j}$ to $\mathcal{H}_{n_B,j,m}$ are given by eigenvectors of $J_{3,n_B,j}$. Then the projection matrices from \mathcal{H}_{n_B} to $\mathcal{H}_{n_B,j,m}$ are $\mathcal{P}_{n_B,j,m} = P_{n_B,j,m} P_{n_B,j}$. We construct a transition matrix

$$\mathcal{P}_{N_B,j,m} = \begin{pmatrix} \mathcal{P}_{n_B=1,j,m} & & & 0 \\ & \mathcal{P}_{n_B=2,j,m} & & \\ & 0 & \ddots & \\ & & & \mathcal{P}_{n_B=N_B,j,m} \end{pmatrix}. \quad (3.37)$$

Finally, we construct the matrix of Hamiltonian in a channel with given (j, m) : $H_{N_B,j,m} = \mathcal{P}_{N_B,j,m}^\dagger H_{N_B} \mathcal{P}_{N_B,j,m}$. It is much smaller than the initial full matrix H_{N_B} and thus diagonalization is faster.

3.4 Gauss elimination for bricks

It was mentioned at the end of subchapter 3.2 that there is one more way to eliminate superfluous bricks. Here this method is presented.

Gauss elimination for bricks is based on an observation that the usual Gauss elimination which can be used to identify linearly dependent vectors, works also for bricks. If a set of composite bricks \mathfrak{B}_i acting on the Fock vacuum gives linearly dependent states, i.e.

$$\sum_i \alpha_i \mathfrak{B}_i |0\rangle = 0, \quad \alpha_i \neq 0, \quad (3.38)$$

then the composite bricks themselves are linearly dependent:

$$\sum_i \alpha_i \mathfrak{B}_i = 0. \quad (3.39)$$

This is not true for general operators. However, it holds for composite bricks because they consist only of creation operators. The idea is to identify linearly dependent states (3.38) and based on this knowledge eliminate unnecessary bricks. The procedure is the following.

1. Choose a sector with occupation numbers \mathbf{n} and assume that the Gauss elimination was already performed for all \mathbf{n}' such that $\mathbf{n} - \mathbf{n}' \geq 0$.
2. Take all bricks \mathcal{B}_i ($i = 1, \dots, q$) with occupation numbers $\hat{\mathbf{n}}_i$ such that $\mathbf{n}_i = \mathbf{n} - \hat{\mathbf{n}}_i$ is nonnegative.
3. Order bricks \mathcal{B}_i such that \mathbf{n}_i is positive for $i = 1, \dots, l$ and vanishes for $i = l+1, \dots, q$. That means that the first l bricks give rise to composite bricks. The last $q - l$ bricks \mathcal{B}_i acting on the Fock vacuum give a state in $\mathcal{H}_{\mathbf{n}}$.
4. Construct the Gram matrix $S_{\mathbf{n}}$. Note that matrix elements $(\mathcal{B}_i^\dagger \mathcal{B}_{i'})|_{\mathbf{n}_i \mathbf{n}_{i'}}$ have size 1×1 for $i, i' > l$.
5. Perform Gauss elimination for $S_{\mathbf{n}}$. It has to be done in such way that first row $i = 1, \dots, l$ are used to eliminate elements in other columns. That is, in the first l steps the pivot element is chosen from the first l rows. In the remaining $q - l$ steps the pivot elements are chosen from the last $l - q$ rows.
6. Bricks \mathcal{B}_i with $i > l$ that correspond to rows which vanish can be removed. They are linearly dependent with other composite bricks.

Using the Gauss elimination one removes all dependent bricks. Still, bases generated in sectors $\mathcal{H}_{\mathbf{n}}$ are overcomplete. It happens for the following reason. Consider occupation numbers $\mathbf{n} = (0, 0, 3, 1, 0)$. If one constructs a block matrix element of an operator A in this sector, then two bricks, $\mathcal{B}_1 = (a_1^\dagger a_1^\dagger)$ and $\mathcal{B}_2 = (a_1^\dagger a_2^\dagger)$ are taken into account. Then,

$$A|_{\mathbf{n}'\mathbf{n}} = \begin{pmatrix} (A\mathcal{B}_1)|_{\mathbf{n}'\mathbf{n}_1} \\ (A\mathcal{B}_2)|_{\mathbf{n}'\mathbf{n}_2} \end{pmatrix}. \quad (3.40)$$

The occupation labels in the smaller sectors are $\mathbf{n}_1 = (0, 0, 1, 1, 0)$, $\mathbf{n}_2 = (0, 0, 2, 0, 0)$. Each of them is one-dimensional. The single basis vector in $\mathcal{H}_{\mathbf{n}_1}$ is $\mathcal{B}_2|0\rangle$ and the basis vector in $\mathcal{H}_{\mathbf{n}_2}$ is $\mathcal{B}_1|0\rangle$. The matrix $A|_{\mathbf{n}'\mathbf{n}}$ has then two columns. One corresponds to $\mathcal{B}_1\mathcal{B}_2|0\rangle$ and the other to $\mathcal{B}_2\mathcal{B}_1|0\rangle$. This is in fact the same vector, so the basis generated in $\mathcal{H}_{\mathbf{n}}$ is overcomplete. This overcompleteness cannot be removed if one would like to preserve gains coming from the recursive nature of the algorithm.

It turned out that with this algorithm all bricks with more than six creation operators were eliminated. That means that all simple bricks which are longer than 6 are expressed in terms of composite bricks.

Motivated by this observation, we found a relation between generators of $SU(3)$. First

we assumed a general form

$$\begin{aligned}
 T^{a_1} T^{a_2} T^{a_3} T^{a_4} T^{a_5} T^{a_6} &= \frac{1}{3} (T^{a_1} T^{a_2} T^{a_3} T^{a_4} T^{a_5} T^{a_6}) \mathbb{1}_3 \\
 &+ A_{i_1 i_2 i_3 i_4 i_5 i_6} (T^{a_{i_1}} T^{a_{i_2}} T^{a_{i_3}} T^{a_{i_4}} T^{a_{i_5}}) T^{a_{i_6}} \\
 &+ B_{i_1 i_2 i_3 i_4 i_5 i_6} (T^{a_{i_1}} T^{a_{i_2}} T^{a_{i_3}} T^{a_{i_4}}) [T^{a_{i_5}} T^{a_{i_6}}] \\
 &+ C_{i_1 i_2 i_3 i_4 i_5 i_6} (T^{a_{i_1}} T^{a_{i_2}} T^{a_{i_3}}) [T^{a_{i_4}} T^{a_{i_5}} T^{a_{i_6}}] \\
 &+ D_{i_1 i_2 i_3 i_4 i_5 i_6} (T^{a_{i_1}} T^{a_{i_2}} T^{a_{i_3}}) (T^{a_{i_4}} T^{a_{i_5}}) T^{a_{i_6}} \\
 &+ E_{i_1 i_2 i_3 i_4 i_5 i_6} (T^{a_{i_1}} T^{a_{i_2}}) [T^{a_{i_3}} T^{a_{i_4}} T^{a_{i_5}} T^{a_{i_6}}] \\
 &+ F_{i_1 i_2 i_3 i_4 i_5 i_6} (T^{a_{i_1}} T^{a_{i_2}}) (T^{a_{i_3}} T^{a_{i_4}}) [T^{a_{i_5}} T^{a_{i_6}}],
 \end{aligned} \tag{3.41}$$

where $[\cdot]$ is the traceless part of a matrix, i.e. $[M] = M - \frac{1}{3}(M)\mathbb{1}_3$. The equation (3.41) can be regarded as a set of equations with unknown coefficients A, B, C, D, E, F . There are over 260 thousand equations labeled by different sets of indices $(a_1, a_2, a_3, a_4, a_5, a_6)$. Indices $(i_1, i_2, i_3, i_4, i_5, i_6)$ are permutations of $(1, 2, 3, 4, 5, 6)$. This gives 4320 free coefficients. Their number can be reduced to 1134 because of symmetry of the trace under cyclic permutations. This set of equations can be solved e.g. with Mathematica¹. The essential statement is that a solution exists. Because of certain relations between $SU(3)$ generators the solution is not unique. There are in fact 432 free parameters. We do not give explicit form of the solution because it is rather complicated. Nevertheless, existence of relation (3.41) implies that there are no bricks that are longer than 6.

Finally, we found that there are 786 bricks for the $SU(3)$ symmetry group.

3.5 Eigenvectors in terms of composite bricks

Recall that we are interested not only in values of energies of the Hamiltonian but also in wavefunctions of the bound states. Here we reconstruct states in the Fock space from eigenvectors of the Hamiltonian in the matrix representation.

Once the Hamiltonian $H_{NB,j,m}$ is diagonalized, its eigenvectors $\{c_l^{\mathbf{q}}\}$ are known. Here, $\mathbf{q} = (n_F, j, m, E)$ are quantum numbers of the corresponding state and l labels elements of the vector. We assume that $\{c_l^{\mathbf{q}}\}$ are given with respect to the orthogonal basis in $\mathcal{H}_{n_F, NB}$. That is, once the Hamiltonian was diagonalized on the subspace $\mathcal{H}_{n_F, NB, j, m}$ the eigenvectors are transformed back to $\mathcal{H}_{n_F, NB}$ with the transition matrix. In what follows the quantum numbers \mathbf{q} are omitted for simpler notation.

Sectors corresponding to occupation numbers \mathbf{n} are sorted in lexicographical order. It is then easy to identify which coefficients c_l correspond to which $\mathcal{H}_{\mathbf{n}}$. The eigenvector $\{c_l\}$ can be given with two labels $\{c_l^{\mathbf{n}}\}$. In each subspace $\mathcal{H}_{\mathbf{n}}$ there is a basis $|e_l^{\mathbf{n}}\rangle$. The ket $|\psi\rangle$ corresponding to $\{c_l^{\mathbf{n}}\}$ is then

$$|\psi\rangle = \sum_{\mathbf{n}, l} c_l^{\mathbf{n}} |e_l^{\mathbf{n}}\rangle. \tag{3.42}$$

The orthogonal basis is given in terms of the orthogonalization matrix $R_{\mathbf{n}}$ and bricks

¹A Mathematica notebook for solving (3.41) is available at http://th.if.uj.edu.pl/~ambrozinski/SU3_relation.zip

acting on basis in lower sectors. Therefore,

$$\begin{aligned} |\psi\rangle &= c^0 |0\rangle + \sum_{\mathbf{n}>0,l} c_l^{\mathbf{n}} |e_l^{\mathbf{n}}\rangle = c^0 |0\rangle + \sum_{\mathbf{n},l} c_l^{\mathbf{n}} \sum_k (R_{\mathbf{n}})_{kl} |v_k\rangle \\ &= c^0 |0\rangle + \sum_{\mathbf{n},l} c_l^{\mathbf{n}} \sum_{i,p} (R_{\mathbf{n}})_{k(i,p)l} \mathcal{B}_i |e_p^{\mathbf{n}i}\rangle. \end{aligned} \quad (3.43)$$

We continue to express $|e_p^{\mathbf{n}i}\rangle$ in terms of basis of yet lower sectors until ψ is given in terms of composite bricks acting on the Fock vacuum

$$|\psi\rangle = \sum_l \alpha_l \left(\prod_i \mathcal{B}_{il} \right) |0\rangle. \quad (3.44)$$

This form of state $|\psi\rangle$ can be then used to construct the wavefunction. Wavefunctions are discussed in Chapter 7.

3.6 Additional variational parameter

The cut Fock space method is effectively a variational method for finding the lowest energies of a system. For a given n_F and N_B the Hilbert space has a finite number of basis states $|e_l\rangle$. A general state is given by a combination $|\psi\rangle = \sum_l b_l |e_l\rangle$. The lowest energy is approximated by the minimum of $\langle\psi|H|\psi\rangle$ with respect to coefficients $\{b_l\}$ with the constraint $\langle\psi|\psi\rangle = 1$. This is precisely the lowest eigenvalue of the matrix $(\langle e_l|H|e_m\rangle)_{lm}$. The second eigenvalue is the minimum of $\langle\psi'|H|\psi'\rangle$ with normalization $\langle\psi'|\psi'\rangle = 1$ and orthogonality condition $\langle\psi'|\psi\rangle = 0$, etc. With increasing N_B the number of variational parameters b_l grows and thus the approximation is more accurate. We now present a way to introduce another variational parameter to the method and show its influence on the final result.

Basis of the Fock space are states

$$|\mathbf{n}, \boldsymbol{\chi}\rangle = |\mathbf{n}\rangle_B \otimes |\boldsymbol{\chi}\rangle_F = \prod_{b,\alpha} (f_\alpha^{b\dagger})^{\chi_\alpha^b} \prod_{a,i} \frac{1}{\sqrt{(n_i^a)!}} (a_i^{a\dagger})^{n_i^a} |0\rangle, \quad (3.45)$$

where $\mathbf{n} = (n_i^a)$ and $\boldsymbol{\chi} = (\chi_\alpha^b)$ denote bosonic and fermionic occupation numbers respectively. These states are not gauge singlets. An orthogonal basis $\{|e_l\rangle\}$ of the space of gauge invariant states \mathcal{H}_{N_B} for given n_F was introduced earlier in this chapter. It can be expressed as linear combinations of states (3.45):

$$|e_l\rangle = \sum_{\mathbf{n}\boldsymbol{\chi}} c_l^{\mathbf{n}\boldsymbol{\chi}} |\mathbf{n}, \boldsymbol{\chi}\rangle. \quad (3.46)$$

Wavefunctions of bosonic states in the configuration representation ${}_B\langle\mathbf{x}|\mathbf{n}\rangle_B$ are given by Hermite functions. The basis can be modified by introducing a parameter $\omega > 0$ in the following way:

$$\begin{aligned} {}_B\langle\mathbf{x}|\mathbf{n}\rangle_{B,\omega} &\equiv \omega^{d/2} {}_B\langle\omega\mathbf{x}|\mathbf{n}\rangle_B, \\ |e_l\rangle_\omega &= \sum_{\mathbf{n}\boldsymbol{\chi}} c_l^{\mathbf{n}\boldsymbol{\chi}} |\mathbf{n}, \boldsymbol{\chi}\rangle_\omega = \sum_{\mathbf{n}\boldsymbol{\chi}} c_l^{\mathbf{n}\boldsymbol{\chi}} |\mathbf{n}\rangle_{B,\omega} \otimes |\boldsymbol{\chi}\rangle_F, \end{aligned} \quad (3.47)$$

where $d = 3(N^2 - 1)$ is dimension of the bosonic configuration space. States $|\mathbf{n}, \boldsymbol{\chi}\rangle_\omega$ satisfy proper orthogonality relations and therefore states $|e_l\rangle_\omega$ are orthogonal.

Matrix elements of the position operator in the modified basis $|\mathbf{n}, \boldsymbol{\chi}\rangle_\omega$ satisfy

$$\begin{aligned} {}_{B,\omega}\langle \mathbf{m} | x_i^a | \mathbf{n} \rangle_{B,\omega} &= \int d^d \mathbf{x} {}_{B,\omega}\langle \mathbf{m} | \mathbf{x} \rangle x_i^a \langle \mathbf{x} | \mathbf{n} \rangle_{B,\omega} \\ &= \omega^{-1} \int d^d(\omega \mathbf{x}) {}_B\langle \mathbf{m} | \omega \mathbf{x} \rangle \omega x_i^a \langle \omega \mathbf{x} | \mathbf{n} \rangle_B \\ &= \omega^{-1} {}_B\langle \mathbf{m} | x_i^a | \mathbf{n} \rangle_B. \end{aligned} \quad (3.48)$$

A similar proof shows that ${}_{B,\omega}\langle \mathbf{m} | p_i^a | \mathbf{n} \rangle_{B,\omega} = \omega {}_B\langle \mathbf{m} | p_i^a | \mathbf{n} \rangle_B$. Finally, it can be read from (2.17), (2.6) and (2.5) that matrix elements of other operators in the orthogonal basis $|e_l\rangle$ yield

$$\begin{aligned} \omega \langle e_l | x_i^a | e_m \rangle_\omega &= \omega^{-1} \langle e_l | x_i^a | e_m \rangle, \\ \omega \langle e_l | p_i^a | e_m \rangle_\omega &= \omega \langle e_l | p_i^a | e_m \rangle, \\ \omega \langle e_l | J_i | e_m \rangle_\omega &= \langle e_l | J_i | e_m \rangle, \\ \omega \langle e_l | G^a | e_m \rangle_\omega &= \langle e_l | G^a | e_m \rangle, \\ \omega \langle e_l | H_K | e_m \rangle_\omega &= \omega^2 \langle e_l | H_K | e_m \rangle, \\ \omega \langle e_l | H_V | e_m \rangle_\omega &= \omega^{-4} \langle e_l | H_V | e_m \rangle, \\ \omega \langle e_l | H_F | e_m \rangle_\omega &= \omega^{-1} \langle e_l | H_F | e_m \rangle. \end{aligned} \quad (3.49)$$

It is significant that matrix elements of J_i and G^a are invariant under ω . It follows that $|e_l\rangle_\omega$ are gauge invariant because $G^a |e_l\rangle = 0$. Therefore, states $|e_l\rangle_\omega$ form an orthogonal basis of the Hilbert space of gauge singlets. Moreover, given an angular momentum multiplet $|j, m\rangle = \sum_l c_l^{j,m} |e_l\rangle$, the scaled combination $|j, m\rangle_\omega = \sum_l c_l^{j,m} |e_l\rangle_\omega$ is also an angular momentum multiplet with the same quantum numbers (j, m) .

We now recall how the energies are calculated to show how ω can be included. First, for given n_F matrices of operators H_K, H_V, H_F, J_i are constructed in the cut space \mathcal{H}_{N_B} . Then, J^2 and J_3 are diagonalized. They are ω -independent. Next, the three matrices $(H_K)_{N_B}, (H_C)_{N_B}, (H_F)_{N_B}$ are projected to the subspaces $\mathcal{H}_{N_B,j,m}$. Their dependence on ω is given by (3.49). Therefore, ω can be taken into account by constructing

$$(H_\omega)_{N_B,j,m} = \omega^2 (H_K)_{N_B,j,m} + \omega^{-4} (H_V)_{N_B,j,m} + \omega^{-1} (H_F)_{N_B,j,m}, \quad (3.50)$$

where all matrices on the right hand side are constructed for $\omega = 1$. Finally, ω is chosen such that the lowest eigenvalue of $(H_\omega)_{N_B,j,m}$ is minimized. This requires diagonalizing $(H_\omega)_{N_B,j,m}$ multiple times. However, subspaces $\mathcal{H}_{N_B,j,m}$ are reasonably small, especially for small j , and this minimization does not consume significant computer resources.

We come to discussing the effect of including ω . Results concerning the energies are given in Tab. 3.1. In the sector $(n_F, j) = (0, 0)$ the smallest eigenvalue with cutoff N_B minimized with respect to ω is smaller than the lowest eigenvalues for cutoff $N_B + 2$ with $\omega = 1$. That is, including the parameter ω effectively increases the cutoff by 2. The effect is similar for $(n_F, j) = (2, 1)$. In the singlet channel for six fermions inclusion of ω effectively rises N_B by almost 1.

In Tab. 3.2 optimal values of ω for different channels are given. It can be seen that all values of ω are similar. They are slightly larger for $n_F \geq 4$. This means that the functions are in general wider for high n_F which may be a slight indication that the spectrum is continuous in these sectors.

N_B	lowest eigenvalues in sector with quantum numbers (n_F, j)					
	$(0, 0)$, no ω	$(0, 0)$ with ω	$(2, 1)$, no ω	$(2, 1)$ with ω	$(6, 0)$, no ω	$(6, 0)$ with ω
0	15	12.9919			15	12.99
1	15	12.9919	17	14.41	9.06	7.83
2	13.327	12.9517	14.35	12.15	6.12	5.10
3	13.327	12.9517	13.03	11.47	4.59	3.74
4	12.8821	12.6322	12.05	11.25		
5	12.8821	12.6322	11.54	11.04		
6	12.7123	12.6203	11.20	10.79		
7	12.7123	12.6203	10.97	10.64		
8	12.6339	12.5911				
9	12.6339	12.5911				
10	12.6038	12.5889				

Table 3.1: The lowest energies in selected sectors. In each case the energy is given with keeping $\omega = 1$ and minimizing the energy with respect to ω .

$j \backslash n_F$	0	1	2	3	4	5	6	7	8
0	1.22		1.21		1.15		1.15		1.14
1/2		1.31		1.23		1.15		1.16	
1	1.25		1.22		1.15		1.15		1.15
3/2		1.27		1.22		1.15		1.15	
2	1.25		1.20		1.15		1.16		1.15

Table 3.2: Optimal values of ω in each (n_F, j) channel. The value depends on the cutoff and is given for the maximal cutoff available.

3.7 Modifications for $SU(2)$

Up to this point the cut Fock space method was discussed in reference to the $SU(3)$ theory. The case of $SU(2)$ is simpler. Some changes can be done to the algorithm so that a higher cutoff can be reached. In this part we briefly discuss these modifications.

For $SU(2)$ there is a relation similar to (3.41), but it decomposes a product of three $SU(2)$ generators:

$$T^a T^b T^c = \frac{1}{2}(T^a T^b)T^c - \frac{1}{2}(T^a T^c)T^b + \frac{1}{2}(T^b T^c)T^a + \frac{1}{2}(T^a T^b T^c)\mathbf{1}_2. \quad (3.51)$$

This implies that there are no bricks longer than three. Some bricks can be eliminated because of invariance of trace under cyclic permutations as for the $SU(3)$ case. The Cayley–Hamilton theorem applied to a matrix M of size 2×2 implies that M^2 can be expressed in terms of (M^2) and (M) . Therefore, there are no bricks of the form $(a_i^\dagger a_i^\dagger b^\dagger)$, where b^\dagger is any creation operator. All independent bricks can be easily identified and there are 35 of them.

The relation (3.51) has further consequences. It implies that there are no single–trace operators of length higher than three. One can calculate all commutators of single–trace operators beforehand and then use them in the program for calculating matrix elements. Because of this, one does not have to calculate the maximally annihilating form of an operator during a run. Instead, one uses the commutators to write $A\mathcal{B}_i = \mathcal{B}_i A + [A, \mathcal{B}_i]$ (cf. (3.29)). This is in principle possible also for $SU(3)$. However, the formula (3.41) limits the single–trace operators to length 6 and in practice there are too many commutators to be calculated and memorized.

Secondly, it is relatively easy to construct operators with definite angular momentum from single–trace operators. Using operators with definite angular momentum allows one to construct matrix elements of the Hamiltonian directly in channels $\mathcal{H}_{n_F N_B j m}$. Then one does not have to diagonalize the matrix representations of J^2 and J_3 but directly the Hamiltonian H . This significantly reduces the time needed for diagonalization and allows one to reach higher cutoffs.

Both of above simplifications are taken into account in [38]. This allowed the authors to reach a cutoff $N_B = 18$ in all fermionic sectors. In this thesis $SU(2)$ case is used only as a guidance for analysis of $SU(3)$ and we are interested in small N_B behavior. Therefore, we do not incorporate modifications discussed above.

3.8 Summary

In this chapter the cut Fock space method was presented. The bosonic and fermionic creation and annihilation operators and the Fock vacuum state were introduced. Because of the Gauss law, only gauge invariant states and operators are relevant. In the matrix notation, creation and annihilation operators are given by operator–valued matrices. Gauge invariant operators are traces of products of such matrices. They are called trace operators. A special class of trace operators, namely those which consist only of creation operators are called bricks. Composite bricks are products of bricks. The whole physical Fock space is generated by composite bricks acting on the empty state.

In the Hilbert space we introduce a cutoff N_B for the maximal number of bosonic excitations. In this way the full space is reduced to a finite dimensional cut Fock space. In this subspace operators are represented by matrices. Because angular momentum and

Hamiltonian conserve the total number of fermions, it is convenient to work with subspaces with definite n_F . It is argued that the spectrum of angular momentum operators is exact for finite cutoff because the angular momentum operators conserve the total number of bosons n_B . The spectrum of the Hamiltonian is recovered only in the $N_B \rightarrow \infty$ limit.

All possible composite bricks acting on the empty generate an overcomplete basis. In subchapters 3.2 and 3.4 we have shown how to reduce the number of bricks to minimum. The three basic relations are

- invariance of trace under cyclic permutations,
- Cayley-Hamilton theorem for matrices with commuting and anticommuting matrix elements (3.6) and (3.12),
- linear dependence of products of three $SU(3)$ generators T^a (3.15).

We argued that more bricks can be removed with Gauss elimination. We found that there are no bricks that are longer than 6. Finally, we explained this by showing existence of a decomposition formula for product of six generators T^a (3.41).

In 3.3 we proposed an algorithm for computing matrix of an operator. The key point is transforming an operator to its maximally annihilating form. For an operator A and a brick \mathcal{B} the maximally annihilating form of $A\mathcal{B}$ (3.29) is given by $\mathcal{B}A + \mathcal{R}$ where \mathcal{R} is the maximally annihilating form of $[A, \mathcal{B}]$. Therefore, calculating the maximally annihilating form of $A\mathcal{B}$ is the same as calculating commutator of A and \mathcal{B} and giving it in a form convenient for further computations. Overcompleteness of basis is taken into account by introducing orthogonalization matrices $R_{\mathbf{n}}$. The algorithm is recursive. Proof of its finiteness is given in Appendix C.

We presented an effective way to diagonalize the Hamiltonian. It is efficient first to diagonalize the matrix of angular momentum J^2 and J_3 . This is because these operators conserve the total number of bosons. Therefore, they can be diagonalized on smaller subspaces which is much faster.

Finally, it was shown how to reconstruct a state in terms of composite bricks acting on the Fock vacuum from eigenvectors of operators in matrix representation. This form of states is used in Chapter 7 where we construct and study wavefunctions.

Chapter 4

Number of gauge invariant states

In the previous Chapter we introduced a set of vectors $|v^k\rangle$ which span a sector $\mathcal{H}_{\mathbf{n}}$ for given occupation numbers \mathbf{n} . It was noted that $|v^k\rangle$ form an overcomplete basis. The proper dimension of $\mathcal{H}_{\mathbf{n}}$ can be read out from the number of nonzero eigenvalues of the Gram matrix $S_{\mathbf{n}}$. However, these eigenvalues bare some numerical errors. Therefore, one would like to cross check if there is a clear distinction between zero and nonzero eigenvalues and if the dimension of $\mathcal{H}_{\mathbf{n}}$ obtained in this way is correct. Secondly, the knowledge of dimensions of sectors a priori provides a check for completeness of the set of bricks. To this end an analytic way of calculating the number of independent $SU(3)$ gauge invariant states in a given sector is presented. It is called character method because the number of states is given by an integral of characters over the group as it is shown below. The analysis in this chapter is based on [45] and modified. Introduction to the group theory and definitions of objects used in this chapter can be found e.g. in [55].

4.1 The character method

A general gauge invariant state in the Fock space can be written in the following form:

$$|s\rangle = t^{a_1 \dots a_n b_1 \dots b_m} a_{i_1}^{a_1 \dagger} \dots a_{i_n}^{a_n \dagger} f_{\alpha_1}^{b_1 \dagger} \dots f_{\alpha_m}^{b_m \dagger} |0\rangle. \quad (4.1)$$

All bosonic and fermionic creation operators are in adjoint $SU(3)$ representation. In this chapter the adjoint representation is denoted by R . Assume that in the combination (4.1) there are n_B^i bosonic creation operators $a_i^{a \dagger}$ for each i and n_F^α fermionic creation operator $f_\alpha^{b \dagger}$ for each α . The state $|s\rangle$ has occupation numbers $\mathbf{n} = (n_B^1, n_B^2, n_B^3, n_F^1, n_F^2)$. In order to simplify notation we introduce

$$\mathbf{n}_B = (n_B^1, n_B^2, n_B^3), \quad n_B = n_B^1 + n_B^2 + n_B^3, \quad (4.2)$$

$$\mathbf{n}_F = (n_F^1, n_F^2), \quad n_F = n_F^1 + n_F^2. \quad (4.3)$$

The state $|s\rangle$ is in the representation

$$Sym(\otimes^{n_B^1} R) \times Sym(\otimes^{n_B^2} R) \times Sym(\otimes^{n_B^3} R) \times Alt(\otimes^{n_F^1} R) \times Alt(\otimes^{n_F^2} R), \quad (4.4)$$

where Sym and Alt are symmetrization and antisymmetrization of the tensor product. Let $D_{\mathbf{n}}$ be the number of independent singlet states in sector $\mathcal{H}_{\mathbf{n}}$. $D_{\mathbf{n}}$ is equal to the number of trivial representations that appear in the product (4.4). From orthogonality

properties of characters it follows [56] that $D_{\mathbf{n}}$ is given by an integral of character over the group $SU(3)$:

$$D_{\mathbf{n}} = \int d\mu \chi_{Sym}^{n_B^1}(R) \chi_{Sym}^{n_B^2}(R) \chi_{Sym}^{n_B^3}(R) \chi_{Alt}^{n_F^1}(R) \chi_{Alt}^{n_F^2}(R), \quad (4.5)$$

where μ is the Haar measure of $SU(3)$. Characters of symmetric and antisymmetric powers of representation R are constructed with Frobenius formula later in this chapter. In order to make the integral (4.5) simpler, we use the generating function

$$G(\mathbf{a}, \mathbf{b}) = \sum_{n_B^i=0}^{\infty} \sum_{n_F^i=0}^{\infty} a_1^{n_B^1} a_2^{n_B^2} a_3^{n_B^3} (-b_1)^{n_F^1} (-b_2)^{n_F^2} D_{\mathbf{n}}. \quad (4.6)$$

Symbols $\mathbf{a} = (a_1, a_2, a_3)$ and $\mathbf{b} = (b_1, b_2)$ are introduced for shorter notation.

Let U be an element of $SU(3)$ in the fundamental representation. U can be decomposed as $U = W\Lambda W^\dagger$ where W is unitary and Λ is diagonal with $\det(\Lambda) = 1$. Then $\Lambda = \text{diag}(z_1, z_2, z_3)$ depends on two parameters because $z_1 z_2 z_3 = 1$. We write $z_j = e^{i\phi_j}$. The character $\chi(R)$ depends on Λ and does not depend on parameters of W . Therefore, it would be convenient to have a Haar measure μ (cf. (4.5)) integrated over parameters of W . This measure is given by the formula (cf. [57])

$$d\mu = \frac{1}{6} \prod_{i=1}^3 \frac{d\phi_i}{2\pi} \delta_P\left(\sum_{i=1}^3 \phi_i\right) \prod_{i<j} |z_i - z_j|^2, \quad (4.7)$$

where $\phi \in [0, 2\pi]$ and $\delta_P(x) = \sum_{k \in \mathbf{Z}} \delta(x - 2\pi k)$. In this parametrization character of an element R in adjoint representation is given by Schur function

$$\chi(R) = \chi(\{z_j\}) = \det(z_j^{l_i+3-i}) / \det(\{z_j^{3-i}\}), \quad (4.8)$$

where $l_i = 3 - i$ is partition of the adjoint representation of $SU(3)$. This is exactly the Weyl determinant formula [58]. The determinants can be calculated explicitly and the character is

$$\begin{aligned} \chi(\{z_i\}) &= \det \left(\begin{bmatrix} 1 & 1 & 1 \\ z_1^2 & z_2^2 & z_3^2 \\ z_1^4 & z_2^4 & z_3^4 \end{bmatrix} \right) / \det \left(\begin{bmatrix} 1 & 1 & 1 \\ z_1 & z_2 & z_3 \\ z_1^2 & z_2^2 & z_3^2 \end{bmatrix} \right) \\ &= \prod_{i<j} (z_i + z_j) = \sum_{i,j} \frac{z_i}{z_j} - 1. \end{aligned} \quad (4.9)$$

The character of R^k is given simply by

$$\chi(R^k) = \chi(\{z_i^k\}) = \sum_{i,j} \frac{z_i^k}{z_j^k} - 1. \quad (4.10)$$

The character of symmetric and antisymmetric powers of $\chi(R)$ is given by the Frobenius formula [56]:

$$\chi_{Sym}^{(n)}(R) = \sum_{\sum_k k i_k = n} \prod_{k=1}^n \frac{1}{i_k!} \frac{\chi^{i_k}(R^k)}{k^{i_k}}, \quad (4.11)$$

$$\chi_{Alt}^{(n)}(R) = \sum_{\sum_k k i_k = n} (-1)^{\sum_k i_k} \prod_{k=1}^n \frac{1}{i_k!} \frac{\chi^{i_k}(R^k)}{k^{i_k}}. \quad (4.12)$$

Finally, we introduce auxiliary functions

$$F_{Sym}(a, \{\phi_i\}) = \sum_{n=0}^{\infty} a^n \chi_{Sym}^{(n)}(R) \quad (4.13)$$

$$F_{Alt}(b, \{\phi_i\}) = \sum_{n=0}^{\infty} (-b)^n \chi_{Alt}^{(n)}(R). \quad (4.14)$$

Functions $F_{Sym}(a, \{\phi_i\})$ and $F_{Alt}(b, \{\phi_i\})$ can be simplified in the following way:

$$\begin{aligned} F_{Sym}(a, \{\phi_i\}) &= \sum_{n=0}^{\infty} a^n \sum_{\sum_k k i_k = n} \prod_{k=1}^n \frac{1}{i_k!} \frac{\chi^{i_k}(R^k)}{k^{i_k}} = \sum_{n=0}^{\infty} \sum_{\sum_k k i_k = n} \prod_{k=1}^n \frac{1}{i_k!} \left(\frac{a^k \chi(R^k)}{k} \right)^{i_k} \\ &= \sum_{n=0}^{\infty} \frac{1}{n!} \left(\sum_k \frac{a^k \chi(R^k)}{k} \right)^n = \exp \left(\sum_{ij} \sum_k \frac{1}{k} \frac{a^k z_i^k}{z_j^k} - \sum_k \frac{a^k}{k} \right) \\ &= \exp \left(- \sum_{ij} \ln \left(1 - \frac{a z_i}{z_j} \right) + \ln(1-a) \right) = (1-a) \prod_{ij} \left(1 - \frac{a z_i}{z_j} \right)^{-1}. \end{aligned} \quad (4.15)$$

Similarly, one can show that

$$F_{Alt}(b, \{\phi_i\}) = (1-b)^{-1} \prod_{ij} \left(1 - b \frac{z_i}{z_j} \right). \quad (4.16)$$

Then the generating function G has the form

$$G(\mathbf{a}, \mathbf{b}) = \int_{[0, 2\pi]^3} d\mu \prod_j F_{Sym}(a_j, \{\phi_i\}) \prod_{\alpha} F_{Alt}(b_{\alpha}, \{\phi_i\}). \quad (4.17)$$

We change the variables

$$\phi_i \rightarrow - \sum_{j \neq i} \phi_j, \quad \phi_N \rightarrow \sum_j \phi_j. \quad (4.18)$$

The jacobian is $1/3$. Integration over the last variable is over $[0, 6\pi]$ giving 3 identical integrals (from the δ_P function). This cancels with the jacobian and $\delta_P(\phi_3)$ is replaced by $\delta(\phi_3)$. The generating function is

$$\begin{aligned} G(\mathbf{a}, \mathbf{b}) &= \frac{1}{6} \left(\frac{(1-b_1)(1-b_2)}{(1-a_1)(1-a_2)(1-a_3)} \right)^2 \int_0^{2\pi} \prod_{i=1}^3 \frac{d\phi_i}{2\pi} \delta(\phi_3) \times \\ &\times \prod_{i \neq j} \left(1 - \frac{z_i}{z_j} \right) \frac{(1-b_1 \frac{z_i}{z_j})(1-b_2 \frac{z_i}{z_j})}{(1-a_1 \frac{z_i}{z_j})(1-a_2 \frac{z_i}{z_j})(1-a_3 \frac{z_i}{z_j})}. \end{aligned} \quad (4.19)$$

4.2 Calculation of the generating function

The integrals are calculated one by one:

$$\begin{aligned}
 G(\mathbf{a}, \mathbf{b}) &= \frac{1}{6} \left(\frac{(1-b_1)(1-b_2)}{(1-a_1)(1-a_2)(1-a_3)} \right)^2 \int_{\mathcal{C}} dz_2 G_1(\mathbf{a}, \mathbf{b}, z_2), \\
 G_1(\mathbf{a}, \mathbf{b}, z_2) &= \int_{\mathcal{C}} dz_1 G_2(\mathbf{a}, \mathbf{b}, z_1, z_2), \\
 G_2(\mathbf{a}, \mathbf{b}, z_1, z_2) &= \frac{1}{z_1 z_2} \prod_{i \neq j} \frac{(z_j - z_i)(z_j - b_1 z_i)(z_j - b_2 z_i)}{(z_j - a_1 z_i)(z_j - a_2 z_i)(z_j - a_3 z_i)},
 \end{aligned} \tag{4.20}$$

where \mathcal{C} is the unit circle on the complex plane. The range of indices i, j is 1, 2, 3. Remember that $z_3 = 1$. The integral is done by residues. After the integrals are calculated, the dimensions D_n of sectors \mathcal{H}_n are read from the Taylor expansion of $G(\mathbf{a}, \mathbf{b})$ around 0. Therefore, in all calculations it is assumed that a_i and b_α are small.

First we perform the integral over z_1 by residues. There are seven simple poles in z_1 variable: $z_1 = 0, a_k, a_k z_2$. The residues are

$$\text{res}_0 G_2 = \frac{(1-z_2)^2 \prod_{i \neq j} \prod_{\alpha} (z_j - b_{\alpha} z_i)}{z_2 \prod_k a_k (1 - a_k z_2) (z_2 - a_k)}, \tag{4.21}$$

where $z_1 = 0, z_3 = 1$,

$$\text{res}_{a_k} G_2 = \frac{(z_2 - 1)(z_2 - a_k)(1 - a_k)}{a_k^2 z_2 (z_2 - a_k^2)(1 + a_k)(1 - a_k z_2)} \prod_{i \neq j} \frac{(z_j - b_1 z_i)(z_j - b_2 z_i)}{\prod_{n \neq k} (z_j - a_n z_i)}, \tag{4.22}$$

where $z_1 = a_k, z_3 = 1$ and

$$\text{res}_{a_k z_2} G_2 = \frac{(1 - a_k z_2)(1 - a_k)(1 - z_2)}{a_k^2 z_2 (1 + a_k)(z_2 - a_k)(1 - a_k^2 z_2)} \prod_{i \neq j} \frac{(z_j - b_1 z_i)(z_j - b_2 z_i)}{\prod_{n \neq k} (z_j - a_n z_i)}, \tag{4.23}$$

with $z_1 = a_k z_2, z_3 = 1$.

$\text{res}_0 G_2$ has four simple poles, $z_2 = 0$ and $z_2 = a_k$. There are six simple poles of $\text{res}_{a_k} G_2$, namely $z_2 = 0, z_2 = a_n$ for $n \neq k$ and $z_2 = a_n a_k$. Finally, $\text{res}_{a_k z_2} G_2$ has four simple poles $z_2 = 0$ and $z_2 = a_n$. None of these functions has poles of higher order.

Now the function $G_1(\mathbf{a}, \mathbf{b}, z_2)$ from (4.20) is

$$G_1(\mathbf{a}, \mathbf{b}, z_2) = \int_{\mathcal{C}} dz_1 G_2(\mathbf{a}, \mathbf{b}, z_1, z_2) = \text{res}_0 G_2 + \sum_k (\text{res}_{a_k} G_2 + \text{res}_{a_k z_2} G_2) \tag{4.24}$$

Finally, $G(\mathbf{a}, \mathbf{b})$ is an integral of $G_1(\mathbf{a}, \mathbf{b}, z_2)$. It is again calculated by residues. The form of the integrals becomes somewhat more complicated:

$$\begin{aligned}
 \text{res}_0 G_1 &= \frac{\prod_{\alpha} b_{\alpha}^3}{\prod_i a_i^3} + \frac{2 \prod_{\alpha} b_{\alpha}^2}{\prod_i a_i^2 \prod_{j < k} (a_j a_k - 1)(a_j - a_k)} \\
 &\times \sum_i \frac{(a_i - 1) \prod_{\alpha} (a_i - b_{\alpha})(a_i b_{\alpha} - 1)(a_m a_n - 1)(a_m - a_n)}{a_i (a_i + 1)}
 \end{aligned}$$

where m and n are such that (i, m, n) is a cyclic permutation of $(1, 2, 3)$.

$$\begin{aligned}
 res_{a_k} G_1 &= \frac{1}{\sum_{i \neq j} (a_j a_j - 1) a_k^2 (1 + a_k) \prod_{i \neq k} (a_k - a_i)} \left(\frac{(a_k - 1) (\prod_{i \neq k} a_i - 1) \prod_{\alpha} b_{\alpha}^2}{a_k \prod_{i \neq k} a_i^2} \right. \\
 &+ \frac{(a_k - 1)^2 (a_k + 1) (\prod_{i \neq k} a_i - 1) \prod_{\alpha} (a_k - b_{\alpha}) (a_k^2 - b_{\alpha}) (a_k b_{\alpha} - 1) (a_k^2 b_{\alpha} - 1)}{a_k (1 + a_k + a_k^2) \prod_{i \neq k} (a_k - a_i) (a_k^2 - a_i) (a_k a_i - 1) (a_k^2 a_i - 1)} \\
 &+ \sum_{i \neq k} \left(\frac{(a_i - a_k) \prod_{\alpha} (a_i - b_{\alpha}) (a_i - a_k b_{\alpha}) (a_k - a_i b_{\alpha}) (a_i b_{\alpha} - 1)}{a_i^2 (a_i - a_k^2) (a_k - a_i^2) (1 + a_i) (a_i a_k - 1) (a_i - a_m) (a_i - a_k a_m) (a_k - a_i a_m)} \right. \\
 &\left. + \frac{(a_k a_i - 1) \prod_{\alpha} (a_i - b_{\alpha}) (a_i a_k - b_{\alpha}) (a_k a_i b_{\alpha} - 1) (a_i b_{\alpha} - 1)}{a_i^2 (a_k - a_i) (a_i - a_m) (a_m - a_i a_k) (1 + a_i) (a_i^2 a_k - 1) (a_i a_k^2 - 1) (a_i a_k a_m - 1)} \right) \Big)
 \end{aligned}$$

where m is assumed to be different then i and k , i.e. (i, k, m) is a permutation of $(1, 2, 3)$.

$$res_{a_k^2} G_1 = \frac{(-1 + a_k)^2 \prod_{\alpha} (a_k - b_{\alpha})^2 (a_k^2 - b_{\alpha}) (-1 + a_k b_{\alpha})^2 (-1 + a_k^2 b_{\alpha})}{a_k^3 (1 + a_k a_k^2) \prod_{i \neq k} (a_k - a_i)^2 (a_k^2 - a_i) (-1 + a_k a_i)^2 (-1 + a_k^2 a_i)}.$$

$$\begin{aligned}
 res_{a_k a_n} G_1 &= -2 \frac{\prod_{\alpha} (a_k - b_{\alpha}) (a_n - b_{\alpha}) (a_k a_n - b_{\alpha}) (-1 + a_k b_{\alpha}) (-1 + a_n b_{\alpha}) (-1 + a_k a_n b_{\alpha})}{(a_k - a_n)^2 (a_k a_n - a_l) (-1 + a_l a_k a_n)} \\
 &\times \prod_{j=k, n} \frac{1}{a_j^2 (1 + a_j) (a_j - a_l) (-1 + a_l a_j) (-1 + a_j a_k a_n)},
 \end{aligned}$$

where $l \neq k, n$.

Finally,

$$\begin{aligned}
 G(\mathbf{a}, \mathbf{b}) &= \frac{1}{6} \left(\frac{(1 - b_1)(1 - b_2)}{(1 - a_1)(1 - a_2)(1 - a_3)} \right)^2 \\
 &\times \left(res_0 G_1 + \sum_k res_{a_k} G_1 + res_{a_k^2} G_1 + \sum_{k < n} res_{a_k a_n} G_1 \right).
 \end{aligned} \tag{4.25}$$

The dimension of $\mathcal{H}_{\mathbf{n}}$ can be read out from Taylor expansion of G . The explicit expressions for residues are rather involved, so it is convenient to use a program for symbolic manipulations, e.g. Mathematica to do the Taylor expansion. The dimension of sectors with given n_B, n_F is given in Table 4.1.

4.3 Comparison with the numerical approach

In this chapter we have shown a method to calculate dimensions $D_{\mathbf{n}}$ of sectors $\mathcal{H}_{\mathbf{n}}$ analytically. A direct, numerical way to find $D_{\mathbf{n}}$ was presented in Chapter 3. First, one constructs the Gramm matrix of scalar products of all vectors that span $\mathcal{H}_{\mathbf{n}}$. Then, $D_{\mathbf{n}}$ is equal to the number of nonzero eigenvalues of the Gramm matrix.

For a cross check of these two approaches we present histograms of eigenvalues in illustrative sectors in Fig. 4.1. The $D_{\mathbf{n}}$ largest eigenvalues (where numerical value of $D_{\mathbf{n}}$ follows from the character method) are marked with red bars. Bars which correspond to smaller eigenvalues are blue. One can see that the large and small eigenvalues are well

n_B	n_F								
	0	1	2	3	4	5	6	7	8
0	1	0	1	4	5	12	11	16	28
1	0	6	12	30	72	114	180	234	240
2	6	18	66	198	444	810	1212	1590	1776
3	11	70	292	870	2048	3926	6135	8010	8780
4	30	228	969	3192	7941	15396	24549	32520	35694
5	75	624	3042	10224	26010	52260	84669	112632	123888
6	186	1632	8328	29376	77030	157348	258150	346292	381908
7	381	4008	21366	77448	207684	431712	717150	967104	1067382
8	885	9156	51078	190500	520782	1097892	1839834	2495124	2760186
9	1785	20108	115894	441212	1225864	2617004	4423238	6024572	6672230
10	3618	42300	249780	971028	2737962	5903544	10048302	13743936	15242292

Table 4.1: Total number of states in sectors with given n_F and n_B .

separated. Also, the number of large eigenvalues agrees with the dimension $D_{\mathbf{n}}$. This holds also in all other sectors. More precisely, the 'zero' eigenvalues are always smaller than 10^{-12} and the 'nonzero' are larger than 10^{-3} .

The agreement also means that all relevant bricks are included. If that was not the case, that there would be not enough large eigenvalues.

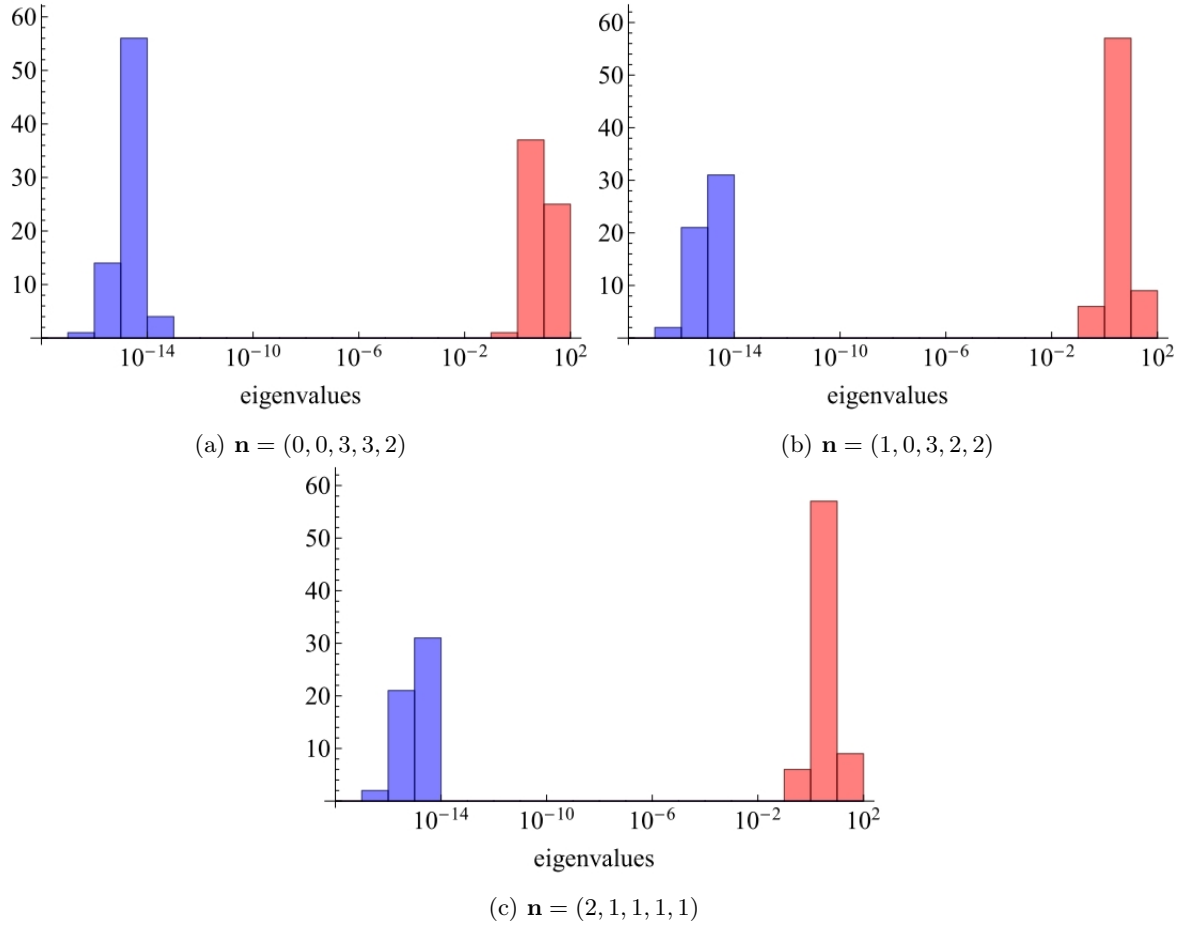


Figure 4.1: Histograms of eigenvalues of the Gram matrices $S_{\mathbf{n}}$ in three different sectors with quantum numbers \mathbf{n} . Red bars correspond to $D_{\mathbf{n}}$ largest eigenvalues where $D_{\mathbf{n}}$ is the dimension of $\mathcal{H}_{\mathbf{n}}$ which follows from the character method.

Chapter 5

The spectrum

Spectrum of a Hamiltonian is a basic characteristic of a model. The main goal of the cut Fock space method is to find eigenvalues of a given operator. Here, we apply this algorithm to find energies of the supersymmetric Yang-Mills quantum mechanics. In particular, it is interesting to identify type of the spectrum, whether it is continuous or discrete. The nature of the spectrum can be identified from behavior of energy levels for growing cutoff [59]. If a given eigenvalue converges fast, then it corresponds to a discrete energy in the continuum limit. A signature of a continuous spectrum are many eigenvalues which decrease slowly (to zero if there is no mass gap) as the cutoff increases. As it was mentioned before, the fermion number and angular momentum are conserved. Therefore, we study the spectrum in channels with definite n_F and j .

First we present the results for the $SU(2)$ theory. We give a short review of other methods and then proceed to detailed analysis of the spectrum obtained with our approach. This part serves as a check of our program and a guide to understand the results for the more complicated model with $SU(3)$ gauge group. Finally, we proceed to analysis of the spectrum of SYMQM with $SU(3)$.

5.1 SYMQM with $SU(2)$ gauge group

5.1.1 Review of other approaches

The $SU(2)$ model has been already extensively studied in [38]. The energies were obtained in all fermionic sectors and all angular momenta for cutoff up to $N_B = 18$. The method used was analogous to our approach, but it included modifications discussed in 3.7. These modifications incorporate computing matrix elements in channels with given angular momentum. This is possible for $SU(2)$ because the algebra of operators is much simpler than in the $SU(3)$ case. One can then rearrange all single-trace operators so that they have definite angular momentum and calculate all commutators.

There exists yet another way to obtain energies in the $SU(2)$ case [42]. However, it is limited to channels with zero angular momentum and $n_F = 0, 2$. In these channels it is very effective and enables one to reach very large cutoff $N_B = 60$ for $n_F = 2$ [43]. We give more details concerning this approach in Chapter 7.

On the other hand, the algorithm proposed in this thesis allows us to calculate energy levels in all (n_F, j) channels. On the other hand, the cutoff is much smaller. It is $N_B = 8 - 11$ depending on n_F . Results of the computations for all n_F , N_B and several angular momenta are shown in Figs 5.1 - 5.4. Values of the energies were checked against

[38] and perfect agreement was found.

An important characteristic of a spectrum is its type – discrete or continuous. It was argued [49] that the two types of spectra reveal a different behavior for a finite cutoff. Energy levels which belong to the discrete spectrum converge very fast, e.g. exponentially. On the other hand, eigenvalues of the Hamiltonian which correspond to the continuous spectrum decrease to 0 like $1/N_B$. Identification of the type of spectrum is the main subject of following paragraphs.

5.1.2 Spectra in sectors with given number of fermions

We start discussing spectra for particular n_F with $n_F = 0$. We first comment on the ‘stepwise’ convergence of eigenvalues in Fig. 5.1. In the bosonic channel the parity is conserved. The creation operator a_i^\dagger has negative parity. Therefore, states with odd n_B (see eq. (3.5)) have negative parity. For a given N_B , all states with $n_B \leq N_B$ are included in the basis of the cut space. When N_B changes from an odd to even value, the basis of odd states does not grow and eigenvalues corresponding to odd states remain constant. Similarly, energy levels of even states do not change when N_B changes from an even to odd value.

For $n_F = 0$ (Fig. 5.1) all energies converge fast with growing cutoff. This behavior is typical for discrete spectrum. The fact that the spectrum is discrete is contrary to what one may naively expect. Indeed, if the three matrices X_i commute then the potential vanishes: $V \equiv -\sum_{i<j} Tr([X_i, X_j]^2) = 0$. The region where the potential vanishes forms a vector subspace in the configuration space which we call flat valleys. Such situation usually generates a continuous spectrum. On the other hand, the potential becomes steeper in the transverse directions as one moves deeper inside the valleys. The transverse oscillations cost more energy and thus the effective potential inside the flat valleys grows. Therefore, the eigenstates of the Hamiltonian with $n_F = 0$ are localized and the spectrum is discrete. A simpler system with similar properties was studied in [60]. The sector with one fermion shares the same behavior (Fig. 5.2).

The picture is different with two fermions (Fig. 5.3). In the $j = 0$ channel the lowest energies approach 0 and the convergence is much slower. This is a signature of a continuous spectrum. This is because inside the flat valley the contributions from interactions of bosonic and fermionic degrees of freedom with the potential have different sign. They cancel exactly causing the effective potential to vanish. The flat valleys are open and the spectrum is continuous. The eigenenergies corresponding to the continuous spectrum will be denoted by E_k^c where $k = 0, 1, \dots$ is the label of the energy level. The two lowest energies E_k correspond to the continuous spectrum, so $E_k^c = E_k$ for $k = 0, 1$. The second excited energy which belongs to the continuous spectrum goes through discrete energy levels. It is marked with triangles in Fig. 5.3. The third energy seems to be $E_3^c = E_5$.

Even with two fermions, the $j = 1$ channel has discrete spectrum (Fig. 5.3). In the next sector, with angular momentum $j = 2$ the spectrum is again continuous. With our data we checked that the spectrum is continuous for all even j and discrete for odd j at least up to $j = 6$. For three fermions the spectrum is continuous for all j .

All these effects, i.e. nonvanishing effective potential in a flat valley, cancellation between bosons and fermions and finally discrete spectrum inside continuous one were already observed for simpler supersymmetric systems [60, 12, 61].

5.1.3 Scaling relations

There are interesting scaling relations for eigenvalues corresponding to the continuous spectrum. They originate from dispersion relations for energies. In [49] the free Hamiltonian in a one dimensional quantum mechanics was studied with the cut Fock space method. For this system there is a standard dispersion relation $E(p) = \frac{1}{2}p^2$. It was shown that in the infinite N limit momentum is related to the label of energy level by $p = \frac{\pi}{\sqrt{2N_B}}(m+1)$. It follows that the energies satisfy

$$E_m^c \approx \frac{\pi^2(m+1)^2}{4N_B} \quad m = 0, 1, \dots \quad (5.1)$$

In the continuum limit the energies fill densely the positive real axis. In [38, 43] it was argued and checked numerically that the scaling of energies are similar for the continuous spectrum in SYMQM. Although the relation (5.1) does not hold precisely, it was shown that $N_B E_m$ converge to nonzero constants and ratios of the energies agree, i.e. $E_m^c/E_k^c \approx (m+1)^2/(k+1)^2$. Corresponding results based on our data are presented in Figs 5.5 and 5.6. Both scaling relations are confirmed for the three lowest energies in the continuous spectrum E_0^c , E_1^c and E_2^c . For the third excited continuous energy we took $E_3^c = E_5$. The scaling relations suggest that $E_3^c = E_5$ is smaller than the theoretical expectation. This can be an effect of too small cutoff or misidentification of the continuous energy.

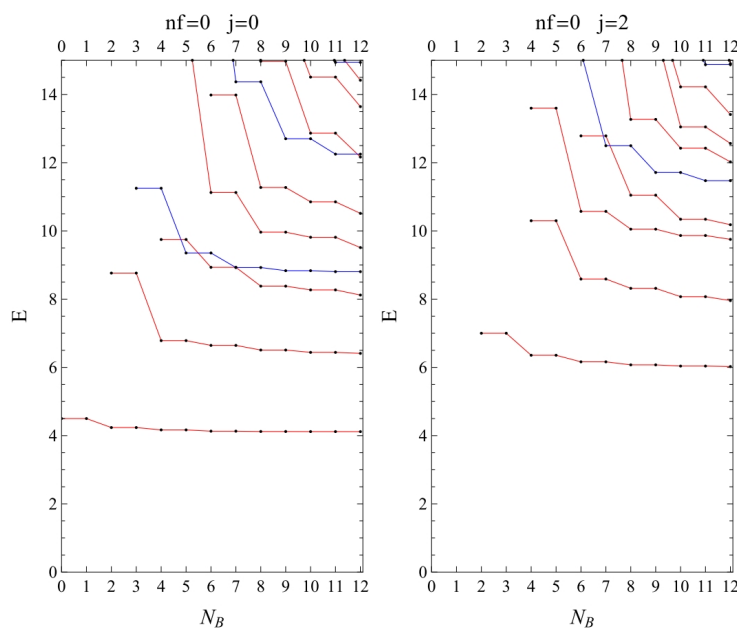


Figure 5.1: Spectrum of the $SU(2)$ theory in the bosonic sector. The maximal cutoff is $N_B = 12$. There are no states with angular momentum $j = 1$ (cf. Appendix B). Energies corresponding to even and odd states are marked with red and blue color respectively.

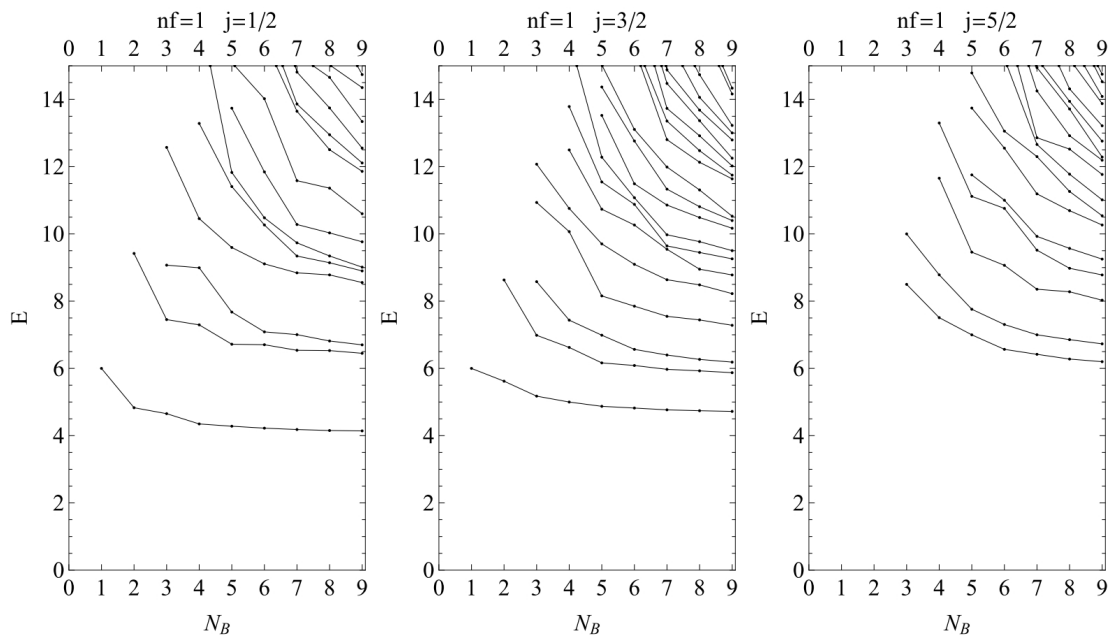


Figure 5.2: Spectrum of the $SU(2)$ theory in sector with a single fermion.

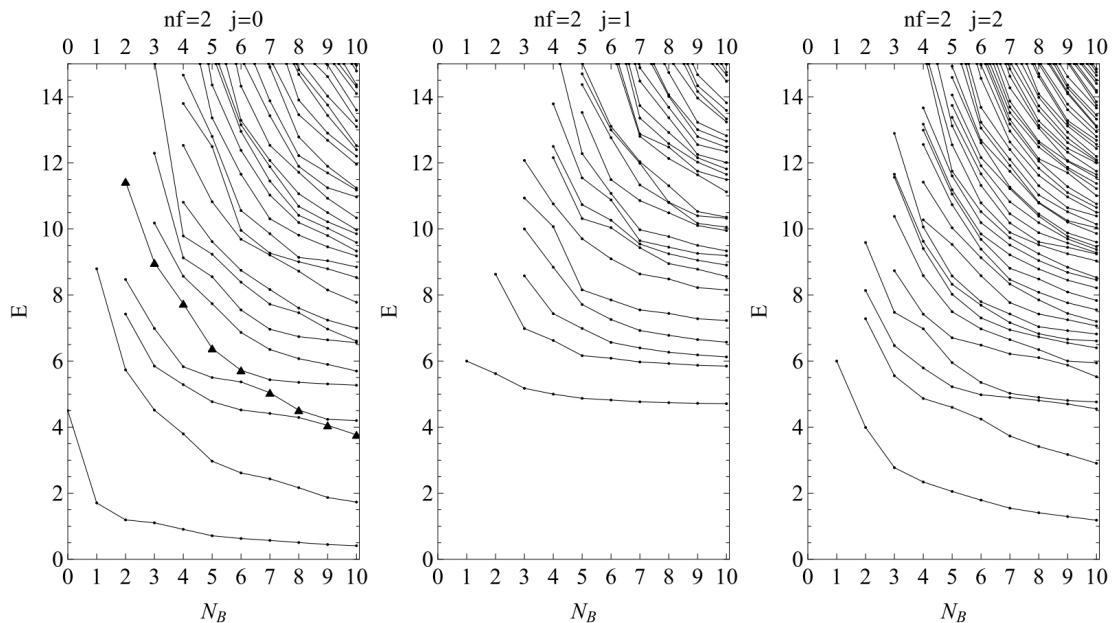
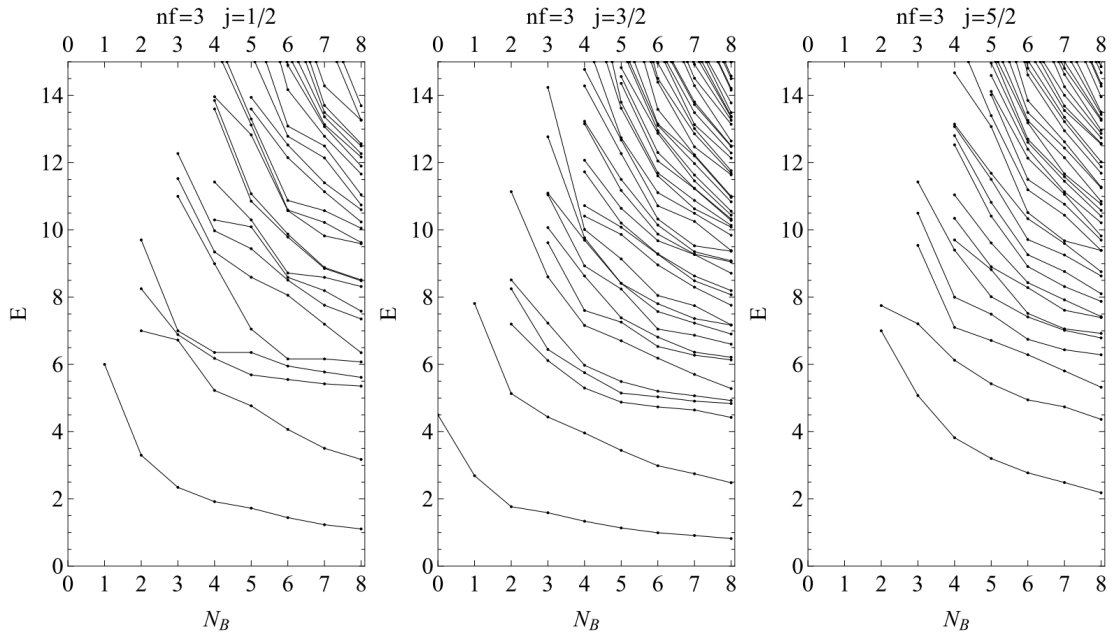
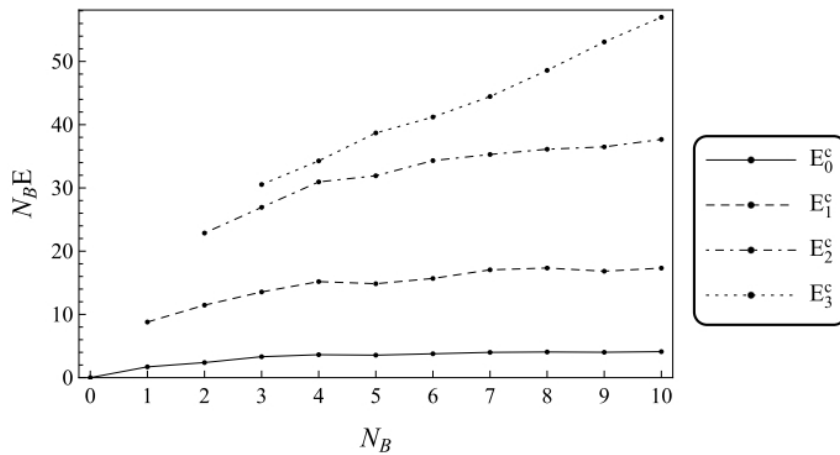


Figure 5.3: Spectrum of the $SU(2)$ theory in sector with two fermions. For $j = 0$ the two lowest energies correspond to continuous spectrum. The third line from the continuous spectrum crosses two discrete energy levels. This line is marked with triangles. Fourth energy from the continuous spectrum is probably the fifth excited energy.


 Figure 5.4: Spectrum of the $SU(2)$ theory in sector with $n_F = 3$.

 Figure 5.5: Scaled energies for $SU(2)$ in channel with $n_F = 2$, $j = 0$. The energies corresponding to the continuous spectrum scaled by the cutoff N_B converge to constant values. This is in agreement with (5.1). The convergence is best for lowest energies. The cutoff is too small for $N_B E_3^c$ to level off or it is misidentified as an energy from the continuous spectrum.

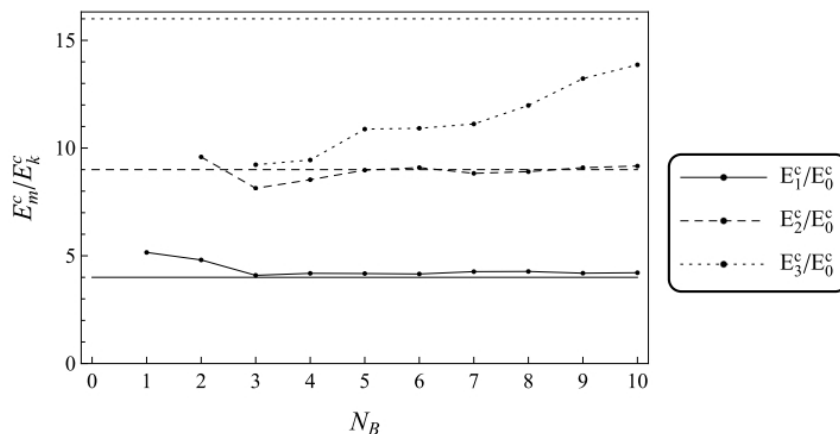


Figure 5.6: Ratios of the energies for $SU(2)$ satisfy the relation $E_m^c/E_k^c \approx (m+1)^2/(k+1)^2$ (flat lines) in the continuum limit. The higher ratio E_3/E_0 has not yet converged for $N_B = 10$.

5.2 The spectrum for the $SU(3)$ gauge group

Here our results for the $SU(3)$ symmetry group are presented. In order to obtain the spectrum we constructed matrices with sizes up to 36000. Computations were performed on a supercomputer Deszno located in the Institute of Physics at Jagiellonian University. 96 cores were used in parallel with the OpenMP interface using up to 256 GB shared memory.

The eigenenergies of the model are shown in Figs 5.7 - 5.15. All energies are obtained in channels with definite total angular momentum j (cf. 3.3.3). For $SU(3)$ there are more degrees of freedom and therefore there are many more states for a given N_B compared to the $SU(2)$ case. This is reflected by a larger density of eigenvalues. Because there are more degrees of freedom, the energies are generally larger for $SU(3)$ than for $SU(2)$. As before, parity is conserved in the bosonic channel.

The general picture is similar to the case of $SU(2)$. For zero and one fermion the spectrum is purely discrete. Unlike in the $SU(2)$ case, the argument from Appendix B doesn't work and there are states with $j = 1$ for $n_F = 0$.

The main difference from $SU(2)$ is that in the sector with two fermions the spectrum is still discrete. It means that there are not enough fermions to cancel with bosonic degrees of freedom and the effective potential does not vanish. The flat valleys remain closed. For the cutoff we were able to reach the continuous spectrum is best manifested for the ground state of $n_F = 6$ and $j = 0$. We checked the scaling of the energies to confirm this conclusion. The result is shown in Fig. 5.16. The scaled energies are given for all n_F in channels with the lowest angular momentum (i.e. $j = 0$ for even n_F and $j = 1/2$ for odd n_F). For $n_F = 0, 1, 2, 3, 4, 6, 8$ we picked the lowest energy. For $n_F = 5, 7$ we chose the first excited energy, because those seem to be better candidates for the continuous spectrum (cf. Figs. 5.12, 5.14). Scaled energies corresponding to the continuous spectrum should be flat for large N_B . All energies are divided by $E(N_B = 1)$ so that the overall scale for each channel is removed. From Fig. 5.16 one can see that the scaled energies become more flat as the number of fermions grows.

As it was mentioned in the Introduction, the Yang–Mills quantum mechanics without fermions was considered as a zeroth order approximation to pure gauge $SU(2)$ theory in a small volume in [30, 31]. In [33, 32] authors give numerical results also for $SU(3)$.

Their results are obtained numerically by a variational technique, which is essentially the same as our method (but restricted to $n_F = 0$). In Table 5.1 we present comparison of the lowest energies in several channels with given angular momentum and parity. The results are consistent. The relative difference usually does not exceed 4%. Naturally, the results differ less in cases where both methods are more precise (i.e. for lowest energies).

sector	cut Fock space	Rayleigh-Ritz	relative difference
0^+	12.5889	12.5887	0.0016%
	15.39	15.38	0.07%
	17.24	17.23	0.06%
0^-	17.75	17.8	-0.28%
1^+	18.77	18	4.1%
	22.4	>20	
1^-	16.52	17.05	-3.2%
	18.5	23	-24%
2^+	14.806	14.854	-3.2%
	17.159	17.26	-0.59%
2^-	18.37	>20	
3^-	16.10	16.5	-2.5%
4^+	17.3	18	-4%

Table 5.1: Comparison of lowest energies in the bosonic sector for the $SU(3)$ case obtained by our method and [32]. Since both approaches are variational, lower values of energies give better approximation to energies in the continuum limit. In the 0^+ sector results are perfectly consistent - eigenvalues differ only at the last digit which was given in [32]. In other channels our results are usually slightly more accurate.

Concluding, the spectrum of the $SU(3)$ theory has discrete and continuous part. In contrary to the $SU(2)$ case, for $SU(3)$ the spectrum is discrete for two fermions. The continuous spectrum is moved to channels with higher n_F because more fermions are needed to have supersymmetric cancelations between fermionic and bosonic degrees of freedom. Only then the effective potential in the flat valleys vanishes. Our results indicate that this occurs for $n_F = 6$.

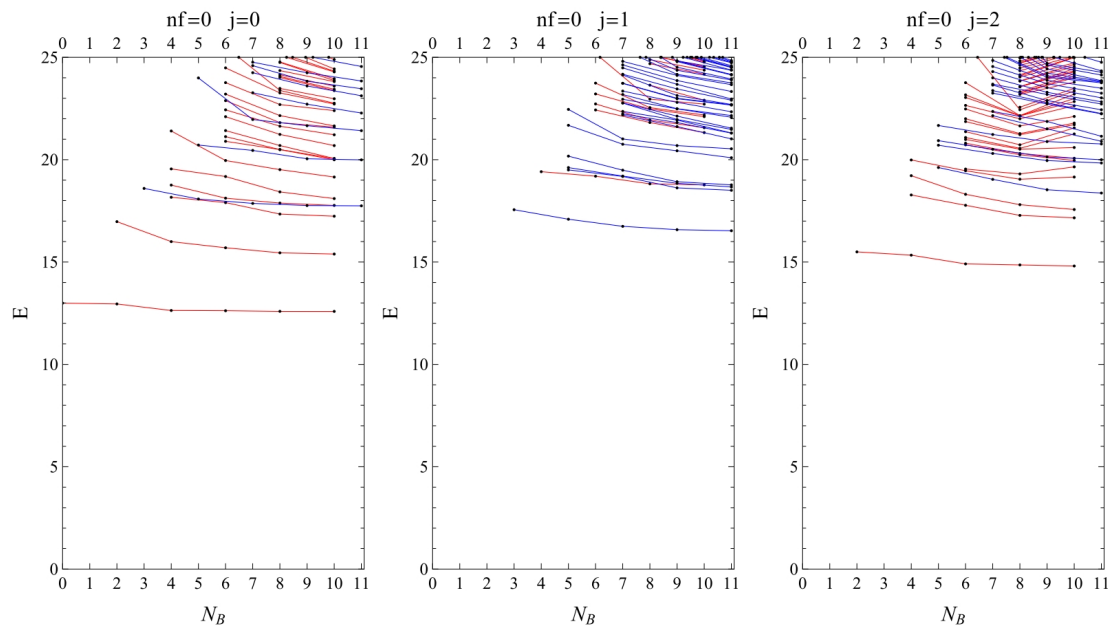


Figure 5.7: Spectrum of the $SU(3)$ theory in the bosonic sector. The maximal cutoff is $N_B = 11$. Energies marked with red correspond to states with positive parity and blue to negative parity. Even energies are marked only for even N_B because they do not change when N_B passes from even to odd value. Conversely, odd energies are marked only for odd N_B .

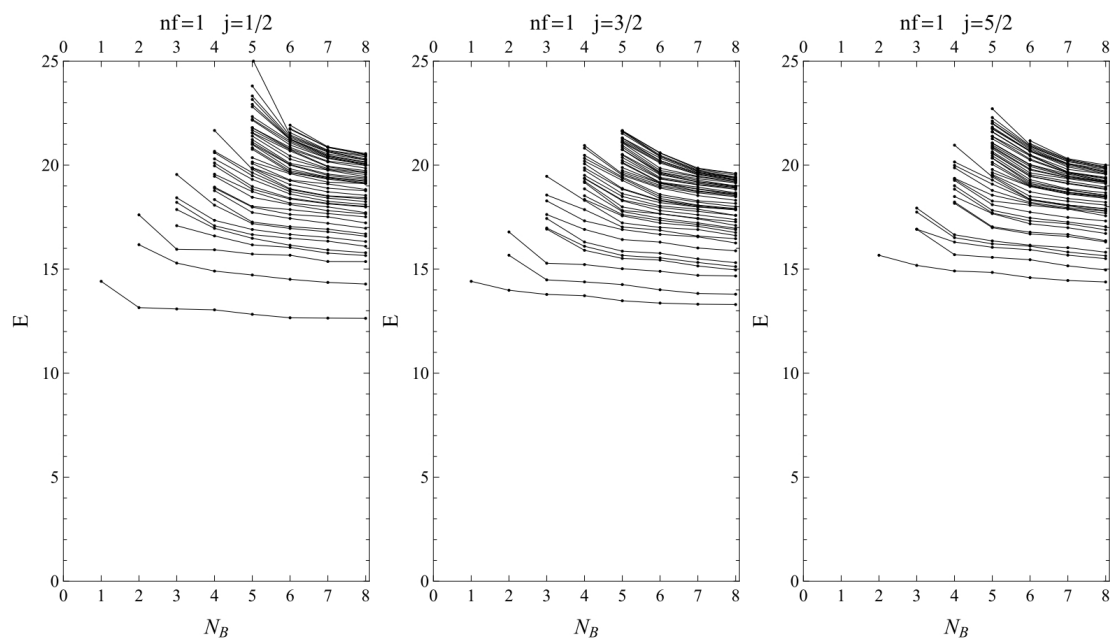


Figure 5.8: Spectrum of the $SU(3)$ theory with a single fermion.

5.2. THE SPECTRUM FOR THE $SU(3)$ GAUGE GROUP

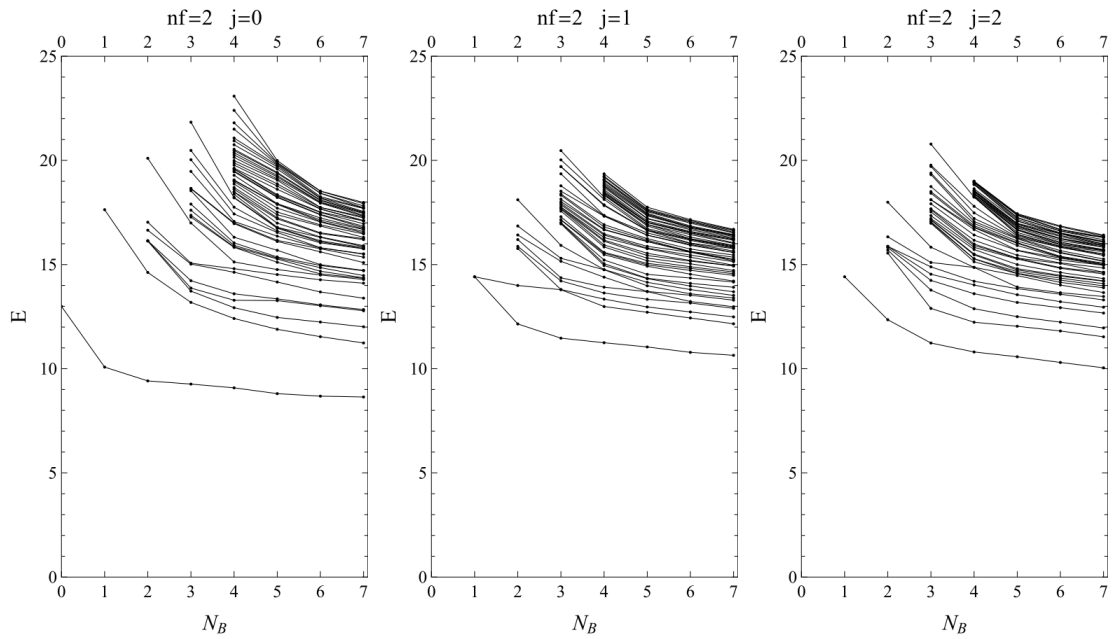


Figure 5.9: Spectrum of the $SU(3)$ theory with two fermions.

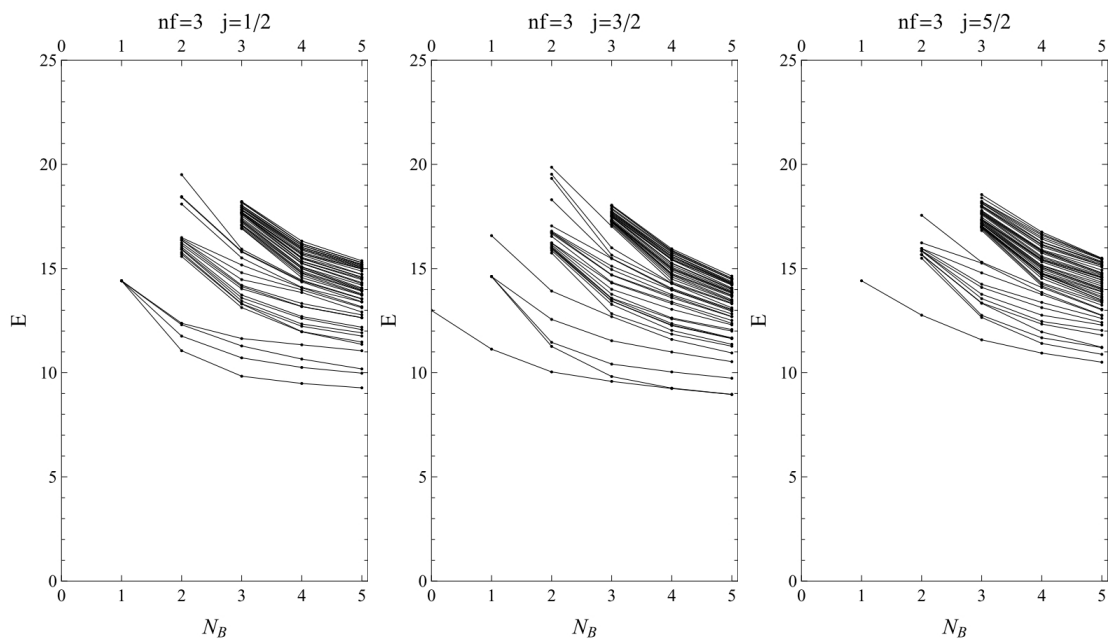


Figure 5.10: Spectrum of the $SU(3)$ theory with $n_F = 3$.

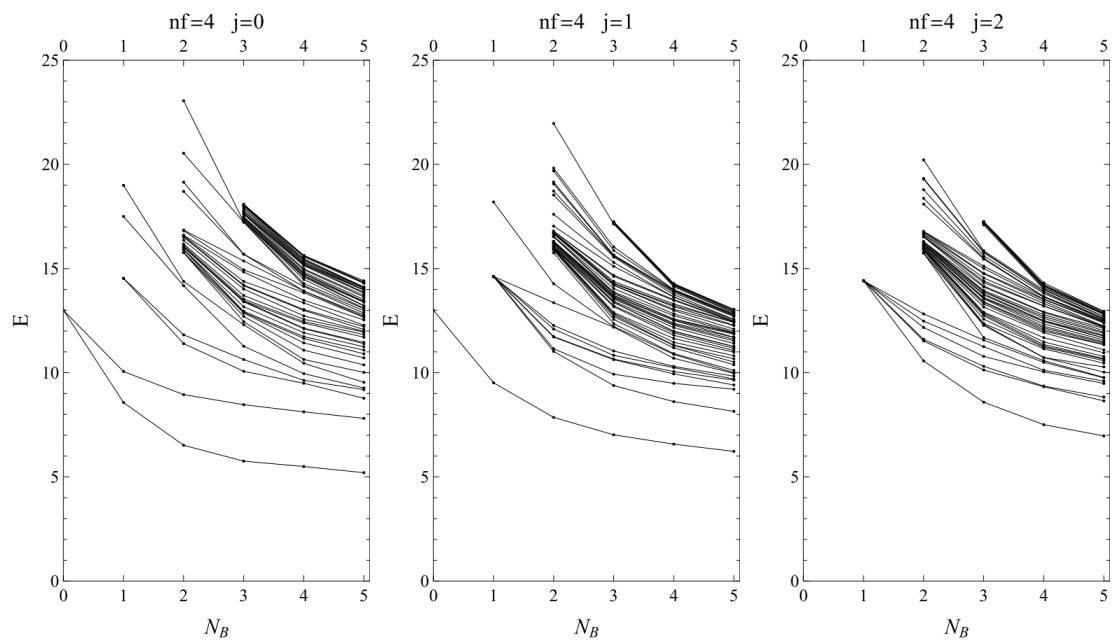


Figure 5.11: Spectrum of the $SU(3)$ theory with $n_F = 4$.

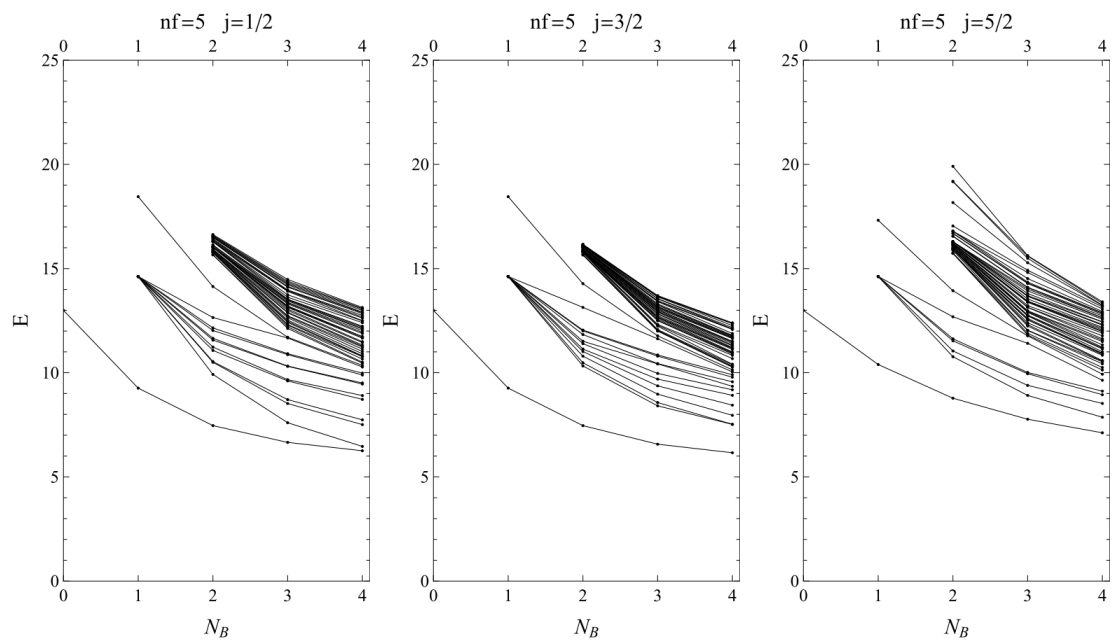


Figure 5.12: Spectrum of the $SU(3)$ theory with $n_F = 5$.

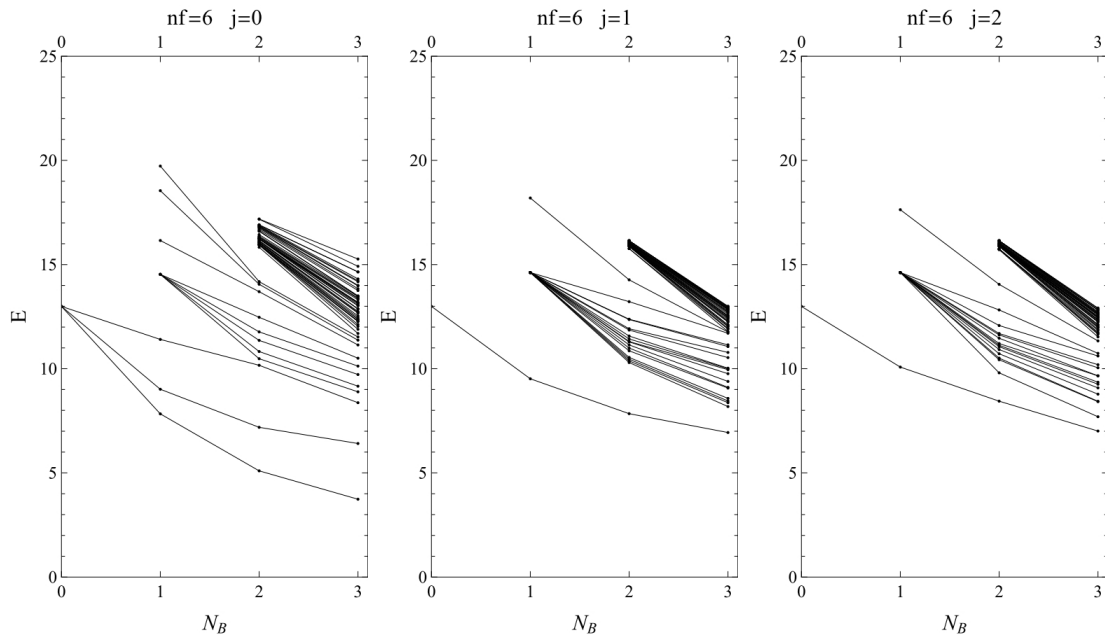


Figure 5.13: Spectrum of the $SU(3)$ theory with $n_F = 6$.

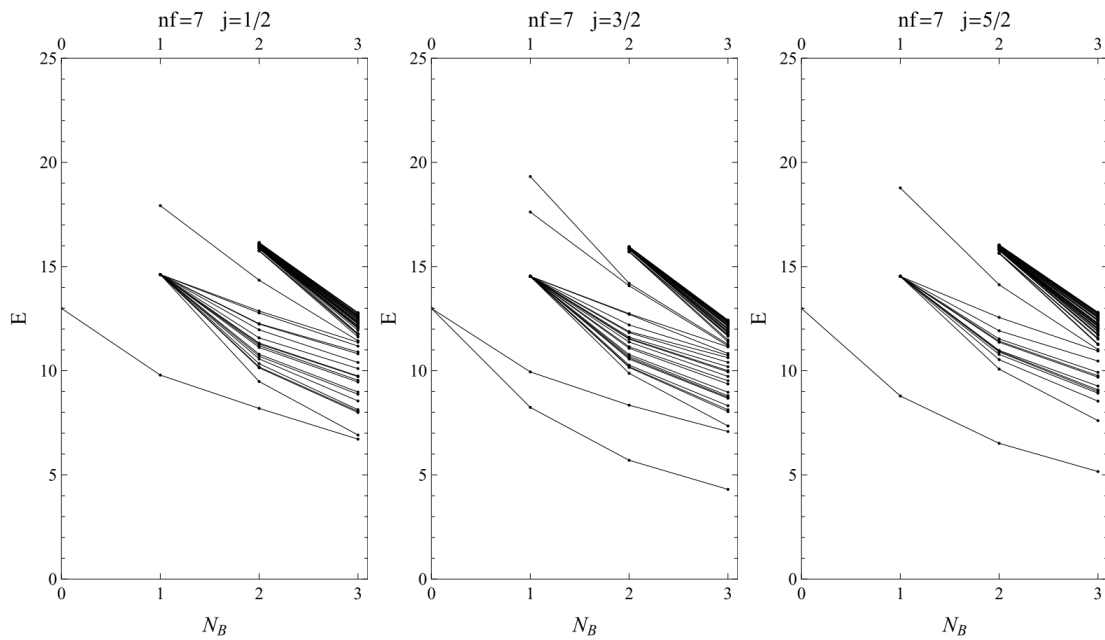


Figure 5.14: Spectrum of the $SU(3)$ theory with $n_F = 7$.

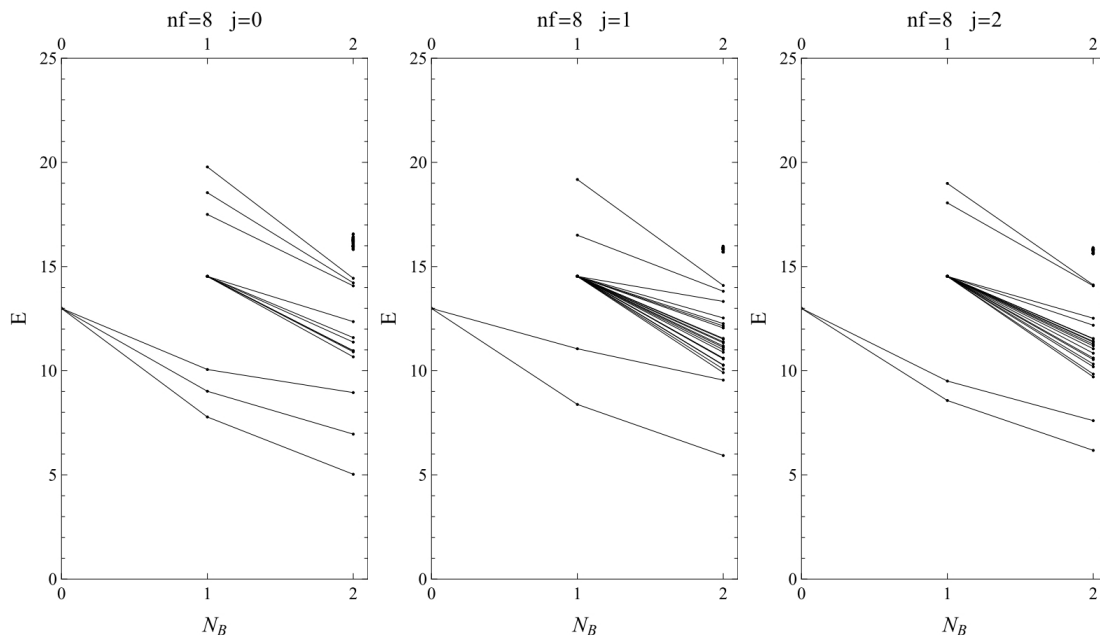


Figure 5.15: Spectrum of the $SU(3)$ theory with $n_F = 8$.

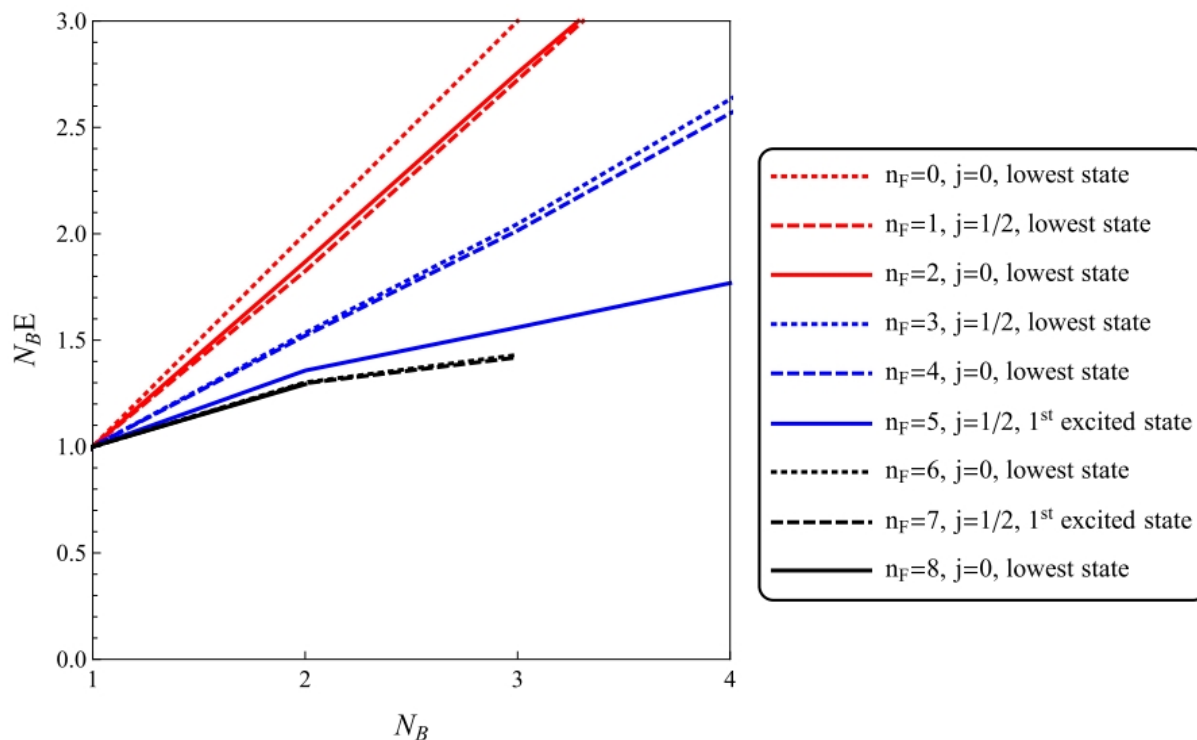


Figure 5.16: Scaled energy $N_B E$ for $SU(3)$ in sectors with $n_F = 3, \dots, 8$. All energies are divided by E for $N_B = 1$. In each channel the lowest j was picked, i.e. $j = 0$ for even n_F and $j = 1/2$ for odd n_F . In most sectors the lowest energy state was picked. For $n_F = 5, 7$ the first excited state was chosen because these seem to be better candidates for states in the continuum spectrum. For states corresponding to the continuum spectrum the scaled energy should be flat.

Chapter 6

Supersymmetry multiplets

Having computed spectrum of the model, we are now interested in its supersymmetric properties. It is known [62] that energy eigenstates of a supersymmetric model form supersymmetry multiplets (or supermultiplets). A supermultiplet is a representation of the supersymmetry algebra (2.16). In each supermultiplet there is a Clifford vacuum $|\Omega\rangle$. It can have any angular momentum j . For $j > 0$ it is degenerate and belongs to a $(2j + 1)$ -dimensional representation of rotational group. By acting with supercharges on $|\Omega\rangle$ one recovers the whole supermultiplet. Other elements of the supermultiplet also form multiplets of angular momentum. The supermultiplet has in total $8j + 4$ states. Half of them has odd and half of them even n_F . In general, these representations are reducible. The only exception is $j = 0$.

A powerful method to identify supermultiplets in organized way is to use supersymmetry fractions [38]. One can check whether two states are elements of the same multiplet by acting with a supercharge on one of them and analyzing the overlap with the other state. A supersymmetry fraction is essentially such an overlap.

In this chapter the parameter ω (cf. Chapter 3) is not included, i.e. here $\omega = 1$.

6.1 Supersymmetry multiplets in the continuum limit

The four supersymmetry generators Q_α introduced in (2.15) satisfy anticommutation relations (2.16) which play a central role in supersymmetric theories. They are however not the only operators which fulfill the algebra (2.16). Moreover, they are somewhat inconvenient because they do not form a spin multiplet. For this reasons we introduce operators \mathcal{Q}_α ($\alpha = \pm$):

$$\begin{aligned}\mathcal{Q}_+^\dagger &= -e^{i\pi/4}Q_4, \\ \mathcal{Q}_-^\dagger &= e^{i\pi/4}Q_3.\end{aligned}\tag{6.1}$$

The overall phase is chosen such that the phase factors simplify when \mathcal{Q}_\pm^\dagger are written in terms of traces. $\mathcal{Q}_\alpha^\dagger$ form a spin doublet. The magnetic quantum number of operator \mathcal{Q}_\pm^\dagger is $m = \pm 1/2$, i.e. $[J_3, \mathcal{Q}_\pm^\dagger] = \pm \frac{1}{2}\mathcal{Q}_\pm^\dagger$. Both \mathcal{Q}_\pm^\dagger rise the fermionic number n_F by $+1$. Their conjugates

$$\begin{aligned}\mathcal{Q}_+ &= e^{i\pi/4}Q_1, \\ \mathcal{Q}_- &= e^{i\pi/4}Q_2\end{aligned}\tag{6.2}$$

also form a spin doublet and have opposite quantum numbers. The new supersymmetry generators fulfill following commutation relations:

$$\begin{aligned}\{\mathcal{Q}_\alpha, \mathcal{Q}_\beta\} &= \{\mathcal{Q}_\alpha^\dagger, \mathcal{Q}_\beta^\dagger\} = 0, \\ \{\mathcal{Q}_\alpha, \mathcal{Q}_\beta^\dagger\} &= 2\delta_{\alpha\beta}H, \\ [H, \mathcal{Q}_\alpha] &= [H, \mathcal{Q}_\alpha^\dagger] = 0.\end{aligned}\tag{6.3}$$

Now we come to discussion of the structure of a supermultiplet. A Clifford vacuum $|\Omega, m\rangle$ is defined by

$$\mathcal{Q}_\alpha |\Omega, m\rangle = 0 \quad \alpha = \pm \frac{1}{2}.\tag{6.4}$$

Assume that it has n_F fermions, angular momentum j and energy E . The magnetic number m is kept explicit. One has to keep in mind that the Clifford vacuum has nothing to do with the vacuum of the model, i.e. the state with the lowest energy. In order to avoid confusion, it will be always called a Clifford vacuum or a vacuum of a supermultiplet. If $E = 0$ then $\mathcal{Q}_\alpha^\dagger |\Omega, m\rangle$ vanishes and $|\Omega, m\rangle$ is a supersymmetry singlet. Indeed,

$$\|\mathcal{Q}_\alpha^\dagger |\Omega, m\rangle\|^2 = \langle \Omega, m | \mathcal{Q}_\alpha \mathcal{Q}_\alpha^\dagger | \Omega, m \rangle = \langle \Omega, m | 2H - \mathcal{Q}_\alpha^\dagger \mathcal{Q}_\alpha | \Omega, m \rangle = 0.\tag{6.5}$$

If this is not the case, new states are created by acting with $\mathcal{Q}_\alpha^\dagger$ on $|\Omega, m\rangle$. With the aid of Clebsh-Gordan coefficients, these states can be arranged in spin multiplets

$$\begin{aligned}|\Omega_-, m\rangle &= \frac{1}{\sqrt{2E}} \sum_\alpha \langle j, m - \alpha, \frac{1}{2}, \alpha | j - \frac{1}{2}, m \rangle \mathcal{Q}_\alpha^\dagger |\Omega, m - \alpha\rangle, \quad m = -j + \frac{1}{2}, \dots, j - \frac{1}{2}, \\ |\Omega_+, m\rangle &= \frac{1}{\sqrt{2E}} \sum_\alpha \langle j, m - \alpha, \frac{1}{2}, \alpha | j + \frac{1}{2}, m \rangle \mathcal{Q}_\alpha^\dagger |\Omega, m - \alpha\rangle, \quad m = -j - \frac{1}{2}, \dots, j + \frac{1}{2}, \\ |\Omega_0, m\rangle &= \frac{1}{2E} \mathcal{Q}_-^\dagger \mathcal{Q}_+^\dagger |\Omega, m\rangle, \quad m = -j, \dots, j.\end{aligned}\tag{6.6}$$

If $j = 0$ then $|\Omega_-, m\rangle = 0$. Otherwise none of these states vanishes. All of them are normalized thanks to the relation of Clebsh-Gordan coefficients

$$\sum_\alpha \left| \langle j \pm \frac{1}{2}, m - \alpha, \frac{1}{2}, \alpha | j, m \rangle \right|^2 = 1 \quad \text{for all } j \geq \frac{1}{2} \text{ and } m = -j, \dots, j.\tag{6.7}$$

Obviously, (6.7) is not valid for $j = 0$ when it is taken with the minus sign, because there is spin $-\frac{1}{2}$ on the left hand side. The three new states have energy E because the supercharges commute with the Hamiltonian. $|\Omega_-, m\rangle, |\Omega_+, m\rangle, |\Omega_0, m\rangle$ are spin multiplets with total angular momentum $j - \frac{1}{2}, j + \frac{1}{2}$ and j respectively. Together with the vacuum $|\Omega, m\rangle$ they form a *supersymmetric multiplet*.

Several remarks concerning supermultiplets are in place. A supersymmetry multiplet is closed under the action of supercharges. That is, \mathcal{Q}_α or $\mathcal{Q}_\alpha^\dagger$ acting on an element of a supermultiplet gives zero or combination of other elements. It follows that none of the three states $|\Omega_-, m\rangle, |\Omega_+, m\rangle, |\Omega_0, m\rangle$ can be a vacuum state of another supermultiplet.

The full supersymmetry multiplet forms a diamond in the (n_F, j) plane (cf. Fig. 6.1). The exception is $j = 0$ – there is no state $|\Omega_-, m\rangle$, i.e. the lower node $(n_F + 1, j - \frac{1}{2})$ in

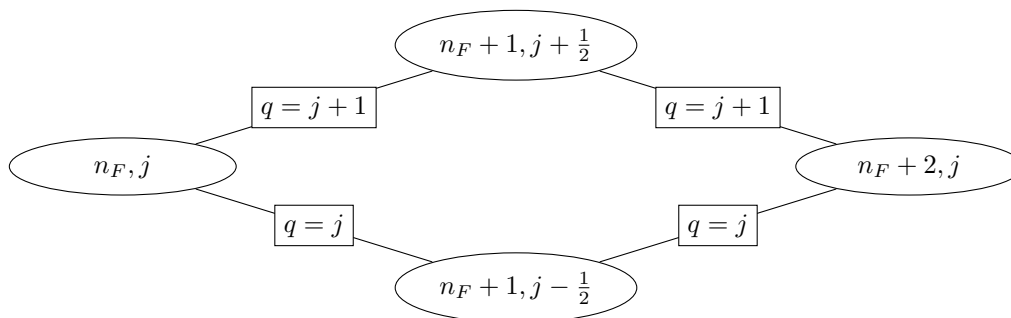


Figure 6.1: Structure of a supermultiplet together with supersymmetry fractions. For $j = 0$ the bottom vertex and the two lower links are absent.

Fig. 6.1 is not present. In the supermultiplet there are $4j + 2$ bosonic states (i.e. states which contain an even number of fermions) and the same number of fermionic states. As a consequence, a supersymmetry multiplet with nonzero energy does not contribute to the Witten index.

For finite N_B there is only a finite number of states in each (n_F, j) channel. In Fig. 6.2 the total number of multiplets in each sector for the $SU(3)$ gauge group and $N_B = 2$ is given. Each circle is a vertex of a diamond or a triangle. These figures are the same as the diamond in Fig. 6.1 and they correspond to supermultiplets. The number inside each diamond or triangle is the number of according supermultiplets for finite N_B . These numbers are determined in such way that the total number of supermultiplets adjacent to a vertex (n_F, j) is the same as the number of angular momentum multiplets in the sector (n_F, j) . This is motivated by the fact that each $SO(3)$ multiplet belongs to exactly one supermultiplet. However, one has to keep in mind that for a finite N_B the supersymmetry is broken and there are actually no supermultiplets. Therefore, the number of supermultiplets determined in this way has no strict meaning. In particular, there is a negative number of $(1, 5/2)$ supermultiplets for $SU(2)$ with $N_B = 2$ (cf. Fig. 6.3).

For $j = 0$ the supermultiplet is an irreducible representation of the algebra (6.3). In this case it consists of four states. For $j > 0$ the representation contains $2j + 1$ irreducible representations of the supersymmetry algebra. An irreducible representation can be constructed starting from $|\Omega, m\rangle$ with a single value of m . Then the other three states in the (small) supermultiplet are $\frac{1}{\sqrt{2E}} Q_\alpha^\dagger |\Omega, m\rangle$ and $\frac{1}{2E} Q_-^\dagger Q_+^\dagger |\Omega, m\rangle$. Each of these states has definite magnetic number, but $Q_\alpha^\dagger |\Omega, m\rangle$ do not have definite total angular momentum. For convenience, in this thesis we use full supermultiplets with complete angular momentum multiplets.

6.2 Supersymmetry fractions

A useful tool to analyze the supermultiplets are supersymmetry fractions. They serve two purposes. First is studying breaking of the supersymmetry for finite cutoff. Second is identifying supermultiplets. Consider two angular momentum multiplets $|n_F j m E\rangle$ and $|n_F + 1 j' m' E'\rangle$. A supercharge Q_α^\dagger maps $|n_F j m E\rangle$ into $|n_F + 1 j' m' E'\rangle$ if they are in the same supermultiplet and $m' = m + \alpha$. A supersymmetry fraction measures the overlap.

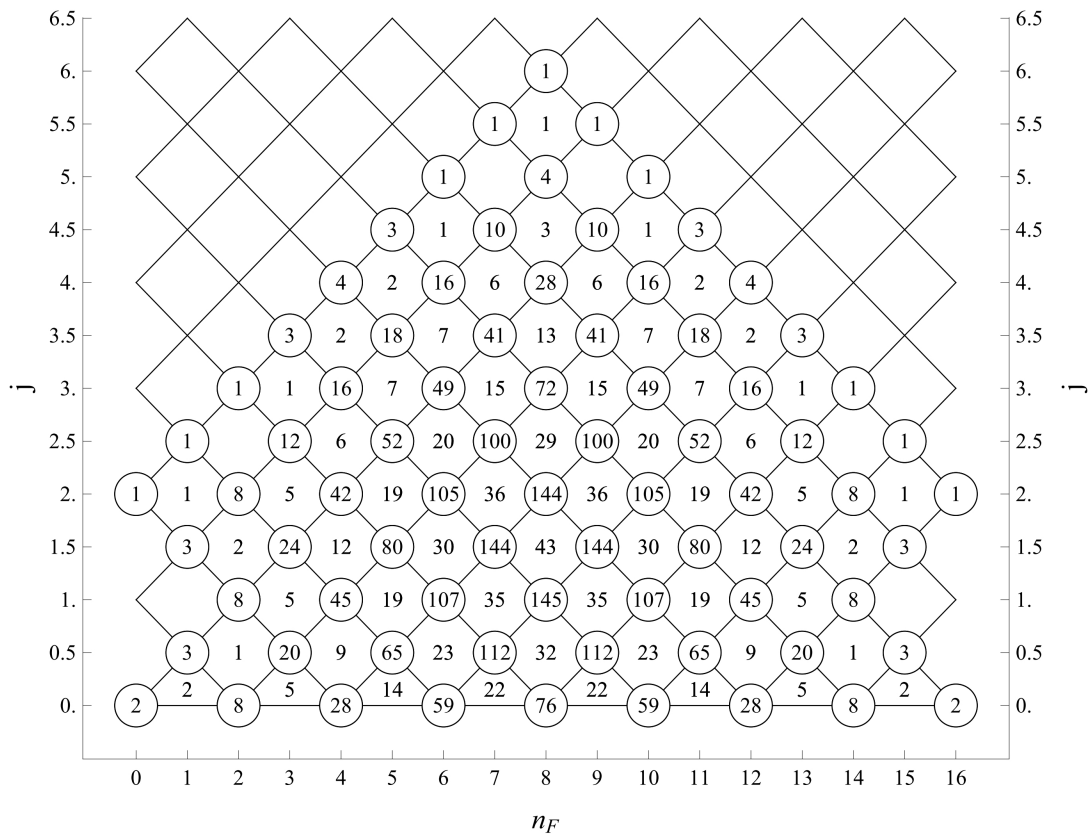


Figure 6.2: Structure of the angular momentum multiplets and supersymmetry multiplets for $SU(3)$ and $N_B = 2$. Numbers in circles represent the number of angular momentum multiplets in a given channel. The numbers in between are the numbers of supersymmetry multiplets (the diamonds).

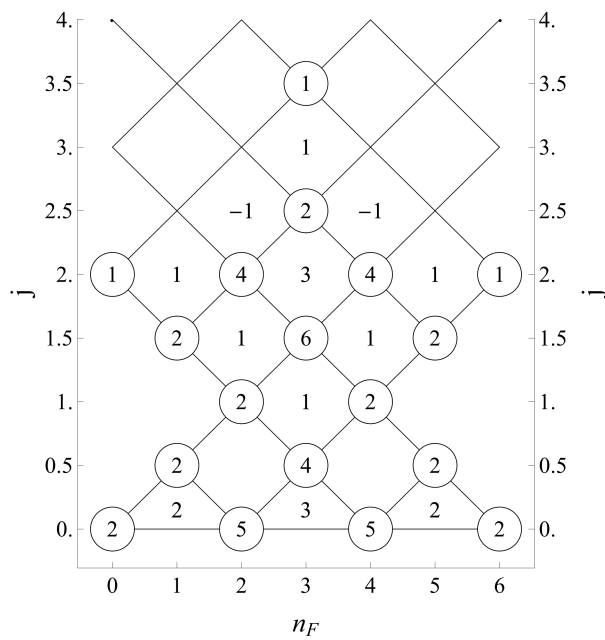


Figure 6.3: Structure of the angular momentum multiplets and supersymmetry multiplets for $SU(2)$ and $N_B = 2$.

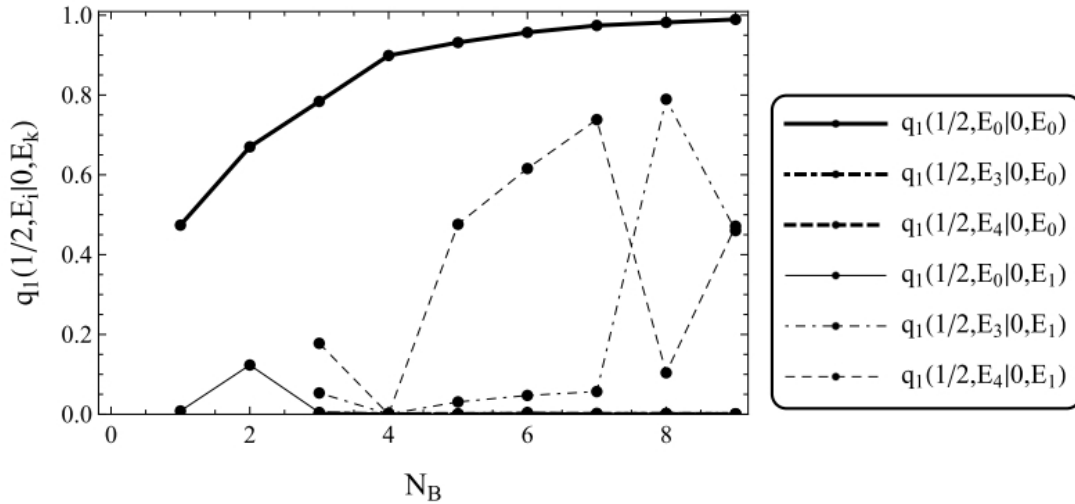


Figure 6.4: Supersymmetry fractions as a function of cutoff. N_B is the cutoff in the sector $n_F = 1$. The cutoff for $n_F = 0$ is higher by 2.

It is defined by

$$q_{n_F}(j' E' | j E) = \frac{1}{4E} \sum_{mm'\alpha} |\langle n_F + 1j' m' E' | \mathcal{Q}_\alpha^\dagger | n_F j m E \rangle|^2. \quad (6.8)$$

Formulas (6.6) together with the anticommutation relations (6.3) give straightforward

$$\begin{aligned} \sum_{mm'\alpha} |\langle \Omega, m | \mathcal{Q}_\alpha | \Omega_+, m' \rangle|^2 &= \sum_{mm'\alpha} |\langle \Omega_+, m | \mathcal{Q}_\alpha | \Omega_0, m' \rangle|^2 = 4E(j+1), \\ \sum_{mm'\alpha} |\langle \Omega, m | \mathcal{Q}_\alpha | \Omega_-, m' \rangle|^2 &= \sum_{mm'\alpha} |\langle \Omega_-, m | \mathcal{Q}_\alpha | \Omega_0, m' \rangle|^2 = 4Ej. \end{aligned} \quad (6.9)$$

These relations specify what are the supersymmetry fractions within a supermultiplet. If the Clifford vacuum $|\Omega, m\rangle$ has n_F fermions, energy E and angular momentum j , then the fractions are

$$\begin{aligned} q_{n_F}\left(j + \frac{1}{2}, E | j, E\right) &= q_{n_F+1}\left(j, E | j + \frac{1}{2}, E\right) = j + 1, \\ q_{n_F}\left(j - \frac{1}{2}, E | j, E\right) &= q_{n_F+1}\left(j, E | j - \frac{1}{2}, E\right) = j. \end{aligned} \quad (6.10)$$

The supersymmetry fractions are denoted by rectangles in Fig. 6.1. The supermultiplet is closed under the action of $\mathcal{Q}_\alpha^\dagger$ so other fractions must necessarily vanish.

6.3 Finite cutoff effects

For a finite cutoff the supersymmetry is broken. Now we analyze restoration of the supersymmetry for growing N_B . For small cutoff the supersymmetry fractions are far from the values given by (6.10). We say that the supersymmetry is recovered when the supersymmetry fractions are close to their exact values. Next we address the problem of identifying superpartners when two supermultiplets are almost degenerate.

Consider a supersymmetry fraction $q_{n_F}(j \pm \frac{1}{2}, E_i | j, E_k)$. For a large cutoff it is expected that the fraction is zero unless corresponding states, labeled with i and k , are in the same supermultiplet. In particular, E_i and E_k should be almost the same if the fraction is nonzero. In contrast, for a small cutoff eigenstates of the cut Hamiltonian do not give a good approximation to exact bound states. In this situation the supersymmetry fractions $q_{n_F}(j \pm \frac{1}{2}, E_i | j, E_k)$ are small but nonzero for many different pairs (i, k) .

Analysis of supersymmetry fractions for growing cutoff provides us the information at which value of N_B supersymmetry is approximately restored. In Fig. 6.4 dependence of supersymmetry fractions $q_1(\frac{1}{2}, E_i | 0, E_k)$ on the cutoff is shown for selected i and k . All states with $(n_F, j) = (0, 0)$ are Clifford vacua, so the exact values of shown supersymmetry fractions are 0 and 1. For the ground state in the bosonic sector there is only one fraction, $q_1(\frac{1}{2}, E_0 | 0, E_0)$, which is significant. It approaches 1 fast and we may say that the supersymmetry between the two corresponding states is essentially restored for $N_B \approx 7$. In general higher cutoffs are required to regain supersymmetry for higher eigenstates. This is because the lowest energy states converge first.

Behavior of fractions $q_1(\frac{1}{2}, E_i | 0, E_1)$, $i = 3, 4$ in Fig. 6.4 is related to an approximate degeneracy of energies with $n_F = 1$ and $N_B = 9$ (cf. Fig. 5.8). We address this case on a general ground. Suppose that with the available cutoff a good approximation of a bound state $|n_F j m E\rangle$ is obtained. Denote its (exact) superpartner a in channel $(n_F + 1, j' = j \pm \frac{1}{2})$ by $|n_F + 1 j' m' E\rangle$. In general, for larger number of fermions cutoffs are smaller and thus the approximation is worse. Therefore, a good approximation of the state $|n_F + 1 j' m' E\rangle$ is given by some combination

$$|n_F + 1 j' m' E\rangle \approx \sum_i c_i |n_F + 1 j' m' E_i\rangle_{N_B}, \quad (6.11)$$

where $|n_F + 1 j' m' E_i\rangle_{N_B}$ are eigenstates of the Hamiltonian for cutoff N_B . The question is which states contribute to the sum (6.11). Each energy E_i has an error Δ_i which is a finite cutoff effect. States which have energies equal within the error Δ mix for higher N_B and give a better approximation of exact eigenstates. Therefore, only these c_i are nonzero for which $|E_i - E| \lesssim \Delta_i$. If the cutoff is not very small and $|n_F + 1 j' m' E\rangle$ is not a highly excited state, then the errors Δ_i are small and the energies E_i have to be almost degenerate. The supersymmetry fractions $q_{n_F}(j' E_i | j E)$ for the cutoff N_B are fully determined by coefficients c_i . In order to calculate values of the fractions first assume that $|n_F j m E\rangle$ is vacuum of a supermultiplet. Then the supersymmetry fraction is

$$\begin{aligned} q_{n_F}(j' E_i | j E) &= \\ &= \frac{1}{4E} \sum_{mm'\alpha} |_{N_B} \langle n_F + 1 j' m' E_i | Q_\alpha^\dagger | n_F j m E \rangle|^2 \\ &= \frac{1}{4E} \sum_{mm'\alpha} \left| |_{N_B} \langle n_F + 1 j' m' E_i | n_F + 1 j' m' E \rangle \langle n_F + 1 j' m' E | Q_\alpha^\dagger | n_F j m E \rangle \right|^2 \\ &= \frac{1}{4E} \sum_{mm'\alpha} |c_i|^2 \left| \frac{1}{\sqrt{2E}} \sum_\beta \langle j, m' - \beta, \frac{1}{2}, \beta | j' m' \rangle \langle n_F j m' - \beta E | Q_\beta Q_\alpha^\dagger | n_F j m E \rangle \right|^2 \\ &= \frac{1}{4E} \sum_{m\alpha} |c_i|^2 \left| \sqrt{2E} \langle j, m, \frac{1}{2}, \alpha | j' m + \alpha \rangle^* \right|^2. \end{aligned} \quad (6.12)$$

Finally, we use the following property of Clebsch-Gordan coefficients:

$$\sum_{m\alpha} \left| \langle j, m, \frac{1}{2}, \alpha | j' m + \alpha \rangle \right|^2 = (2j' + 1) \quad (6.13)$$

and obtain

$$q_{n_F}(j' E_i | j E) = \left(j' + \frac{1}{2} \right) |c_i|^2. \quad (6.14)$$

If $|n_F j m E\rangle$ is not a Clifford vacuum then it is $|\Omega_+, m\rangle$ or $|\Omega_-, m\rangle$ from (6.6). One can show by an analogous proof that then

$$q_{n_F}(j' E_i | j E) = \left(j + \frac{1}{2} \right) |c_i|^2. \quad (6.15)$$

In both cases $q_{n_F}(j' E_i | j E)$ is the exact supersymmetry fraction multiplied by $|c_i|^2$. Concluding, the supersymmetry fractions $q_{n_F}(j' E_i | j E)$ add up to the exact value. Therefore, if one finds several fractions $q_{n_F}(j' E_i | j E)$ which sum up almost to $j + \frac{1}{2}$ or $j' + \frac{1}{2}$ then the superpartner of $|n_F j m E\rangle$ is given by (6.11) where c_i are determined up to phases.

Consider again the supersymmetry fractions $q_1(\frac{1}{2}, E_i | 0, E_1)$ (Fig. 6.4). For N_B up to 7 the fraction $q_1(\frac{1}{2}, E_4 | 0, E_1)$ grows while $q_1(\frac{1}{2}, E_3 | 0, E_1)$ is close to 0. For $N_B = 8$ the two fractions interchange. This is because the energy of the state $|1, \frac{1}{2}, E_4\rangle$ decreases faster than the energy of $|1, \frac{1}{2}, E_3\rangle$ and labels of energies are swapped at $N_B = 8$. For $N_B = 9$ the fractions are 0.46 and 0.47 and sum up to 0.93. Based on earlier analysis we conclude that a good approximation to the superpartner $|\Omega_+, m\rangle$ (cf. (6.6)) of the first excited state in the bosonic sector $|0, 0, E_1\rangle$ is given by a combination of the third and fourth state:

$$|\Omega_+, m\rangle \approx \sqrt{0.46} e^{i\alpha_1} |1, \frac{1}{2}, m, E_3\rangle_{N_B=9} + \sqrt{0.47} e^{i\alpha_2} |1, \frac{1}{2}, m, E_4\rangle_{N_B=9}. \quad (6.16)$$

Such situation as described above, with several supersymmetry fractions which add up almost to an exact value is in fact very common. The main reason for this is that because large number of degrees of freedom density of eigenstates is large. Therefore, states that correspond to different but close energies mix easily for a finite cutoff. Obviously, these states disentangle for a cutoff which is high enough. Nevertheless, if energies of different supermultiplets are almost degenerate, the needed cutoff is very large.

All above considerations address only the case of discrete spectrum. This is because the continuous spectrum appears in channels with many fermions. There the density of energy states is higher while the available cutoff is small. This makes the analysis of supersymmetry fractions yet more demanding.

6.4 Detailed analysis of supersymmetry fractions

A general method for identifying superpartners was presented. Here more examples are considered. In particular, full identification of a supermultiplet with a Clifford vacuum in sector $(0, 0)$ is carried out. In Tables 6.1 - 6.4 supersymmetry fractions for several (n_F, j) channels are shown. A fraction $q_{n_F}(j + \frac{1}{2} E' | j E)$ can take values either $j + \frac{1}{2}$ or $j + 1$ depending on whether corresponding states are in $(n_F - 1, j + \frac{1}{2})$ or (n_F, j) supermultiplet

respectively. Analogously, $q_{n_F}(j - \frac{1}{2}E'|jE) = j + \frac{1}{2}$ or j if the states are in $(n_F - 1, j - \frac{1}{2})$ of (n_F, j) supermultiplet. Because the cutoff we are able to reach are not very large, the supersymmetry fractions are in general significantly smaller than their values in the continuum limit. Still, they give valuable information on at least some supermultiplets.

In Tab. 6.1 there are shown supersymmetry fractions $q_1(\frac{1}{2}E_i|0, E_k)$. All states from the $(0, 0)$ sector are vacua of a $(0, 0, E)$ supermultiplet. Therefore, for all of them there should be a supersymmetry fraction equal to 1 with some states with $(n_F, j) = (1, \frac{1}{2})$. The states from channel $(1, \frac{1}{2})$ belong to one of three supermultiplets, $(0, 0, E)$, $(0, 1, E)$ or $(1, \frac{1}{2}, E)$. Therefore, only some of them share nonzero supersymmetry fractions with states in the $(0, 0)$ sector.

The first two columns of Tab. 6.1 were already analyzed in the previous part of this chapter. It was stated that the ground states in $(0, 0)$ and $(1, \frac{1}{2})$ sectors are elements of the same multiplet. The superpartner of the first excited bosonic state, $|0, 0, 15.48\rangle$ is a combination of third and fourth excited states in the channel $(1, \frac{1}{2})$. The third column is related to the singlet $|0, 0, 17.47\rangle$. There are five fractions which correspond to doublets in single fermion sector that add up to 0.83. Energies of these doublets range from 17.88 to 18.85. These states will possibly mix for higher cutoff and give the superpartner of $|0, 0, 17.47\rangle$. This is consistent with the energy dependence on the cutoff (cf. Fig. 5.8). For $E \sim 18$ all energies decrease by $\Delta E \sim 1$ when N_B changes from 8 to 9. Therefore, the error bars to these energies are of order 1. All five energies are the same within error bars and thus the states can mix before the continuum limit is reached.

Consider fractions $q_2(0, E_i|\frac{1}{2}, E_k)$ (Tab. 6.2). In the first column there are two significant fractions $q_2(0, 13.34|\frac{1}{2}, 12.72)$ and $q_2(0, 13.45|\frac{1}{2}, 12.72)$ which add up to 0.92. This is evidence that a combination of states $|2, 0, 13.34\rangle$ and $|2, 0, 13.45\rangle$ gives the last state of the supermultiplet $(0, 0, 12.6)$. In the second column the largest element is $q_2(0, 15.67|\frac{1}{2}, 14.48) = 0.3$. If $|1, \frac{1}{2}, 14.48\rangle$ is vacuum of a supermultiplet, then the exact value of the fraction is 0.5. If this is the case then there should be a fraction $q_2(1, E|\frac{1}{2}, 14.48) \approx 1.5$. Indeed, there is $q_2(1, 15.62|\frac{1}{2}, 14.48) = 0.65 \times 1.5$.

Finally, we study supersymmetry fractions $q_0(j', E'|1, E)$ with $j' = \frac{1}{2}$ (Tab. 6.3) and $j' = \frac{3}{2}$ (Tab. 6.4). Since the bosonic state is always a vacuum of a supermultiplet, the exact values of fractions are 1 and 2 respectively. For the bosonic ground state with $j = 1$ the relevant fractions are $q_0(\frac{1}{2}, 17.5|1, 16.66) = 0.77$ and $q_0(\frac{3}{2}, 17.44|1, 16.66) = 0.76 \times 2$. It is remarkable that in both $(n_F = 1, j')$ channels the approximation of the energies is of the same quality ($E \approx 17.5$) as well as the fractions $q \approx 0.76 \times q_{exact}$. For the first excited bosonic state the susy fractions are rather poor: $q_0(\frac{1}{2}, 20.75|1, 18.79) = 0.53$ and $q_0(\frac{3}{2}, 20.74|1, 18.79) + q_0(\frac{3}{2}, 20.82|1, 18.79) = 0.52 \times 2$. Again, the approximation of energies and fractions are similar for $|1, \frac{1}{2}, 20.74\rangle$ and $|1, \frac{3}{2}, 20.82\rangle$.

Analysis of all other sectors is similar. Summary of identified supermultiplets is given in Tab. 6.5. Also values of supersymmetry fractions are given to indicate how strong is the identification. Clearly, large difference of energies in a supermultiplet means that states did not yet converge and one should not expect large values of fractions. Supersymmetry fractions given in Tab. 6.5 are normalized, i.e. divided by exact values.

6.5 Summary

In Fig. 6.5 all identified supermultiplets are shown. Triangles with vertices in sectors $(n_F, 0)$, $(n_F + 1, \frac{1}{2})$, $(n_F + 2, 0)$ and all diamonds are fully identified supermultiplets. They

are marked with blue color. The triangles which have vertices at (n_F, j) , $(n_F+1, j-\frac{1}{2})$ and $(n_F+1, j+\frac{1}{2})$ are marked with green color and represent diamonds with one element not identified. Green lines correspond to two states out of three in a multiplet with Clifford vacuum in $(n_F, 0)$. Not identified states are marked with a question mark in Tab. 6.5. There are also many energies in between for which there were no supersymmetry fractions much different from 0. In the continuum limit all states should group in supersymmetric multiplets. The method which was used for finding the energies is variational, so all energies are approximated from above. For this reason all states in Fig. 6.5 are shifted to the lowest energy in the corresponding multiplet.

We succeeded to fully identify four supermultiplets (cf. Tab. 6.5). In general, it is easier to identify states which 'open' the multiplet, i.e. the vacuum in the sector with n_F fermions and two states with $n_F + 1$ fermions. The remaining state which 'closes' the supermultiplet is significantly harder to find. This is because with more fermions the lowest energy state has smaller energy than in those with less fermions and the density of eigenenergies is higher (see Figs 5.7 - 5.15). Therefore, even if the Clifford vacuum is a low excited state, the state which closes the supermultiplet has $n_F + 2$ fermions and is highly excited. For excited states one needs a higher cutoff before the convergence is reached. On the other hand, the available cutoff gets smaller for more fermions.

	E	$n_F = 0, j = 0$					
		12.6	15.48	17.47	17.88	18.32	19.76
$n_F = 1, j = 1/2$	12.72	0.99	-	-	-	-	-
	14.48	-	-	-	-	-	-
	15.52	-	0.01	-	-	-	-
	15.88	-	0.46	-	-	-	-
	15.96	-	0.47	0.01	-	-	-
	16.46	-	-	-	-	-	-
	16.69	-	-	-	-	-	-
	16.97	-	-	-	-	-	-
	17.09	-	-	-	-	-	-
	17.5	-	-	-	-	-	-
	17.58	-	-	-	-	-	-
	17.88	-	-	0.11	0.03	-	-
	18.26	-	-	-	-	-	-
	18.32	-	-	-	-	-	-
	18.52	-	-	0.2	0.14	0.04	0.02
	18.62	-	-	0.42	0.03	0.05	-
	18.73	-	-	0.06	0.02	0.01	-
	18.85	-	-	0.05	0.61	0.01	-
	18.96	-	-	-	-	-	-
	19.08	-	-	-	-	-	-
	19.21	-	-	-	0.02	0.03	0.02
	19.3	-	-	-	-	-	-
	19.46	-	-	-	-	-	-
	19.66	-	-	0.01	0.03	0.11	0.06
	19.73	-	-	-	-	0.52	-
	19.75	-	-	-	-	-	-
	20.03	-	-	-	-	-	-
	20.11	-	-	-	-	-	-
	20.38	-	-	-	-	-	-
	20.47	-	-	-	-	-	-
	20.57	-	-	-	-	-	-
	20.74	-	-	-	-	-	0.03
	20.75	-	-	-	-	-	-
	20.79	-	-	-	-	-	-
	20.92	-	-	-	-	0.02	0.01
	20.99	-	-	-	-	-	-
	21.16	-	-	-	-	-	-
	21.17	-	-	-	-	-	0.01
	21.33	-	-	-	-	-	-
	21.34	-	-	-	-	-	0.01
	21.49	-	-	-	-	-	-
	21.5	-	-	-	-	-	0.1
21.57	-	-	-	-	-	-	
21.64	-	-	-	-	-	0.3	

 Table 6.1: Supersymmetry fractions between sectors $(n_F, j) = (0, 0)$ and $(1, 1/2)$.

E	$n_F = 1, j = 1/2$			
	12.72	14.48	15.52	15.88
8.8	-	-	-	-
11.57	-	-	-	-
12.47	-	-	-	-
13.34	0.71	-	-	-
13.45	0.21	-	-	-
14.23	-	-	-	-
14.64	-	-	-	-
14.82	-	0.11	-	-
15.09	-	-	-	-
15.55	-	-	-	-
15.67	-	0.3	-	-
$\vdots(4)$				
16.61	-	-	0.09	0.02
16.83	-	-	0.12	0.04
17.05	-	-	0.14	0.01
$\vdots(7)$				
18.05	-	-	0.04	0.28

Table 6.2: Supersymmetry fractions between sectors with $(n_F, j) = (1, 1/2)$ and $(2, 0)$.

E	$n_F = 0, j = 1$			
	16.66	18.79	19.02	19.11
$\vdots(9)$				
17.5	0.77	-	-	-
$\vdots(12)$				
19.46	-	0.11	-	0.14
$\vdots(4)$				
20.11	-	-	0.02	0.14
20.38	-	-	-	0.4
$\vdots(3)$				
20.75	-	0.53	-	-
20.79	-	0.1	0.04	0.04
$\vdots(6)$				
21.49	-	-	0.4	-

Table 6.3: Supersymmetry fractions between bosonic sector with $j = 1$ and fermionic sector with $j = 1/2$.

	E	$n_F = 0, j = 1$			
		16.66	18.79	19.02	19.11
$n_F = 1, j = 3/2$	$\vdots(12)$ 17.44	0.14	-	-	-
	17.55	1.52	0.04	0.01	-
	$\vdots(16)$ 19.38	-	0.1	-	0.24
	$\vdots(6)$ 20.1	-	-	-	0.15
	$\vdots(3)$ 20.41	-	0.02	-	0.92
	20.54	-	0.04	-	-
	20.58	-	0.02	0.03	0.14
	20.66	-	-	-	-
	20.74	-	0.73	-	0.02
	20.75	-	-	-	-
	20.79	-	0.12	-	-
	20.82	-	0.31	-	-
	20.88	-	-	-	-
	20.93	-	0.11	-	-
	$\vdots(9)$ 21.47	-	-	0.38	-
	21.52	-	-	0.8	-

Table 6.4: Supersymmetry fractions between bosonic sector with $j = 1$ and fermionic sector with $j = 3/2$. Rows with no supersymmetry fractions greater than 0.1 are omitted. Numbers of omitted states are given in brackets.

(n_F, j)	energy				fractions			
	(n_F, j)	$(n_F + 1, j - \frac{1}{2})$	$(n_F + 1, j + \frac{1}{2})$	$(n_F + 2, j)$	$\tilde{a}_{n_F}(j - \frac{1}{2})$	$\tilde{a}_{n_F}(j + \frac{1}{2})$	$\tilde{a}_{n_F+1}(j j - \frac{1}{2})$	$\tilde{a}_{n_F+1}(j j + \frac{1}{2})$
(0,0)	12.6	-	12.72	13.4*	-	.99	-	.92*
(0,0)	15.48	-	15.92*	?	-	.93*	-	?
(0,0)	17.88	-	18.85	?	-	.61	-	?
(0,0)	18.32	-	19.7*	?	-	.63*	-	?
(0,1)	16.66	17.5	17.55	?	.77	.76	?	?
(0,1)	18.79	20.75	20.78*	?	.53	.52	?	?
(0,1)	19.11	20.38*	20.41	?	.54*	.53*	?	?
(0,2)	14.89	15.27	15.29	17.06	.9	.95	.75*	.67*
(0,2)	17.41	18.47	18.49	?	.72	.79	?	?
(0,2)	17.79	18.94	18.98*	?	.66	.71*	?	?
(0,2)	18.7	20.8	20.83*	?	.6	.63*	?	?
(0,3)	16.1	16.75	16.8	?	.86	.9	?	?
(0,3)	18.77	20.9*	21.02	?	.5*	.66	?	?
(1,1/2)	14.48	15.67	15.62	?	.6	.65	?	?
(1,1/2)	15.52	16.93*	16.72	?	.52	.75	?	?
(1,3/2)	13.39	13.86	13.97	14.96	.83*	.88*	.2*	.18
(1,3/2)	13.96	14.97	15.05	?	.73*	.8*	?	?
(1,3/2)	14.83	15.81	16.14	?	.71*	.71*	?	?
(1,5/2)	16.13	17.61	17.94	?	.49	.57*	?	?
(2,0)	8.8	-	9.84	12.74	-	.83	-	.58
(2,1)	10.97	13.	12.93	?	.62	.71*	?	?
(2,2)	10.43	12.68	12.72	?	.59*	.59	?	?

Table 6.5: Energies and supersymmetry fractions in identified supermultiplets. Fractions are divided by the value they should take in continuum. The closer the normalized supersymmetry fraction is to one, the higher is the quality of identification of a supermultiplet. Stars mean that the fraction is summed over two states and energies are averaged. Question marks stand for unidentified states and corresponding supersymmetry fractions in a supermultiplet. Dashes stand for states which do not appear in a supermultiplet.

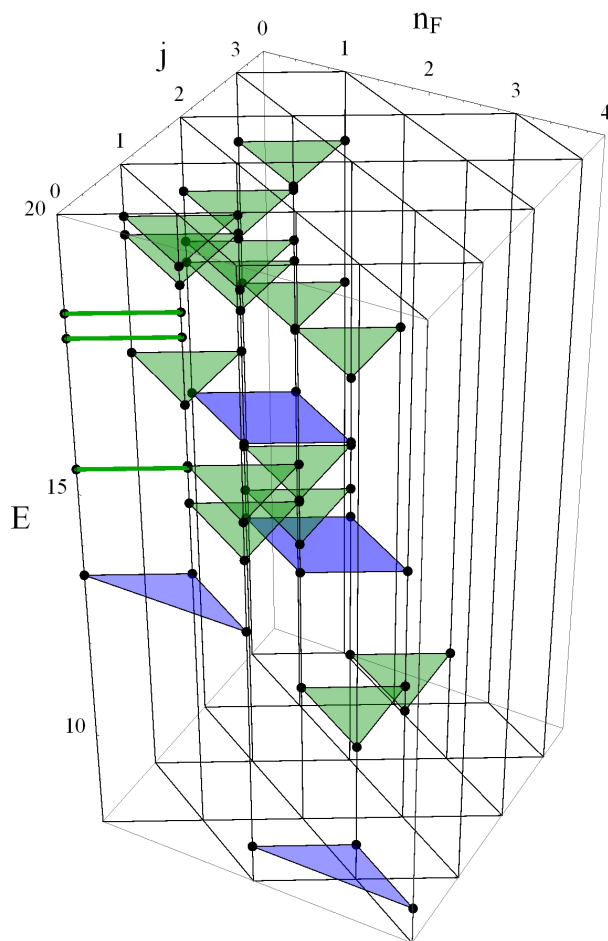


Figure 6.5: All identified supermultiplets. The diamond and two triangles with two vertices at $j = 0$ are completely identified multiplets. The other triangles correspond to diamonds with one state unidentified. Lines correspond to triangle multiplets with one vertex not identified.

Chapter 7

Wavefunctions

This chapter is dedicated to wavefunctions in coordinate representation for $SU(2)$ and $SU(3)$ gauge groups. The wavefunctions of supersymmetric Yang–Mills quantum mechanics in two dimensions are studied in great detail. The complete solution of the model, i.e. explicit formulae for wavefunctions and corresponding energies was given for $SU(2)$ gauge group [23]. Later, wavefunctions of the vacuum were found for general $SU(N)$ [8]. For $D = 4$ only s–waves of $SU(2)$ were analyzed so far [42]. In this thesis a new, more general approach is proposed. In principle, it can be used to study wavefunctions with arbitrary angular momentum and for any $SU(N)$ gauge group. It is used here to analyze the cases of $SU(2)$ and $SU(3)$.

We will now briefly review the approach of [42]. It is a numerical technique to obtain energies and eigenstates of s–waves in $D = 4$ for $SU(2)$. The idea of this method applied to the two–fermion sector is following. There is one symmetric and one antisymmetric combination of spinors that create two fermions. Each of these two can be contracted in three different ways to give a gauge and rotationally invariant operator. These six operators acting on the Fock vacuum generate a basis $|e_m\rangle$. A most general gauge invariant state with $j = 0$ is a combination of these basis states, where the coefficients are functions $h_m(r, u, v)$ of three bosonic variables:

$$|\psi\rangle = \sum_{m=1}^6 h_m(r, u, v) |e_m\rangle. \quad (7.1)$$

The three invariants (r, u, v) are discussed later in this chapter. The Schrödinger equation $H|\psi\rangle = E|\psi\rangle$ is a system of six coupled differential equations for functions h_m in a three dimensional space. There exists an ‘angular momentum’ L related to a differential operator in variables (r, u, v) . Eigenstates of the angular momentum are 6–component ‘spherical harmonics’. They are functions of two angle variables u and v . The spherical harmonics can be found analytically. Finally, one can introduce a basis for the radial part of functions with given L . There is a natural cutoff in this complete set of functions. It is equivalent to the cutoff for the number of bosonic excitations which is used in this paper. With this method one can reach $N_B = 60$ [43]. A limitation of this approach is that it addresses rotationally invariant states. In particular, it gives no information about sectors with odd number of fermions.

Here we propose a new approach. One starts with an angular momentum multiplet expressed in terms of composite bricks acting on the empty state. States in the Fock space are in one to one correspondence with wavefunctions in the configuration space. Because

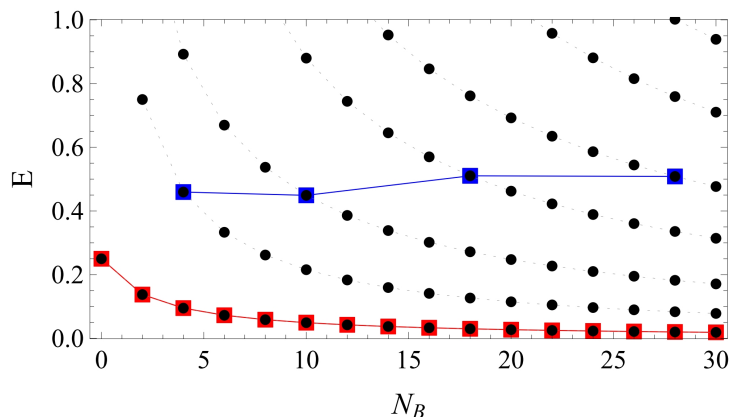


Figure 7.1: Two ways to analyze non-localized energy eigenstates. Circles are energies of the free one-dimensional quantum mechanics. Blue line represents fixed energy limit with $E_* = 0.5$. Red line corresponds to the ground states for each N_B .

of fermions, the wavefunctions are multi-component. It is shown how to construct a rotationally invariant single-component function $\rho(x)$. This function is an analogue to probability density of bosonic variables. Next, the structure of the potential is studied in a fixed gauge and some characteristic directions in the configuration space are chosen. These are the flat valley (i.e. a direction in which the potential vanishes) and two steep directions, where the potential grows fastest. Finally, sections of wavefunctions along these directions are studied.

The main purpose of analyzing the wavefunctions is exploring the difference between states corresponding to discrete and continuous spectra. In 7.3.2 we discuss the expected behavior of bound and scattering states. We argue that the localized states are well approximated by the cut Fock basis already for finite cutoff. On the other hand, the scattering states are non-localized and they can be reconstructed only when one goes to high N_B .

There are two ways to study scattering states. First is to inspect the limit of constant energy $E = E_* = \text{const}$ while $N_B \rightarrow \infty$. It was mentioned in Chapter 5 that the eigenenergies corresponding to the continuous spectrum decrease slowly to 0 as one increases N_B . Therefore, at every few values of the cutoff there is a state with energy $E \approx E_*$. Such limit was studied in [43] for $SU(2)$. It was observed that a periodic function is recovered as the cutoff grows. When N_B increases, new peaks are reconstructed. Period of the function agrees with the dispersion relation for energy E_* . For $SU(2)$ the constant energy analysis requires increasing cutoff by about 10 at each step.

Another approach to address scattering states is to fix the energy level (e.g. the lowest state) and raise N_B one by one. Then the energy converges to zero. One does not recover a periodic function. Instead, the probability density is smeared over an increasing range. Explanation of this behavior is given in detail later. This type of analysis is easier from the numerical point of view, because one does not need large cutoff.

7.1 Structure of fermionic wavefunctions

In Chapter 3 it was shown how to obtain eigenstates of the Hamiltonian. These eigenstates are expressed in terms of creation operators acting on a Fock vacuum. In this part of the theses we study their wavefunctions in the configuration space.

Let $\mathbf{n} = (n_i^a)$ and $\boldsymbol{\chi} = (\chi_\alpha^b)$ denote bosonic and fermionic occupation numbers respectively. n_i^a take integer, nonnegative values while χ_α^b are 0 or 1. As before, $a, b = 1, \dots, N^2 - 1$ are color indices, $i = 1, 2, 3$ is the spatial index and $\alpha = \pm \frac{1}{2}$ is the Weyl spinor index. Labels \mathbf{n} and $\boldsymbol{\chi}$ have $3(N^2 - 1)$ and $2(N^2 - 1)$ components respectively. The basis of the Fock space with no restriction to gauge-singlet states is

$$|\mathbf{n}, \boldsymbol{\chi}\rangle = |\mathbf{n}\rangle_B \otimes |\boldsymbol{\chi}\rangle_F = \prod_{b,\alpha} (f_\alpha^{b\dagger})^{\chi_\alpha^b} \prod_{a,i} \frac{1}{\sqrt{(n_i^a)!}} (a_i^{a\dagger})^{n_i^a} |0\rangle. \quad (7.2)$$

These states satisfy relations

$$a_i^{a\dagger} a_i^a |\mathbf{n}, \boldsymbol{\chi}\rangle = n_i^a |\mathbf{n}, \boldsymbol{\chi}\rangle, \quad f_\alpha^{b\dagger} f_\alpha^b |\mathbf{n}, \boldsymbol{\chi}\rangle = \chi_\alpha^b |\mathbf{n}, \boldsymbol{\chi}\rangle, \quad (7.3)$$

where no sum over indices is performed. Bosonic states $|\mathbf{n}\rangle_B$, bosonic creation and annihilation operators $a_i^{a\dagger}$, a_i^a and the Fock vacuum $|0\rangle$ depend on the parameter ω introduced in 3.6. In this chapter the index ω will remain implicit.

The coordinates in the bosonic $3(N^2 - 1)$ -dimensional configuration space are $\mathbf{x} = (x_i^a)$. A ket $|\mathbf{x}\rangle_B$ is defined by the relation

$$\hat{x}_i^a |\mathbf{x}\rangle_B = x_i^a |\mathbf{x}\rangle_B, \quad (7.4)$$

where \hat{x}_i^a is the position operator. Wavefunction of bosonic states $|\mathbf{n}\rangle_B$ are simply wavefunctions of eigenstates of the harmonic oscillator

$${}_B\langle \mathbf{x} | \mathbf{n} \rangle_B = \prod_{a,i} \sqrt{\frac{\omega}{2^{n_i^a} (n_i^a)!}} \pi^{-1/4} \exp(-(\omega x_i^a)^2 / 2) H_{n_i^a}(\omega x_i^a), \quad (7.5)$$

where $H_n(x)$ is the Hermite polynomial.

In order to handle the fermionic states, a representation of $|\boldsymbol{\chi}\rangle_F$ is needed. In what follows we incorporate the matrix representation of fermions [63]. In this notation fermionic creation and annihilation operators are represented by matrices and wavefunctions are columns. For the simplest case of one fermionic type there is a vacuum state $|0\rangle_F$ and a state with one fermion $|1\rangle_F$. The states and operators are represented as follows:

$$|0\rangle_F = \begin{pmatrix} 0 \\ 1 \end{pmatrix}, \quad f^\dagger = \begin{pmatrix} 0 & 1 \\ 0 & 0 \end{pmatrix}, \quad (7.6)$$

$$|1\rangle_F = \begin{pmatrix} 1 \\ 0 \end{pmatrix}, \quad f = \begin{pmatrix} 0 & 0 \\ 1 & 0 \end{pmatrix}. \quad (7.7)$$

Then the action of creation and annihilation operators is

$$f^\dagger |0\rangle_F = |1\rangle_F, \quad f |1\rangle_F = |0\rangle_F, \quad f |0\rangle_F = f^\dagger |1\rangle_F = 0. \quad (7.8)$$

A wavefunction of a general state $|\phi\rangle$ is a two-component function

$$\phi(x) = \begin{pmatrix} \phi_1(x) \\ \phi_0(x) \end{pmatrix}. \quad (7.9)$$

Wavefunctions associated with the zero- and one-fermion part are given by scalar products

$$\phi_\chi(x) = \langle x, \chi | \phi \rangle, \quad \chi = 0, 1. \quad (7.10)$$

This representation naturally generalizes to a larger number of fermionic types. Consider again SYMQM. The label $\boldsymbol{\chi}$ has $2(N^2 - 1)$ components, each taking values 0 or 1. Therefore, $\boldsymbol{\chi}$ has $2^{2(N^2-1)}$ possible values and the wavefunction is a column of size $2^{2(N^2-1)}$. Elements of the column are bosonic wavefunctions labeled by $\boldsymbol{\chi}$.

Consider a general state $|\phi\rangle$. Its expansion in basis states is given by

$$|\phi\rangle = \sum_{\boldsymbol{n}, \boldsymbol{\chi}} c(\boldsymbol{n}, \boldsymbol{\chi}) |\boldsymbol{n}, \boldsymbol{\chi}\rangle \quad (7.11)$$

with some complex coefficients $c(\boldsymbol{n}, \boldsymbol{\chi})$. Then the $\boldsymbol{\chi}$ -component of the wavefunction of $|\phi\rangle$ is the scalar product

$$\phi_{\boldsymbol{\chi}}(\boldsymbol{x}) \equiv \langle \boldsymbol{x}, \boldsymbol{\chi} | \phi \rangle = \sum_{\boldsymbol{n}_i} c(\boldsymbol{n}, \boldsymbol{\chi}) \langle \boldsymbol{x} | \boldsymbol{n} \rangle_B. \quad (7.12)$$

The fact that a wavefunction has many components introduces a major difficulty to analyzing them in a direct way. For $SU(2)$ the column $(\phi_{\boldsymbol{\chi}}(\boldsymbol{x}))$ has $2^{2 \times 3} = 64$ and for $SU(3)$ it has $2^{2 \times 8} = 65536$ elements. Fortunately, we consider only states in sectors with definite number of fermions. Then $(\phi_{\boldsymbol{\chi}}(\boldsymbol{x}))$ has only $\binom{2(N^2 - 1)}{n_F}$ elements that are nonzero. Still, the direct study of $\phi_{\boldsymbol{\chi}}(\boldsymbol{x})$ is complicated. For example, consider a multiplet $|\phi^m\rangle$ with angular momentum j . Then $|\phi^m\rangle$ is represented by a $(2j + 1) \times \binom{2(N^2-1)}{n_F}$ -component complex-valued bosonic functions in a $3(N^2 - 1)$ -dimensional bosonic space. For instance, for $SU(3)$, $j = 1$ and $n_F = 2$ these are 360 functions of 24 variables.

7.2 Probability density from fermionic wavefunctions

A wavefunction carries full information about a state. In particular, it depends on fermionic occupation numbers and angular momentum. In order to simplify the wavefunctions, we would like to integrate out fermionic degrees of freedom and angles which correspond to rotations in the physical space. To this end we introduce the probability distribution $\rho(\boldsymbol{x})$. Take an angular momentum multiplet $|\phi^m\rangle$. Then the probability density is defined as

$$\rho(\boldsymbol{x}) = \sum_{m\boldsymbol{\chi}} |\phi_{\boldsymbol{\chi}}^m(\boldsymbol{x})|^2, \quad (7.13)$$

which sums over fermionic occupation numbers and the magnetic quantum number. Studying $\rho(\boldsymbol{x})$ is easier since it is a single-component real function. Still, it depends on many variables. However, there are some simplifications. It is shown in Appendix D that $\rho(\boldsymbol{x})$ is invariant under rotations. It is also gauge invariant because the original states $|\phi^m\rangle$ are such. Because of these symmetries $\rho(\boldsymbol{x})$ depends only on $3(N^2 - 1) - (N^2 - 1) - 3 = 2N^2 - 5$ invariants of gauge and rotation transformations.

One more step needs to be taken before $\rho(\boldsymbol{x})$ can be considered as a probability density integrated over rotations and gauge transformations. Suppose we are interested in calculating the expectation value of an observable A in a state given by a wavefunction $\psi(\boldsymbol{x})$ and $A(\boldsymbol{x})$ is invariant under rotations and action of gauge group. Rotations are parameterized by 3 angles $\boldsymbol{\theta} = (\theta_1, \theta_2, \theta_3)$. Gauge transformations depend on $N^2 - 1$

angles $\boldsymbol{\alpha} = (\alpha_1, \dots, \alpha_{N^2-1})$. Then there are $2N^2 - 5$ variables left. They will be denoted by $\mathbf{y} = (y_1, \dots, y_{2N^2-5})$. A depends only on \mathbf{y} . The mean value of A is

$$\begin{aligned} \langle \psi | A | \psi \rangle &= \int d\mathbf{x} A(\mathbf{x}) |\psi(\mathbf{x})|^2 = \int d\mathbf{y} d\boldsymbol{\alpha} d\boldsymbol{\theta} A(\boldsymbol{\alpha}, \boldsymbol{\theta}, \mathbf{y}) |\psi(\boldsymbol{\alpha}, \boldsymbol{\theta}, \mathbf{y})|^2 |J(\boldsymbol{\alpha}, \boldsymbol{\theta}, \mathbf{y})| \\ &= \int d\mathbf{y} A(\mathbf{y}) |\psi(\mathbf{y})|^2 \int d\boldsymbol{\alpha} d\boldsymbol{\theta} |J(\boldsymbol{\alpha}, \boldsymbol{\theta}, \mathbf{y})| = \int d\mathbf{y} A(\mathbf{y}) |\psi(\mathbf{y})|^2 J(\mathbf{y}), \end{aligned} \quad (7.14)$$

where J is the Jacobian. The integral was reduced from $3(N^2 - 1)$ to $2N^2 - 5$ dimensional. $N^2 + 2$ variables were integrated out, so the Jacobian $J(\mathbf{y})$ is proportional to r^{N^2+2} . In order to take the Jacobian into account, the function $\rho(\mathbf{x})$ will be multiplied by r^{N^2+2} .

Concluding, $r^{N^2+2}\rho(\mathbf{x})$ is the probability density, summed over fermionic degrees of freedom and integrated over angles which correspond to rotations and gauge transformations. The integration over rotational angles is performed by summing over members of the angular momentum multiplet. In order to further simplify the analysis we will choose some interesting directions in the configurations space.

7.3 Wavefunctions for $SU(2)$ gauge group

7.3.1 Invariants

For the $SU(2)$ gauge group a general wavefunction depends on 9 variables x_i^a . It was argued previously that $\rho(\mathbf{x})$ defined in (7.13) depends on $2N^2 - 5 = 3$ gauge and rotation invariants. For $SU(2)$ they can be found explicitly. If $\mathbf{x} = (x_i^a)$ is treated as a 3×3 matrix then it transforms under rotations and $SU(2)$ in the following way:

$$\mathbf{x} \rightarrow \mathbf{x}' = U \mathbf{x} V^\dagger \quad (7.15)$$

where U, V are both $SO(3)$ matrices. U corresponds to gauge transformation (in adjoint representation) and V to rotation in the configuration space. It is known that one can diagonalize \mathbf{x} with U and V [64, 65]. We define $\mathbf{y} = \text{diag}(y_1, y_2, y_3)$ by

$$\mathbf{x} = U \mathbf{y} V^\dagger. \quad (7.16)$$

The diagonal terms y_i are defined uniquely up to permutations and reflection of two of them. These symmetries give 24-fold degeneracy. We impose additional constraint $y_1 \geq y_2 \geq |y_3|$ so that the diagonal elements are uniquely defined. Under this constraint y_i are proper invariants of gauge transformations and rotations. It convenient to introduce other set of invariants [42]:

$$\begin{aligned} r^2 &= y_1^2 + y_2^2 + y_3^2 = \sum_{i,a} (x_i^a)^2, \\ r^3 v &= y_1 y_2 y_3 = \det(x_i^a), \\ r^4 u &= y_1^2 y_2^2 + y_2^2 y_3^2 + y_3^2 y_1^2 = \sum_{a,b,i < j} ((x_i^a)^2 (x_j^b)^2 - x_i^a x_j^a x_i^b x_j^b). \end{aligned} \quad (7.17)$$

Note that if r vanishes, then the other two variables are undetermined. If $u = 0$ then also $v = 0$. Moreover, two of these variables are bounded, $0 \leq u \leq 1/3$, $|v| \leq 3^{-3/2}$. The potential takes the form $V = \frac{1}{2} r^4 u$.

We will be interested in two directions in the configuration space, namely the flat valley and the steepest direction. Potential vanishes when $u = 0$. Since then also v vanishes, the flat valley is one-dimensional and can be parameterized by r . In terms of y_i the potential vanishes when two variables vanish, i.e. only y_1 is nonzero.

The potential grows fastest for $u = 1/3$ which implies $v = \pm 3^{-3/2}$. There are thus two steep directions and both are one dimensional. In terms of y_i the steep direction is $y_1 = y_2 = r/\sqrt{3}$, $y_3 = \pm r/\sqrt{3}$.

Although the wavefunction $\rho(\mathbf{x})$ depends on \mathbf{y} , in practice it is given as an explicit function of \mathbf{x} (7.16). Therefore, we calculate $\rho(\mathbf{x})$ along certain directions which correspond to values of invariants in the flat and steep directions. The directions are parameterized as $\mathbf{x} = r\hat{\mathbf{x}}$ where $|\hat{\mathbf{x}}| = 1$. Versor of the flat direction is denoted by $\hat{\mathbf{x}}_{flat}$. Versors of the two steep directions are $\hat{\mathbf{x}}_{steep}$ and $\hat{\mathbf{x}}'_{steep}$.

$$\hat{\mathbf{x}}_{flat} = \begin{pmatrix} 1 & 0 & 0 \\ 0 & 0 & 0 \\ 0 & 0 & 0 \end{pmatrix}, \quad \hat{\mathbf{x}}_{steep} = \frac{1}{\sqrt{3}} \begin{pmatrix} 1 & 0 & 0 \\ 0 & 1 & 0 \\ 0 & 0 & 1 \end{pmatrix}, \quad \hat{\mathbf{x}}'_{steep} = \frac{1}{\sqrt{3}} \begin{pmatrix} -1 & 0 & 0 \\ 0 & -1 & 0 \\ 0 & 0 & -1 \end{pmatrix}. \quad (7.18)$$

For $\hat{\mathbf{x}}_{flat}$ and $\hat{\mathbf{x}}_{steep}$ the invariants y_i are the diagonal elements. $\hat{\mathbf{x}}'_{steep}$ corresponds to $y_1 = y_2 = -y_3 = 1/\sqrt{3}$. Note that $r\hat{\mathbf{x}}'_{steep} = -r\hat{\mathbf{x}}_{steep}$. In the following we will drop $\hat{\mathbf{x}}'_{steep}$ and slightly abuse the notation by taking $r\hat{\mathbf{x}}_{steep}$ with positive and negative r . This way, both steep directions are included. This is done merely for the convenience to include both steep directions on one plot.

7.3.2 Bound and scattering states – models and expectations

Here we recall what is the characteristic behavior of states associated with discrete and continuous spectrum in general quantum mechanical models. It will serve us as a hint to analyze wavefunctions of SYMQM. The states which correspond to discrete spectrum are bound states, i.e. their wavefunctions are localized. That is, the probability density is centered at minimum of the potential and vanishes as one moves away to infinity. Because the basis of the Fock space consists of localized states, the bound states can be well approximated for finite N_B .

Bound states are typical for a potential which grows to infinity in all directions or at least $V(x) > V_0$ for $|x| > r_0$ (then there may be discrete energies smaller than V_0). In the considered model the potential has flat valleys and neither condition is fulfilled. However, although the potential has a flat valley, its width shrinks as one moves outwards. The transverse oscillations cost more energy as one moves along the valley and an effective potential is generated. The effective potential is unbounded from above and vanishes only at the origin. On the other hand, because of the supersymmetry, interactions of the potential with bosonic degrees of freedom may cancel and then the effective potential vanishes. However, in the purely bosonic channel such cancelations cannot take place simply because there are no fermions. Therefore, the effective potential is present for $n_F = 0$ and the spectrum is discrete. Surprisingly, the effective potential does not vanish also for nonzero but small n_F . Only in sectors rich in fermions the supersymmetric cancelations are possible.

For n_F large enough the continuous spectrum appears. The continuous spectrum is associated with scattering states. They are not localized and non-normalizable. The scattering states are concentrated in regions where the potential is flat. The probability

density does not decay for $|x| \rightarrow \infty$. A scattering state cannot be well approximated for finite N_B because the basis of cut Fock space consists of localized functions. Instead, such state is reconstructed step by step as the cutoff grows.

In order to better understand what is the behavior of scattering states, consider a three dimensional, quantum mechanical, free Hamiltonian $H = \frac{1}{2} \sum_{i=1}^3 p_i^2$. This simple system can be solved analytically. Its spectrum in all channels with definite angular momentum is continuous and ranges from zero to infinity. For vanishing angular momentum the wavefunctions are just the spherical waves

$$\langle \vec{x} | E \rangle = \sqrt{\frac{2p}{\pi}} \frac{\sin(pr)}{r}, \quad (7.19)$$

where $p = \sqrt{2E}$ [66].

One way to analyze scattering states is to fix E and observe how the functions approach the spherical wave. However, as it was mentioned in the introduction to this chapter, states with given E appear at every few N_B . The cutoff that we are able to explore is too small to perform this analysis. Instead, we analyze the ground state and thus take the limit $E \rightarrow 0$.

For $E \rightarrow 0$ the wavefunction (7.19) converges to a flat function. With the cut Fock space method one does not exactly recover a ground state of the theory, but rather an approximation which improves for growing cutoff. Therefore, one should expect that the ground state will be approximated by a roughly flat function. Because N_B effectively gives an infrared cutoff (cf. Chapter 3), the flat function is smeared over a finite region which grows with N_B .

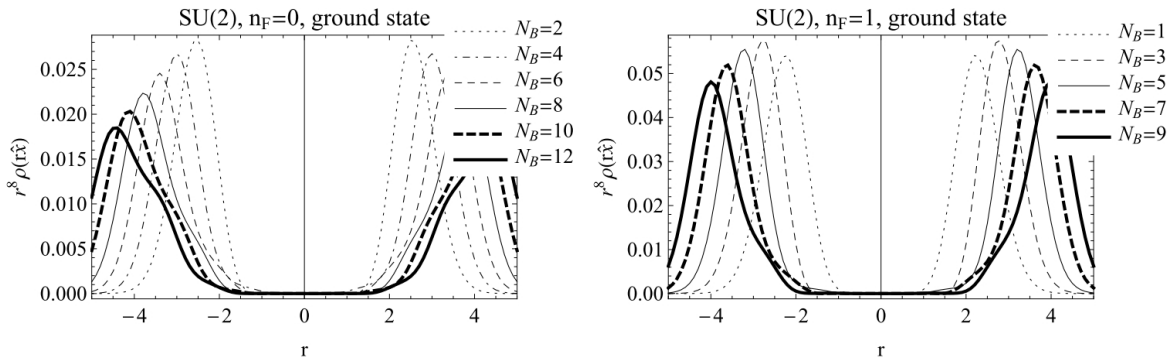


Figure 7.2: Wavefunctions of lowest eigenstates for free $SU(2)$ with $n_F = 0$ and $n_F = 1$. As there is no potential, the wavefunctions depend only on the radius r . The angular momentum for $n_F = 0$ is $j = 0$ and $j = 1/2$ for $n_F = 1$. Wavefunction with $n_F = 2$ is exactly the same as in the sector with $n_F = 0$. It is obvious since the free Hamiltonian has no fermionic terms.

For comparison, consider the free Yang–Mills quantum mechanics with $SU(2)$ symmetry $H = Tr(p_i p_i)$. Because of symmetry of the Hamiltonian, the wavefunctions should depend only on one invariant r . Therefore, instead of $r^{N^2+2} = r^6$ we multiply the probability density $\rho(\mathbf{x})$ by r^8 . The function $r^8 \rho(\mathbf{x})$ is then the probability density integrated over all variables apart from the radius. Wavefunctions of ground state in channels with $n_F = 0, 1$ for finite cutoffs are shown in Fig. 7.2. One can see that the wavefunction move outside as the cutoff grows. This is in agreement with what was expected.

7.3.3 Interacting case – results

Finally, consider the interacting case. Profiles of wavefunctions with $n_F = 0, 1, 2, 3$ are presented in Fig. 7.3. They correspond to the ground states, which for $n_F = 0, 2$ and $n_F = 1, 3$ are in channels with $j = 0$ and $j = 1/2$ respectively.

For $n_F = 0$ the wavefunction converges to a fixed shape. In fact, the wavefunction moves a little deeper into the flat valley. Convergence is seen for $N_B \approx 4$. In the steep direction the wavefunction initially decreases with N_B and finally converges for $N_B \approx 4$. We shall also note that the values of wavefunction are of the same order inside and outside of the valley. The wavefunction in the steep direction is the same for positive and negative r . This is because for $n_F = 0$ the parity is conserved. The two steep directions are related by the parity transformation. The behavior of wavefunction in $n_F = 1$ sector is essentially the same. The wavefunction converges to a fixed shape although the rate of convergence is slower. For $n_F > 0$ the parity symmetry is broken wavefunctions are different for $r > 0$ and $r < 0$.

Channels $n_F = 2, 3$ correspond to continuous spectrum and thus the behavior of wavefunctions is very different. In both cases, the probability density moves deeper into the flat valleys as the cutoff grows. In turn, in the steep directions the wavefunctions get significantly smaller. That is, the probability density concentrates along the flat valleys.

As it was observed in Chapter 5, there are discrete energies immersed in the continuous spectrum for $n_F = 2, 3$. The two plots in Fig. 7.4 show the second excited state of $(n_F, j) = (3, 1/2)$. We see that the wavefunction vanishes along the whole the valley. Indeed, values of the wavefunction are of the order of numerical errors. In the steep direction the function decreases and approaches the origin as the cutoff grows. This behavior may be considered strange. However, this is merely a consequence of looking only along the steep and flat directions. A combined plot gives a more complete picture. First, we introduce another flat direction

$$\hat{\mathbf{x}}'_{flat} = \begin{pmatrix} 0 & 1 & 0 \\ 0 & 0 & 0 \\ 0 & 0 & 0 \end{pmatrix}. \quad (7.20)$$

It can be mapped into the flat direction $\hat{\mathbf{x}}_{flat}$ defined in (7.18) with gauge transformations and rotations. On the other hand, it is orthogonal to $\hat{\mathbf{x}}_{steep}$. One can see that the probability density is concentrated around the origin with some preference of the flat direction. This is similar to the behavior of ground state in the purely bosonic sector (cf. Fig. 7.3). The difference is that the wavefunction vanishes along the bottom of the valley.

In conclusion, lowest energy states with $n_F = 0, 1$ fermions are localized near the origin and thus they are bound states. Ground states in channels with $n_F = 2, 3$ fermions penetrate the valley and are scattering states. There are also bound states for $n_F = 2, 3$. These observations are in agreement with conclusions of Chapter 5 where the discrete spectrum in $n_F = 0, 1$ sectors and continuous spectrum for $n_F = 2, 3$ were identified.

7.3. WAVEFUNCTIONS FOR SU(2) GAUGE GROUP

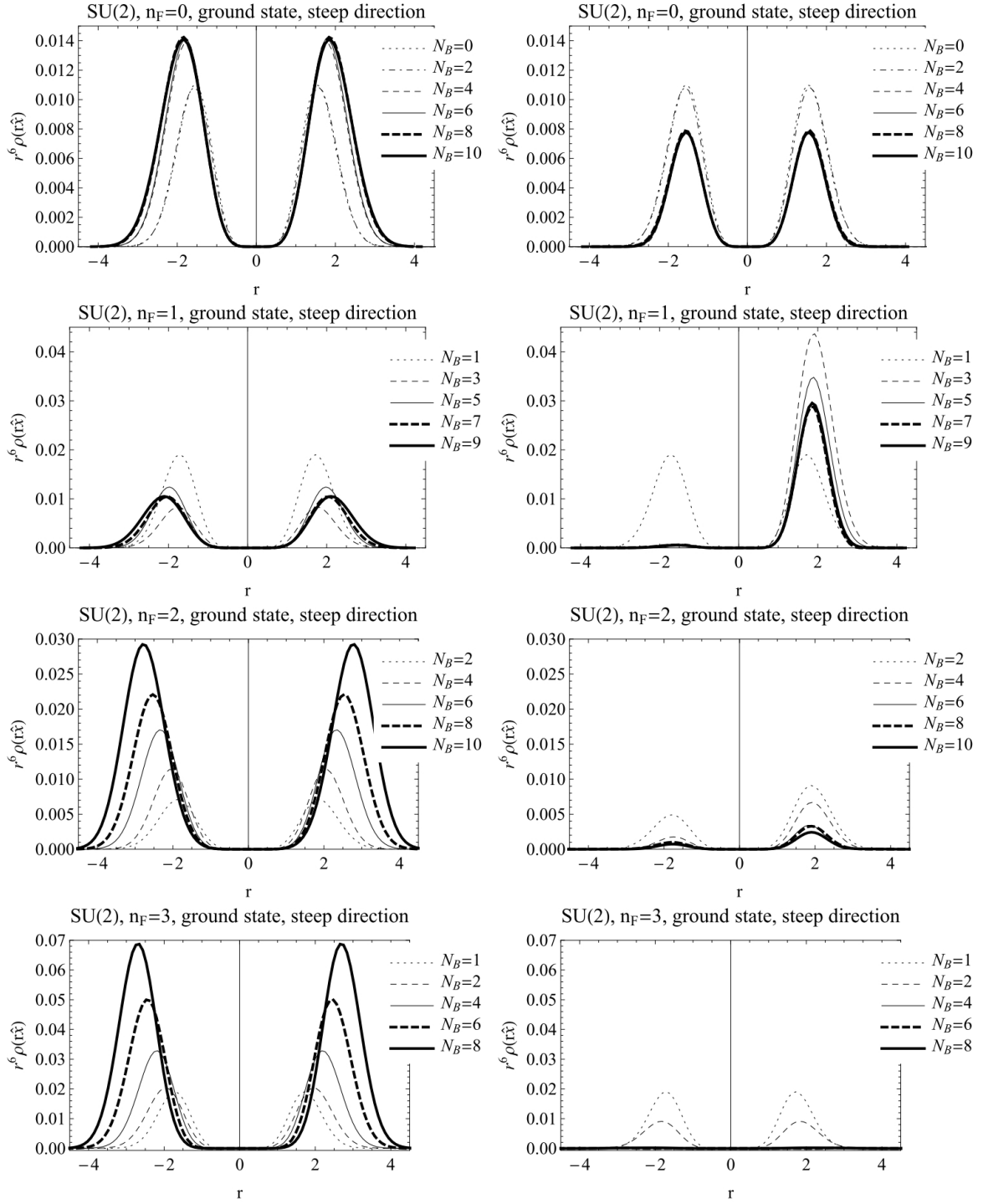


Figure 7.3: Plots of wavefunctions of ground states in sectors $n_F = 0, 1, 2, 3$. The angular momentum is $j = 0$ for $n_F = 0, 2$ and $j = 1/2$ for $n_F = 1, 3$. The versor is $\hat{x} = \hat{x}_{flat}$ for the flat direction and $\hat{x} = \hat{x}_{steep}$ for the steep direction.

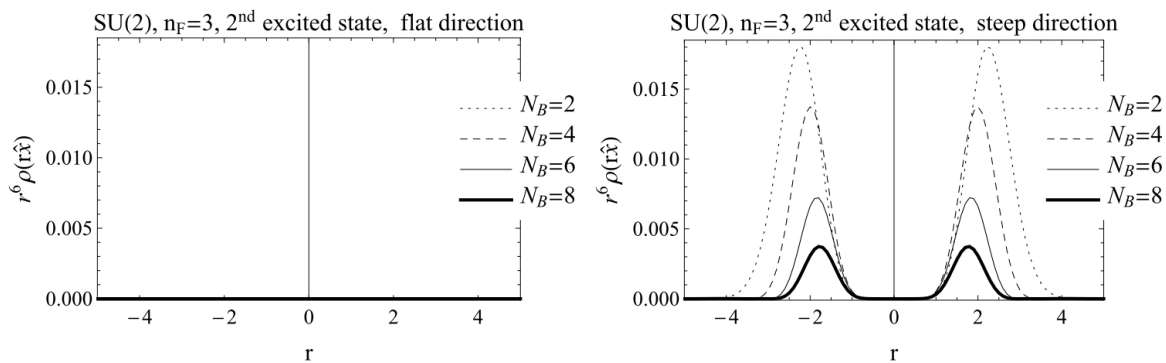


Figure 7.4: Plots of wavefunctions of the second excited state in sector with three fermions and $j = 1/2$.

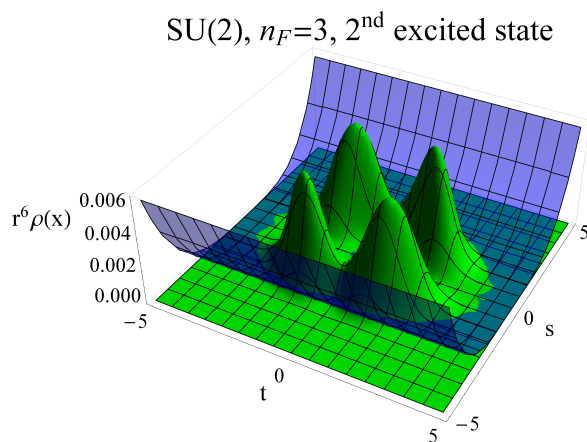


Figure 7.5: Second excited states for $n_F = 3$, $j = 1/2$, $N_B = 8$. The parametrization is $\mathbf{x} = t\hat{\mathbf{x}}'_{flat} + s\hat{\mathbf{x}}'_{steep}$. The blue surface represents the potential.

7.4 Wavefunctions for $SU(3)$ gauge group

Now we analyze wavefunctions for the $SU(3)$ gauge group. There are 24 bosonic degrees of freedom x_i^a . Equivalently, they are expressed in terms of three hermitean traceless 3×3 matrices $X_i = x_i^a T^a$. The gauge transformation of X_i is $X_i \rightarrow U X_i U^\dagger$, where $U \in SU(3)$. The potential and wavefunctions are gauge invariant. Therefore, analyzing any of them along the orbits of gauge transformations gives no new information about dynamics of the system. One would like to eliminate these directions. This can be achieved in two ways. One is to find gauge invariants, as is was done for $SU(2)$. However, these are difficult to find for $SU(3)$. Another way is to fix the gauge. This procedure is straightforward and eliminates precisely $N^2 - 1 = 8$ degrees of freedom of X_i .

7.4.1 Fixing the gauge

The procedure of gauge fixing consists of several steps. One starts with a general U in the fundamental representation of $SU(3)$ and a general set of three traceless, hermitean matrices X_i . In the first step U is used to diagonalize X_1 . This done, there is a residual gauge transformation that leaves X_1 unchanged. In following steps the gauge transformations are used to impose additional constraints on X_2 and X_3 . The procedure continues until no more constraints on X_i can be introduced.

Consider first a generic case. The gauge transformation U can be chosen such that X_1 is diagonalized and the diagonal elements are in the increasing order. Once X_1 is diagonalized, the gauge is fixed up to transformations with $U = \text{diag}(e^{i\phi}, e^{i\psi}, e^{-i\phi-i\psi})$. Now the question is how this gauge freedom can be used to fix matrix elements of X_2 . First, consider a general matrix $M = (m_{ij})$. The transformation applied to M is

$$UMU^\dagger = \begin{pmatrix} m_{11} & e^{i\phi-i\psi}m_{12} & e^{2i\phi+i\psi}m_{13} \\ e^{-i\phi+i\psi}m_{21} & m_{22} & e^{i\phi+2i\psi}m_{23} \\ e^{-2i\phi-i\psi}m_{31} & e^{-i\phi-2i\psi}m_{32} & m_{33} \end{pmatrix}. \quad (7.21)$$

One can see that U can be used to set the off-diagonal matrix elements $(X_2)_{12}$ and $(X_2)_{23}$ to be real and positive. In the generic case this additional condition fixes the gauge completely. The conditions on matrices X_i can be translated to constraints on coordinates x_i^a :

$$\begin{aligned} x_1^1 = x_1^2 = x_1^4 = x_1^5 = x_1^6 = x_1^7 = x_2^2 = x_2^5 = 0, \\ x_1^8 \leq \frac{\sqrt{3}}{2}x_1^3 \leq 0. \end{aligned} \quad (7.22)$$

The space of configurations in the fixed gauge is 16-dimensional.

There are many nongeneric cases in which the procedure presented above does not completely fix the gauge. For example, if $X_1 = 0$ then after the first step the residual gauge group is the full $SU(3)$. It is then used to diagonalize X_2 and set $(X_3)_{12}$ and $(X_3)_{23}$ positive.

Other special case is when X_1 is not zero, but the two lowest eigenvalues are equal. Then the remaining gauge freedom after the first step is

$$U = \begin{pmatrix} U_2 & 0 \\ 0 & 0 \end{pmatrix}, \quad (7.23)$$

where U_2 is a general $U(2)$ matrix. Then it is used to diagonalize the upper-left 2×2 block of X_2 with increasing order of eigenvalues. There still remains a gauge freedom with $U = \text{diag}(e^{i\phi}, e^{i\psi}, e^{-i\phi-i\psi})$. It is utilized to set the coefficients $(X_2)_{13}$ and $(X_2)_{23}$ positive.

A third degenerate case is when all three eigenvalues of X_1 are different but $(X_2)_{12} = 0$. Then after fixing $(X_2)_{23} > 0$ there is still a freedom of one phase in U . It is used to set $(X_2)_{13}$ to be positive.

These are not all special cases. Moreover, all of these three contain some degenerate 'subcases'. Therefore, some care has to be taken in order to completely fix the gauge. The complete procedure is presented in Appendix E. It is chosen in such a way that the conditions (7.22) are always fulfilled after the final step of gauge fixing.

One may question the necessity to completely fix the gauge rather than to restrict the gauge fixing to (7.22). However, when the gauge is only partially fixed, some gauge freedom still remains. This leads to 'false' flat valleys as will be shown later.

7.4.2 Flat and steep directions

After the gauge is fixed, a wavefunction depends on 16 coordinates, which are encoded in matrices X_i . This is still too many to analyze behavior of the wavefunctions. Again,

we consider flat and steep directions. The potential is given by

$$V = - \sum_{i < j} Tr([X_i, X_j]^2) = - \sum_{i < j} Tr([X_i, X_j]^2). \quad (7.24)$$

V is nonnegative and has flat valleys. Indeed, each $i[X_i, X_j]$ is hermitean, so $-[X_i, X_j]^2$ is semipositive definite and so is the trace. The potential vanishes only if $[X_i, X_j] = 0$ for all i, j . These equations together with constraints (7.22) give six different solutions. There is one six-parameter solution

$$X_i^{val} = x_i^3 T^3 + x_i^8 T^8. \quad (7.25)$$

The other five solutions do not satisfy additional constraints which follow from fixing the gauge. More precisely, although they satisfy (7.22), they fall into the special cases mentioned before. The special cases impose additional constraints which are not fulfilled by these solutions. An example of such 'false valley' is

$$\begin{aligned} X_1 &= 0, \\ X_2 &= \frac{1}{2} \begin{pmatrix} x_2^3 + \frac{1}{\sqrt{3}}x_2^8 & x_2^1 & 0 \\ x_2^1 & -x_2^3 + \frac{1}{\sqrt{3}}x_2^8 & 0 \\ 0 & 0 & -\frac{2}{\sqrt{3}}x_2^8 \end{pmatrix}, \\ X_3 &= \frac{1}{2} \begin{pmatrix} x_3^3 + \frac{1}{\sqrt{3}}x_3^8 & x_2^1 x_3^1 / x_2^3 & 0 \\ x_2^1 x_3^1 / x_2^3 & -x_3^3 + \frac{1}{\sqrt{3}}x_3^8 & 0 \\ 0 & 0 & -\frac{2}{\sqrt{3}}x_3^8 \end{pmatrix}. \end{aligned} \quad (7.26)$$

One can easily check that it satisfies (7.22) and the potential vanishes on this configuration. However, if $X_1 = 0$ then the gauge symmetry is used to diagonalize X_2 . The matrix X_2 in (7.26) is not diagonal and thus this set of matrices does not fulfill all gauge constraints.

The probability density $\rho(\mathbf{x})$ is invariant under rotations. Therefore, we would like to construct rotational invariants from (7.25). The two vectors $\vec{v}_3 = (x_1^3, x_2^3, x_3^3)$ and $\vec{v}_8 = (x_1^8, x_2^8, x_3^8)$ transform under rotations like ordinary vectors. There are three rotation invariants, namely \vec{v}_3^2 , \vec{v}_8^2 , $\vec{v}_3 \cdot \vec{v}_8$. They can be rewritten in terms of other parameters which will be more useful for later purposes:

$$\begin{aligned} r^2 &= \vec{v}_3^2 + \vec{v}_8^2, \\ \tan \theta &= |\vec{v}_8| / |\vec{v}_3|, \\ \cos \phi &= \frac{\vec{v}_3 \cdot \vec{v}_8}{|\vec{v}_8| |\vec{v}_3|}. \end{aligned} \quad (7.27)$$

This gives us the complete description of the flat valley.

Second interesting direction is the one in which the potential grows fastest. The scaling of the potential is known, $V(r\mathbf{X}) = r^4 V(\mathbf{X})$. It is therefore enough to find such configuration \mathbf{X} , normalized by the condition $\sum_i Tr(X_i^2) = 1$, which maximizes $V(\mathbf{X})$. First observe that we can assume $Tr(X_i^2) = \frac{1}{3}$ for each i . Indeed, if this assumption is not fulfilled, there exists a rotation matrix R_{ij} such that $X'_i = R_{ij} X_j$ where R_{ij} satisfies $Tr(X'_i{}^2) = \frac{1}{3}$. The potential is invariant under rotations, so $V(\mathbf{X}') = V(\mathbf{X})$.

Consider one component of the potential, namely $V(X_1, X_2) = -Tr([X_1, X_2]^2)$. Maximizing this component with $Tr(X_i^2) = \frac{1}{3}$ and constraints from the gauge fixing gives a

unique solution. It is

$$X_1 = \begin{pmatrix} -\frac{1}{\sqrt{6}} & 0 & 0 \\ 0 & 0 & 0 \\ 0 & 0 & \frac{1}{\sqrt{6}} \end{pmatrix}, \quad X_2 = \begin{pmatrix} 0 & 0 & \frac{1}{\sqrt{6}} \\ 0 & 0 & 0 \\ \frac{1}{\sqrt{6}} & 0 & 0 \end{pmatrix}. \quad (7.28)$$

Obviously, maximum of the potential is not greater than sum of maxima of the three components, i.e.

$$\max_{\mathbf{X}} V(\mathbf{X}) \leq - \sum_{i < j} \max_{X_i, X_j} Tr([X_i X_j]^2). \quad (7.29)$$

Suppose that there exists a matrix X_3 such that $Tr(X_3^2) = \frac{1}{3}$ and $Tr([X_1, X_2]^2) = Tr([X_2, X_3]^2) = Tr([X_1, X_3]^2)$ with X_1, X_2 given by (7.28). If it is true, then the set (X_1, X_2, X_3) necessarily maximizes the potential. There are two such matrices X_3 :

$$X_3 = \begin{pmatrix} 0 & 0 & -\frac{i}{\sqrt{6}} \\ 0 & 0 & 0 \\ \frac{i}{\sqrt{6}} & 0 & 0 \end{pmatrix}, \quad X'_3 = \begin{pmatrix} 0 & 0 & \frac{i}{\sqrt{6}} \\ 0 & 0 & 0 \\ -\frac{i}{\sqrt{6}} & 0 & 0 \end{pmatrix}. \quad (7.30)$$

Concluding, there are two one-dimensional steep directions, just as for the $SU(2)$ gauge group. In particular, these solutions are invariant under rotations. That is, for a given $SO(3)$ matrix R_{ij} the configuration $X'_i = R_{ij} X_j$ is gauge-equivalent to X_i . In other words, rotations of the two steep directions are special cases of gauge transformations.

For consistency with previous paragraphs, we denote the versors of the two steep directions by $\hat{\mathbf{x}}_{steep}$ and $\hat{\mathbf{x}}'_{steep}$. As in the $SU(2)$ case, $-\hat{\mathbf{x}}'_{steep}$ can be transformed with the gauge transformation to $\hat{\mathbf{x}}_{steep}$. Therefore, in all profiles we use only one steep direction $\hat{\mathbf{x}}_{steep}$ and let r to be positive and negative.

7.4.3 Analysis of wavefunctions

Consider first the noninteracting case. The Hamiltonian has only the kinetic part, $H = Tr(p_i p_i)$. As in the $SU(2)$ case the wavefunction depends only on the radius. Therefore, the probability density has to be multiplied by r^{23} . The profile of the probability distribution in the noninteracting case is shown in Fig. 7.6. One can see that indeed the wavefunction moves outwards as the cutoff grows.

Let us now come to the interacting case. Previously it was shown that $\rho(\mathbf{x})$ needs to be multiplied by a factor r^{N^2+2} so that it can be considered as the probability density integrated over the gauge group and rotations. For $SU(3)$, $r^{N^2+2} = r^{11}$. However, additional factor has to be taken into account.

The flat valleys are three dimensional. They are parameterized by the radius r and two angles θ, ϕ (cf. (7.27)). It turns out that $\rho(\mathbf{x})$ does not depend on two angles, but only on the radius r . Therefore, it is convenient to consider probability density integrated over the gauge group, rotations and the two angles θ and ϕ . Another r^2 has to be included and finally, $\rho(\mathbf{x})$ has to be multiplied by r^{13} .

For the steep direction the situation is reversed. Spatial Rotations are included in gauge rotations. Thus, $\rho(\mathbf{x})$ needs to be multiplied only by r^9 which comes from integration over the gauge group. However, for consistency $\rho(\mathbf{x})$ in the steep direction is also multiplied by r^{13} . Only then one can compare wavefunctions in the two directions.

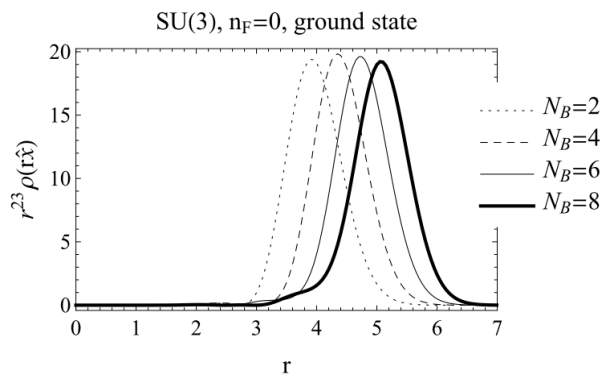


Figure 7.6: Plot of the wavefunctions of ground state in the noninteracting case for $n_F = 0$ and $j = 0$.

First, consider the ground state in the purely bosonic sector (Fig. 7.7). One can see that the probability distribution converges for $N_B \approx 8$. The profile in the steep direction is suppressed compared to the flat direction. Moreover, it penetrates the valley deeper than the region where the potential is nonzero. All these effects are similar to the case of $SU(2)$, yet there are some differences. First, the convergence is slower. Secondly, the steep direction is suppressed stronger than for $SU(2)$. This may be caused by higher dimension of the configuration space. There are more allowed directions, so the steepest one is naturally more disfavored. For $n_F = 2$ behavior of the probability distribution is very similar. The convergence is even slower, but rather clear.

Next, take the first excited state for $n_F = 7$. One can see that in the flat direction the probability density grows while in the steep direction it is suppressed. This may be the first step of the characteristic behavior of wavefunctions of scattering states, which was observed for $SU(2)$ (cf. Fig. 7.3). On the other hand, bound states for $SU(3)$ share the same tendencies for small cutoffs. Therefore, a firm statement can be given only from analysis for higher N_B .

Finally, consider the other states presented in Fig 7.8 – the first excited state for $n_F = 5$ and the ground state for $n_F = 6$. These are the candidates for the scattering states with minimal number of fermions (see Chapter 5). The probability distribution moves outwards as the cutoff grows. However, this effect is not stronger than for the lowest eigenstate for $n_F = 2$ and $N_B \leq 5$. Therefore, the asymptotic behavior of these profiles remains unclear.

Concluding, analysis of wavefunctions for the $SU(3)$ gauge group is more delicate than for $SU(2)$. In sectors with small number of fermions, the convergence is slower than for $SU(2)$, but is clearly seen in our data. Moreover, suppression of the steep direction is stronger. For five and six fermions the wavefunctions share some behavior of scattering states, but it could be a small-cutoff effect. Finally, the first excited state with seven fermions is a candidate for a scattering state. This is in agreement with scaling relations for continuous spectrum (cf. Chapter 5).

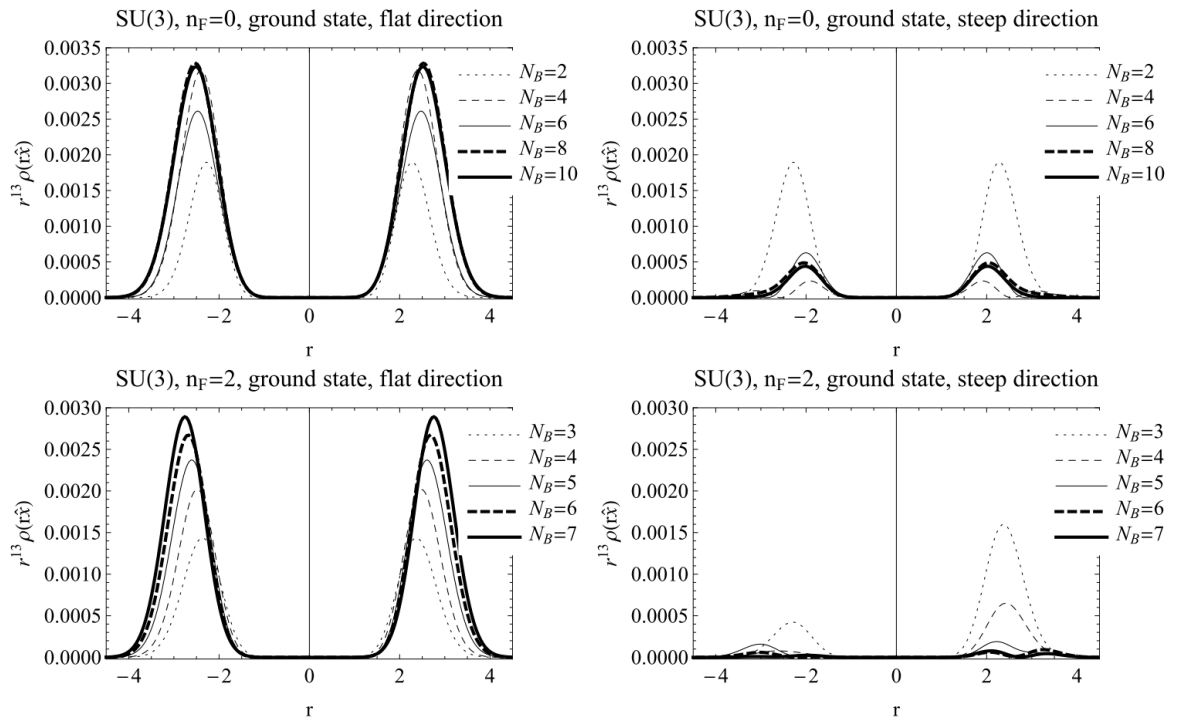


Figure 7.7: Plots of wavefunctions of ground states in sectors $n_F = 0$. The angular momentum is $j = 0$.

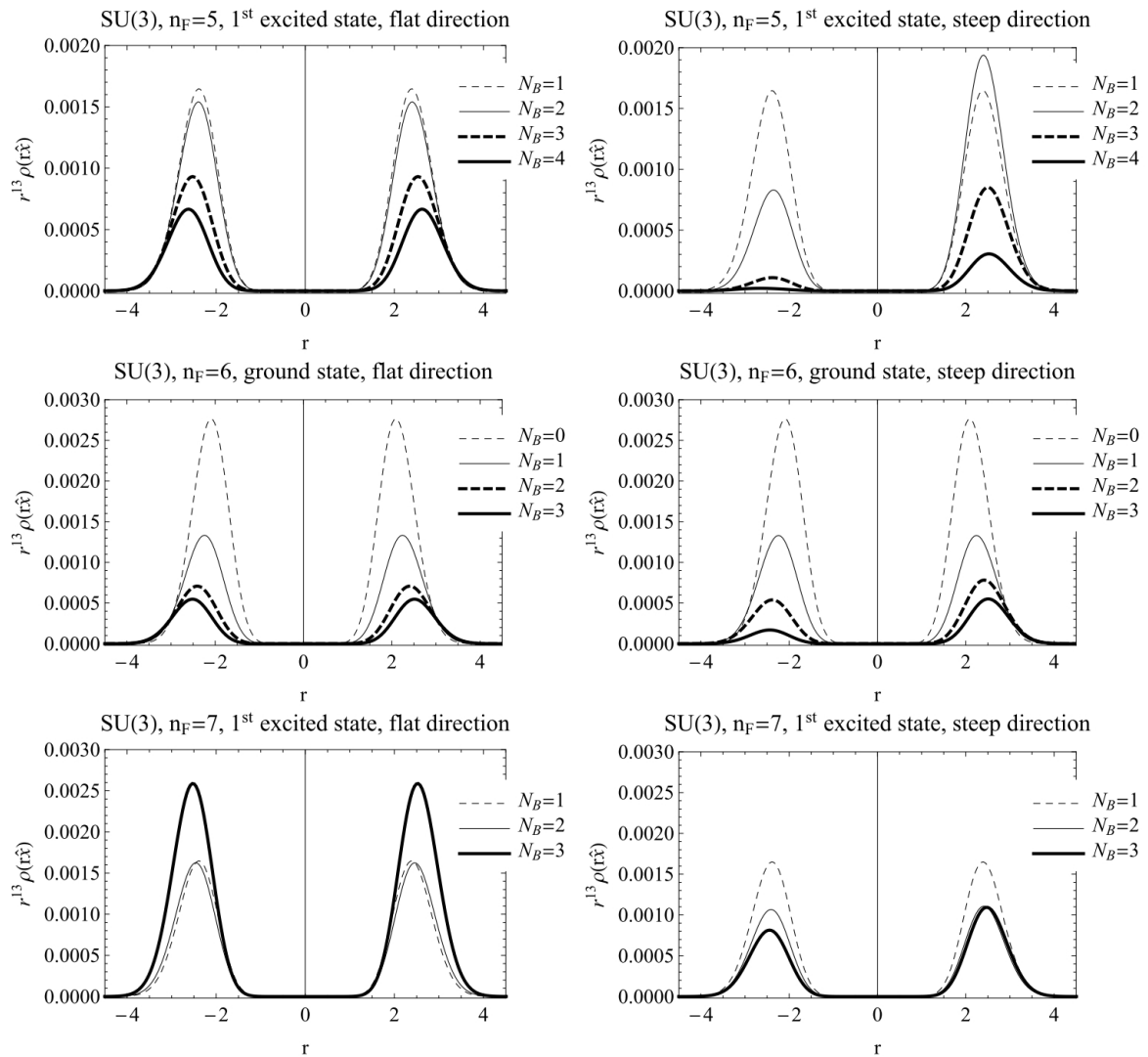


Figure 7.8: Plots of wavefunctions of ground states in sectors $n_F = 0$. The angular momentum is $j = 0$.

Chapter 8

Summary

In this thesis the cut Fock space approach was used to study the supersymmetric Yang-Mills quantum mechanics in $D = 4$. Central results concern the theory with $SU(3)$ gauge group. However, substantial part of the analysis is redone also for $SU(2)$, mainly for comparison. Our studies cover the following topics:

- construction of the basis of cut Fock space,
- algorithm for constructing matrix representation of operators H , J_i and Q_α in occupation number basis,
- spectrum of the model obtained numerically,
- restoration of supersymmetry in the continuum limit,
- wavefunctions of energy eigenstates.

These points will be now discussed in order.

The Fock space consists of states which are singlets of the gauge group $SU(N)$. Basis of the Hilbert space is generated by so called bricks (cf. [52]). A brick is a trace of product of creation operators contracted with $SU(N)$ generators, e.g. $(a_1^\dagger a_2^\dagger) \equiv a_1^{a_1^\dagger} a_2^{b_1^\dagger} Tr(T^a T^b)$. The whole Hilbert space is spanned by composite bricks (i.e. products of bricks) acting on the empty state. The set of vectors generated in this way is overcomplete. This is because the set of all possible bricks is not independent. Eliminating dependent bricks is nontrivial but essential for performance of the numerical algorithm. In 3.2 we addressed this problem for $SU(3)$. Many bricks can be eliminated with the following relations:

- invariance of the trace under cyclic permutations,
- Cayley-Hamilton theorem for matrices with commuting (3.6) and anticommuting (3.12) matrix elements,
- symmetric combination of product of three $SU(3)$ generators reduces to shorter bricks.

After these relations are exploited to reduce the number of bricks, the Gauss elimination algorithm can be applied. With this method one eliminates all dependent bricks. It was found that all bricks consisting of more than six creation operators can be reduced to shorter ones. This fact was explained by showing that there exists a solution to (3.41). It follows from (3.41) that a trace of product of seven or more $SU(3)$ generators can be expressed by a combination of products of shorter traces. Finally, the number of

independent bricks is finite and 786 bricks were found. The structure of $SU(2)$ group is simpler and there are only 35 independent bricks.

After construction of the occupation number basis, a cutoff N_B for the maximal number of bosonic excitations is introduced. Because of the Pauli exclusion principle, the total number of fermions n_F is limited by $2(N^2 - 1)$, so no cutoff for n_F is needed. The resulting cut Fock space is spanned by composite bricks which consist of at most N_B bosonic and any number of fermionic creation operators. In this finite-dimensional space operators are represented by matrices. In 3.3 a recursive algorithm for calculating matrix elements of the Hamiltonian and other relevant operators is introduced. In Appendix C finiteness of this procedure is proven. The Hamiltonian and angular momentum conserve the total number of fermions, so their matrix elements can be generated in each sector with given n_F independently. Supersymmetry generators change the number of fermions by one, so they are represented by matrices which act between sectors.

The program was used to construct matrix representations of angular momentum, Hamiltonian and supersymmetry generators for certain cutoffs in (or between) sectors with given n_F . Construction of these matrices was performed with a parallel program on a supercomputer Deszno at the Jagiellonian University. The main limitation was the amount of available memory (256 GB). First, matrices of angular momentum were diagonalized. Then, the Hamiltonian was diagonalized in subspaces corresponding to given total angular momentum j and the third component m .

The Hilbert space \mathcal{H} can be split into subspaces $\mathcal{H}_{\mathbf{n}}$, $\mathbf{n} = (n_F^1, n_F^2, n_B^1, n_B^2, n_B^3)$ with definite occupation numbers of bosons and fermions for corresponding labels \mathbf{n} . In Chapter 4 a group theoretical approach was used to calculate dimensions $D_{\mathbf{n}}$ of $\mathcal{H}_{\mathbf{n}}$. Our analysis is an extension of a method discussed in [45] where sectors with total number of bosons $n_B = n_B^1 + n_B^2 + n_B^3$ and total number of fermions $n_F = n_F^1 + n_F^2$ are considered. An essential component of this technique is the generating function

$$G(a_1, a_2, a_3, b_1, b_2) = \sum_{n_B^i=0}^{\infty} \sum_{n_F^{\alpha}=0}^{\infty} a_1^{n_B^1} a_2^{n_B^2} a_3^{n_B^3} (-b_1)^{n_F^1} (-b_2)^{n_F^2} D_{\mathbf{n}}. \quad (8.1)$$

$D_{\mathbf{n}}$ is expressed as an integral of character over the $SU(N)$ group. The generating function was calculated by residues and an explicit result was given in (4.25). Then, $D_{\mathbf{n}}$ were extracted from Taylor expansion of G . The dimensions were checked against the number of independent vectors determined numerically in the computer program and an agreement was found (cf. Fig. 4.1). The dimensions of channels with definite total occupation numbers n_B and n_F were given in Tab. 4.1. It is in perfect agreement with earlier results [45]. As expected, dimensions $D_{\mathbf{n}}$ grow fast with n_B .

In Chapter 5 we analyzed the spectrum for $SU(2)$ and $SU(3)$ cases. Dependence of the eigenenergies on the cutoff N_B is crucial for identifying type of the spectrum. Discrete energy levels converge very fast to the exact value. On the contrary, if the continuous spectrum is present, then all eigenvalues E_m converge slowly to zero for fixed m . From another point of view, one can recognize a continuous spectrum by a distribution of eigenenergies that fill densely a full interval as N_B grows. The spectrum for $SU(2)$ was already found with a great precision in [38] and served as a check of our program. A perfect agreement was established. The spectrum is purely discrete for $n_F = 0, 1$ (cf. Figs 5.1–5.2). It is continuous for two and three fermions (cf. Figs 5.3–5.4). Moreover, there are discrete energy levels immersed in the continuous part. For the $SU(3)$ case the cutoffs we were able to reach were significantly smaller than for $SU(2)$, especially for large

n_F . However, a number of regularities already appear. Our results in the purely bosonic part of the Hilbert space were compared with [32] where no fermions were considered. Very good agreement was found (cf. Tab. 5.1). It was argued in [38, 43] that eigenenergies corresponding to the continuous spectrum should satisfy the scaling relation (5.1):

$$E_m \propto \frac{(m+1)^2}{N_B}, \quad (8.2)$$

where m is the label of the energy. Therefore, the scaled energy $N_B \times E_m$ should approach a constant when $N_B \rightarrow \infty$. This effect is seen clearly for $SU(2)$ for at least the two lowest energies in the $(n_F, j) = (2, 0)$ sector (cf. Fig. 5.5). Ratios of the lowest energies also agree with the prediction of (5.1), i.e. $E_m/E_0 \approx (m+1)^2$ (cf. Fig. 5.6). For $SU(3)$ the scaled energies grow approximately linearly with increasing N_B for $n_F \leq 4$ and seem to be approximately constant for $n_F = 5, 6, 7, 8$ (Fig. 5.16). Therefore, the spectrum is purely discrete for $n_F \leq 4$. It seems to be continuous for $n_F = 6, 7, 8$. The intermediate sector $n_F = 5$ is disputable. Because of the particle–hole symmetry, the energy levels for $8 < n_F \leq 16$ are the same as for $16 - n_F$ fermions. Therefore, supersymmetric cancelations can happen only in the middle sectors. Only then there are enough fermionic degrees of freedom. For a more detailed picture concerning the type of spectrum a higher cutoff would be needed.

In Chapter 6 we studied supersymmetric structure of the model for a finite cutoff. Finite N_B breaks the supersymmetry. This is because the supercharges \mathcal{Q}_α do not conserve the number of bosons. However, the supersymmetry is being restored as N_B grows. For exact supersymmetry massive states form supersymmetry multiplets. For a given state one can act on it with \mathcal{Q}_α and $\mathcal{Q}_\alpha^\dagger$ to recover the other states in its supermultiplet. To check how much the supersymmetry is broken for a given cutoff we used supersymmetry fractions

$$q_{n_F}(j'E'|jE) = \frac{1}{4E} \sum_{mm'\alpha} |\langle n_F + 1j'm'E' | \mathcal{Q}_\alpha^\dagger | n_F jmE \rangle|^2, \quad (8.3)$$

where $|n_F jmE\rangle$ is a state with n_F fermions, total angular momentum j , the third component of angular momentum m and energy E . Values of supersymmetry fractions are known when the supersymmetry is exact. $q_{n_F}(j'E'|jE)$ is j or $j + \frac{1}{2}$ if the two corresponding states are in the same multiplet and zero otherwise. Therefore, supersymmetry fractions can be used to measure the SUSY breaking. We found that at least for some low energy states the supersymmetry fractions converge to their exact values (cf. Fig. 6.4). They were used to identify supermultiplets. Four complete supermultiplets were fully identified. More supermultiplets were found with one state in the channel with highest n_F missing. Complete list of identified supermultiplets is given in Tab. 6.5 and an overview picture is presented in Fig. 6.5. We concluded that within the available cutoff, some supersymmetry is already restored at low energies and small number of fermions.

Finally, in Chapter 7 we studied the wavefunctions. For a given state $|\phi\rangle$ the probability density $|\phi_\chi(\mathbf{x})|^2$ in the configuration space is a multi-component function. The label χ corresponds to occupation numbers of fermions and variable \mathbf{x} is a $3(N^2 - 1)$ -dimensional coordinate. As we are not interested in particular dependence on fermionic degrees of freedom, sum over χ was performed. For an angular momentum multiplet $|\phi^m\rangle$ a sum over elements of the multiplet eliminates dependence on rotations. The probability

distribution

$$\rho(\mathbf{x}) \equiv \sum_{m\mathbf{x}} |\phi_{\mathbf{x}}^m(\mathbf{x})|^2 \quad (8.4)$$

is a real, single-component function. $\rho(\mathbf{x})$ is gauge and rotationally invariant. This is proven in Appendix D.

We were interested in behavior of the wavefunctions inside and outside flat valleys of the potential. To this end we identified the directions in the configurations space in which the potential vanishes and grows most rapidly. For $SU(2)$ this was done with invariants (7.17) introduced in [42]. There is one direction in the space of gauge and rotation invariants where the potential is flat and there are two steep directions. We observed that the low energy wave functions converge to a fixed shape as the cutoff grows. They are a little stretched along the flat valleys, as one may expect. On the contrary, the scattering states penetrate the flat valleys deeper for increasing N_B (Fig. 7.3). They remain localized in the steep direction.

For $SU(3)$ structure of the potential was studied in a fixed gauge. The full procedure of fixing the gauge is given in Appendix E. As for $SU(2)$, there are two one-dimensional steep directions. The flat direction is six dimensional. The flat valley can be parameterized by three angles which correspond to rotations and three rotation invariants. As it was pointed out, $\rho(\mathbf{x})$ does not depend on rotations. Moreover, it turned out that in all studied cases $\rho(\mathbf{x})$ depends only on the radius $r = (x_i^a x_i^a)^{1/2}$. For small n_F the energy eigenstates correspond to discrete energy levels. Convergence of $\rho(\mathbf{x})$ to a fixed shape is observed (Fig. 7.7). The available cutoff for large n_F is small and the studies of wavefunctions in these sectors are preliminary.

To summarize, we analyzed the supersymmetric Yang-Mills quantum mechanics in four dimensions with $SU(2)$ and $SU(3)$ gauge groups. The case of $SU(2)$ was already considered before and served mainly as a check of the program for numerical calculations. Results for $SU(3)$ with fermions are original. Only the purely bosonic channel was addressed in earlier papers. The studies were performed with the cut Fock space method. On the technical side, we identified independent bricks which generate basis of the Hilbert space and developed a recursive algorithm for constructing matrices of relevant operators in the occupation number basis. The program worked nicely. Results are consistent with previous results for $SU(2)$ and the purely bosonic sector for $SU(3)$. Dimensions of $\mathcal{H}_{\mathbf{n}}$ calculated analytically and numerically agree.

The numerical results provide information about dynamics of zero modes of the supersymmetric Yang-Mills theory. In the sector with no fermions the spectrum is discrete. Although the potential has flat valleys, the transverse oscillations give rise to an effective potential. It prevents wavefunctions from propagating in these directions. The situation is identical for small number of fermions. Only in channels rich in fermions the supersymmetric cancelations of bosonic and fermionic degrees of freedom is possible. Then the effective potential vanishes and flat valleys are open. The spectrum becomes continuous. For $SU(2)$ this happens already for two fermions and for $SU(3)$ the smallest required number of fermions is $n_F = 5$ or 6. Because of the particle-hole symmetry, spectra for number of fermions large enough are again discrete.

The supersymmetry is broken for finite cutoff N_B . It is recovered for $N_B \rightarrow \infty$ and then all states are grouped in supermultiplets. A full angular momentum and supersymmetry multiplet is labeled by (n_F, j, E) where (n_F, j) are the number of fermions and total angular momentum of the Clifford vacuum (cf. Chapter 6). All $8j + 4$ states of the

multiplet are degenerate and have energy E . Restoration of the supersymmetric structure takes place first for low energy states and is best seen for small n_F . Four supermultiplets were completely identified and for eighteen more there is one state missing (due to the finite cutoff effects).

Finally, the wavefunctions were analyzed. In earlier papers [42, 43] only wavefunctions of s-waves were studied (and thus only channels with two fermions were available). In this thesis we developed a new method that gives access to all (n_F, j) sectors. We have shown for $SU(2)$ that the bound states converge to a fixed shape for $N_B \rightarrow \infty$. On the other hand, the scattering states penetrate the flat valleys of the potential deeper as the cutoff grows. Analogous study of the $SU(3)$ case shows similar behavior of bound states.

Appendix A

Symmetries

In this chapter we discuss symmetries of the Hamiltonian. The Hamiltonian conserves angular momentum, total number of fermions and supercharge. Apart from these there is a particle–hole symmetry which relates sectors with n_F and $2(N^2 - 1) - n_F$ fermions. All these symmetries were mentioned in Chapter 2. Here they are analyzed in more detail. In the following part we use definitions of operators introduced in Chapter 2. Recall definition of the Hamiltonian:

$$\begin{aligned}
 H &= H_K + g^2 H_V + g H_F, \\
 H_K &= \frac{1}{2} p_i^a p_i^a, \\
 H_V &= \frac{1}{4} f^{abc} f^{ade} x_i^b x_j^c x_i^d x_j^e, \\
 H_F &= \frac{i}{2} f^{abc} \psi^{a\dagger} \gamma^0 \gamma^k \psi^b x_k^c.
 \end{aligned} \tag{A.1}$$

The Majorana spinor ψ is

$$\psi^a = e^{i\pi/4} \begin{pmatrix} -f_1^a \\ -f_2^a \\ f_2^{a\dagger} \\ -f_1^{a\dagger} \end{pmatrix}. \tag{A.2}$$

A.1 Number of fermions

The operator of the total number of fermions is

$$n_F = \sum_{\alpha,a} f_\alpha^{a\dagger} f_\alpha^a. \tag{A.3}$$

It is more convenient to write it in terms of ψ . One can find that the matrix γ^5 is given by

$$\gamma^5 = \begin{pmatrix} -1 & 0 & 0 & 0 \\ 0 & -1 & 0 & 0 \\ 0 & 0 & 1 & 0 \\ 0 & 0 & 0 & 1 \end{pmatrix}. \tag{A.4}$$

Then, it is easy to check that

$$n_F = 8 - \frac{1}{2}\psi^{a\dagger}\gamma^5\psi^a. \quad (\text{A.5})$$

The kinetic part and potential obviously do not change the number of fermions. One needs to show that H_F commutes with $\psi^{a\dagger}\gamma^5\psi^a$:

$$\begin{aligned} [H_F, \psi^{a\dagger}\gamma^5\psi^a] &= \frac{i}{2}f^{abc}[\psi^{a\dagger}\gamma^0\gamma^k\psi^b, \psi^{d\dagger}\gamma^5\psi^d]x_k^c \\ &= \frac{i}{2}f^{abc}x_k^c (\psi^{a\dagger}\gamma^0\gamma^k\gamma^5\psi^b - \psi^{a\dagger}\gamma^5\gamma^0\gamma^k\psi^b) \\ &= \frac{i}{2}f^{abc}x_k^c\psi^{a\dagger} (\gamma^0\gamma^k\gamma^5 - \gamma^5\gamma^0\gamma^k) \psi^b \\ &= 0. \end{aligned} \quad (\text{A.6})$$

Finally, conservation of the total number of fermions is proven.

This symmetry is in practice the most important one in calculating spectrum of SYMQM. One can consider each sector with definite n_F separately and the full Hilbert space splits into $2(N^2 - 1)$ parts. Taking a channel with definite n_F is easier than e.g. taking states with definite angular momentum.

A.2 Parity

In Chapter 2 we noted that the Hilbert space breaks the parity symmetry. It is a consequence of the condition that ψ has to be a Majorana spinor. We will now show how this happens in detail. Color indices are irrelevant for this discussion and are implicit throughout this part.

First, take a Dirac spinor ψ . It can be parameterized in a convenient way by two 2-component spinors ζ and χ . These can be used to form left- and right-handed spinors

$$\psi_L = \begin{pmatrix} \zeta \\ 0 \end{pmatrix}, \quad \psi_R = \begin{pmatrix} 0 \\ \chi \end{pmatrix}. \quad (\text{A.7})$$

Next, ζ is used to build a Majorana spinor ψ_M . In turn, χ is used to construct an 'anti-Majorana' spinor $\psi_{\bar{M}}$, i.e. $\psi_{\bar{M}}$ satisfies the Majorana condition with a '-' sign $(\psi_{\bar{M}})_C = -\psi_{\bar{M}}$. The explicit formulas are

$$\psi_M = \psi_L + (\psi_L)_C = \begin{pmatrix} \zeta \\ \bar{\zeta} \end{pmatrix}, \quad \psi_{\bar{M}} = \psi_R - (\psi_R)_C = \begin{pmatrix} \bar{\chi} \\ \chi \end{pmatrix}, \quad (\text{A.8})$$

where $\bar{\zeta} \equiv -\sigma_2\zeta^*$. A sum of ψ_M and $\psi_{\bar{M}}$ gives a general, Dirac spinor

$$\psi = \frac{1}{\sqrt{2}}(\psi_M + \psi_{\bar{M}}) = \frac{1}{\sqrt{2}} \begin{pmatrix} \zeta + \bar{\chi} \\ \bar{\zeta} + \chi \end{pmatrix}. \quad (\text{A.9})$$

The parity transformation interchanges the left- and right-handed spinors. Indeed,

$$\psi \rightarrow \psi_P \equiv \frac{1}{\sqrt{2}} \begin{pmatrix} \zeta_P + \bar{\chi}_P \\ \bar{\zeta}_P + \chi_P \end{pmatrix} = \gamma^0\psi = \frac{1}{\sqrt{2}} \begin{pmatrix} \bar{\zeta} + \chi \\ \zeta + \bar{\chi} \end{pmatrix}. \quad (\text{A.10})$$

It follows that $\zeta_P = \chi$ and $\chi_P = \zeta$. One can also see that $(\psi_{\bar{M}})_C$ is a Majorana spinor while $(\psi_M)_C$ is 'anti-Majorana'.

We quantize the system by imposing standard anticommutation relations on ζ and χ :

$$\begin{aligned} \{\zeta_\alpha, \zeta_\beta\} &= \{\zeta_\alpha^\dagger, \zeta_\beta^\dagger\} = 0, & \{\zeta_\alpha, \zeta_\beta^\dagger\} &= \delta_{\alpha\beta}, \\ \{\chi_\alpha, \chi_\beta\} &= \{\chi_\alpha^\dagger, \chi_\beta^\dagger\} = 0, & \{\chi_\alpha, \chi_\beta^\dagger\} &= \delta_{\alpha\beta}. \end{aligned} \quad (\text{A.11})$$

Then the Dirac spinor ψ satisfies

$$\{\psi_\alpha, \psi_\beta\} = \{\psi_\alpha^\dagger, \psi_\beta^\dagger\} = 0, \quad \{\psi_\alpha, \psi_\beta^\dagger\} = \delta_{\alpha\beta}. \quad (\text{A.12})$$

The empty state $|0\rangle$ is defined by

$$\zeta_\alpha |0\rangle = \chi_\alpha |0\rangle = 0. \quad (\text{A.13})$$

The other states in the Hilbert space are generated by repeatedly acting with ζ_α^\dagger and χ_α^\dagger on $|0\rangle$.

We are interested in parity–transformation of states. The parity–transformed empty state satisfies conditions

$$(\zeta_P)_\alpha |0\rangle_P = (\chi_P)_\alpha |0\rangle_P = 0. \quad (\text{A.14})$$

We see that $|0\rangle_P = |0\rangle$, i.e. $|0\rangle$ is invariant under parity. Take now a different state, e.g. $|s\rangle = \zeta_1^\dagger |0\rangle$. The transformed state is

$$|s\rangle_P = (\zeta_P)_1^\dagger |0\rangle = (\chi)_1^\dagger |0\rangle. \quad (\text{A.15})$$

Recall that for the Yang–Mills quantum mechanics to be supersymmetric a condition $\psi = \psi_M$ has to be imposed. Therefore, ψ contains only ζ and not χ . The Hilbert space consists of the empty state $|0\rangle$ and all states obtained by acting with ζ_α^\dagger on it. Therefore, $|s\rangle$ is an element of the Hilbert space, but $|s\rangle_P$ is not. In fact, only $|0\rangle$ survives the parity transformation. We can see that the parity is broken on the level of the Hilbert space.

A.3 Particle – hole symmetry

The particle–hole transformation of operators is the following:

$$\begin{aligned} \psi^a &\rightarrow \psi_{ph}^a = e^{i\pi/4} \begin{pmatrix} f_2^{a\dagger} \\ -f_1^{a\dagger} \\ f_1^a \\ f_2^a \end{pmatrix} = \gamma^0 \gamma^5 \psi^a, \\ x_i^a &\rightarrow -x_i^a. \end{aligned} \quad (\text{A.16})$$

In the view of the discussion on parity, it is important to note that ψ_{ph} is a Majorana spinor. Now, it has to be shown that it is a symmetry of the Hamiltonian. Obviously, the kinetic terms and potential do not change under the particle–hole transformation. Proof for the last term is following:

$$\begin{aligned} H_F &\rightarrow -\frac{i}{2} f^{abc} \psi_{ph}^{a\dagger} \gamma^0 \gamma^k \psi_{ph}^b x_k^c = -\frac{i}{2} f^{abc} \psi^{a\dagger} \gamma^5 \gamma^0 \gamma^0 \gamma^k \gamma^0 \gamma^5 \psi^b x_k^c \\ &= \frac{i}{2} f^{abc} \psi^{a\dagger} \gamma^0 \gamma^k \psi^b x_k^c = H_F. \end{aligned} \quad (\text{A.17})$$

Therefore, this is a true symmetry.

The name of this symmetry lies in the transformation of states. The transformation of fermionic operators is

$$f_1^a \rightarrow -f_2^{a\dagger}, \quad f_2^a \rightarrow f_1^{a\dagger}. \quad (\text{A.18})$$

Therefore, the definition of empty state transforms into

$$f_\alpha^{a\dagger} |0\rangle_{ph} = 0, \quad (\text{A.19})$$

i.e. $|0\rangle_{ph}$ is the state with the maximal number of fermions

$$|0\rangle_{ph} = \prod_{a,\alpha} f_\alpha^{a\dagger} |0\rangle. \quad (\text{A.20})$$

One can readily see that a state $|\phi\rangle$ with n_F fermions transforms to state $|\phi\rangle_{ph}$ with $2(N^2 - 1) - n_F$ fermions. It follows that the spectra in corresponding fermionic sectors are the same and one needs to study only $n_F \leq N^2 - 1$.

A.4 Conservation of supercharge

The proof of supercharge conservation is much simpler in the Majorana representation. The Gamma matrices in this representation are

$$\begin{aligned} \gamma^0 &= \begin{pmatrix} 0 & \sigma_2 \\ \sigma_2 & 0 \end{pmatrix}, & \gamma^1 &= \begin{pmatrix} 0 & -\sigma_1 \\ -\sigma_1 & 0 \end{pmatrix}, \\ \gamma^2 &= \begin{pmatrix} \mathbf{1} & 0 \\ 0 & -\mathbf{1} \end{pmatrix}, & \gamma^3 &= \begin{pmatrix} 0 & -\sigma_3 \\ -\sigma_3 & 0 \end{pmatrix}. \end{aligned} \quad (\text{A.21})$$

Note that $(\gamma^0)^T = -\gamma^0$, $(\gamma^i)^T = \gamma^i$. In Majorana representation the alpha matrices are real, i.e. $\Gamma_k = \Gamma_k^*$, where $*$ denotes complex conjugation. It follows that $\Sigma_{jk}^* = -\Sigma_{jk}$.

The charge conjugation matrix is

$$C = \begin{pmatrix} 0 & -i\sigma_2 \\ -i\sigma_2 & 0 \end{pmatrix}. \quad (\text{A.22})$$

The Majorana condition for spinor ψ written explicitly reads

$$\psi_\alpha^a = (\psi_C)_\alpha^a \equiv -iC_{\alpha\beta}(\gamma^0)_{\gamma\beta}\psi_\gamma^{a\dagger} = \psi_\alpha^{a\dagger}. \quad (\text{A.23})$$

Supercharges are also self-conjugate. Indeed,

$$\begin{aligned} Q_\alpha^\dagger &= (\Gamma_k^* \psi^{a\dagger})_\alpha p_k^a - igf^{abc}(\Sigma_{jk}^* \psi^{a\dagger})_\alpha x_j^b x_k^c \\ &= (\Gamma_k \psi^a)_\alpha p_k^a - igf^{abc}(-\Sigma_{jk} \psi^a)_\alpha x_j^b x_k^c = Q_\alpha. \end{aligned} \quad (\text{A.24})$$

The Hamiltonian has a particularly simple form

$$H = \frac{1}{2} \{Q_\alpha, Q_\alpha^\dagger\} = Q_\alpha Q_\alpha, \quad (\text{A.25})$$

where no summation over α is performed. Obviously, it commutes with Q_α .

Conservation of supercharge gives rise to supersymmetry multiplets. These multiplets consist of four states in different n_F channels. One can combine multiplets of the supersymmetry and angular momentum. This gives rise to $8j+4$ -dimensional representation of the two algebras. It consists of $2j+1$ states with angular momentum j and n_F fermions, angular momentum multiplets with $j' = j + 1/2$ and $j' = j - 1/2$ in $n_F + 1$ channel and a multiplet with $j' = j$ with $n_F + 2$. These multiplets are studied in detail in Chapter 6.

Appendix B

Absence of vector states in the bosonic sector for $SU(2)$

It is shown that for the $SU(2)$ gauge group there are no states with angular momentum $j = 1$ and no fermions. This proof is done after [31]. For a proof by contradiction, assume that $\psi_i(x)$ is a wavefunction with $j = 1$. Variable x_i^a has an adjoint color index $a = 1, 2, 3$ and space index $i = 1, 2, 3$. For convenience it will be treated as a matrix where a stands for the row index and i for the column index. Gauge transformations and rotations are represented by orthogonal matrices $R, S \in SO(3)$ and they act on x_i^a as left and right multiplication respectively

$$x_i^a \rightarrow x_i'^a = R^{ab} x_j^b S_{ji}. \quad (\text{B.1})$$

The wavefunction is a gauge singlet and vector with respect to rotations:

$$\psi_i(x') \equiv \psi_i(RxS) = \psi_j(x) S_{ji} \quad (\text{B.2})$$

The matrix x can be diagonalized with two matrices $R, S \in SO(3)$ [64], i.e. $x = RdS$ where d is a diagonal matrix. Then

$$\psi_i(x) = \psi_j(d) S_{ji}. \quad (\text{B.3})$$

Let us fix the index i . Consider a diagonal matrix $D \in SO(3)$ such that $D_{ii} = -1$ and the other two diagonal elements are -1 and 1 . Clearly, d and D commute. It follows that

$$\psi_i(d) = \psi_i(DDd) = \psi_i(DdD) = \psi_j(d) D_{ji} = -\psi_i(d). \quad (\text{B.4})$$

This implies $\psi_i(d) = 0$ and it holds for each $i = 1, 2, 3$ and all d . From (B.3) it follows that $\psi_i(x) = 0$ for all x . The wavefunction must vanish identically and therefore a vector state cannot exist.

*APPENDIX B. ABSENCE OF VECTOR STATES IN THE BOSONIC SECTOR
FOR SU(2)*

Appendix C

Finiteness of the recursive algorithm

In 3.3 we presented a recursive algorithm for finding matrix elements of operators in the Fock space representation. In each step of this algorithm one needs to find matrix elements of other operators (cf. formula (3.29)). It needs to be shown that such procedure is finite. This is done in this chapter. All symbols defined here are introduced in 3.3.

In a given step of the algorithm a matrix element $A|_{\mathbf{n}'\mathbf{n}}$ is calculated. Assume that the annihilation rank ν of A is not smaller than the annihilation rank $\bar{\nu}$ of A^\dagger . Otherwise, one would construct matrix element of A^\dagger and use the relation $A|_{\mathbf{n}'\mathbf{n}} = (A^\dagger|_{\mathbf{n}\mathbf{n}'})^\dagger$.

Let $L(A)$ be the length of the trace operator A and $|\mathbf{n}| = \sum_\alpha n_F^\alpha + \sum_i n_B^i$ be a norm of the occupation number \mathbf{n} . We define *recursion level* of the block $A|_{\mathbf{n}'\mathbf{n}}$ by

$$R(A, \mathbf{n}', \mathbf{n}) = L(A) + |\mathbf{n}| + |\mathbf{n}'|. \quad (\text{C.1})$$

It will be shown that one needs only matrix elements with smaller recursion level to construct the block $A|_{\mathbf{n}'\mathbf{n}}$.

There is a triangle inequality for $L(A)$, $|\mathbf{n}|$ and $|\mathbf{n}'|$. Namely, each quantity is not greater than the sum of the two others. In particular, $|\mathbf{n}| \leq L(A) + |\mathbf{n}'|$. If A consisted only of creation operators, then we would have $|\mathbf{n}'| = L(A) + |\mathbf{n}|$. However, we assumed that $\nu \geq \bar{\nu}$, so A contains at least one annihilation operator. Therefore, $|\mathbf{n}'| < L(A) + |\mathbf{n}|$.

First we show that $(A\mathcal{B}_i)|_{\mathbf{n}'\mathbf{n}_i}$, which are building blocks of $A|_{\mathbf{n}'\mathbf{n}}$ (formula (3.29)) have recursion levels smaller than $R(A, \mathbf{n}', \mathbf{n})$. The operator \mathcal{B}_i is a brick, so it is composed only of creation operators and therefore $L(\mathcal{B}_i) + |\mathbf{n}_i| = |\mathbf{n}|$. It is easy to check that the maximally annihilating permutation of $A\mathcal{B}_i$ is $\mathcal{B}_i A$. Therefore, the maximally annihilating form of $A\mathcal{B}_i$ is $\pm \mathcal{B}_i A + \mathcal{R}$. The sign is '-' if both, A and \mathcal{B}_i are fermionic and '+' otherwise. The remainder $\mathcal{R} = \sum_k \alpha_k \prod_l C_{kl}$ is a combination of products of trace operators. The length of operator \mathcal{R} is defined by $L(\mathcal{R}) = \max_k \sum_l L(C_{kl})$.

\mathcal{R} originates from commutators of operators in the product $A\mathcal{B}_i$. A commutator of creation and annihilation operator is proportional to identity. Therefore, each commutation removes two operators from the product, so $L(\mathcal{R}) < L(A) + L(\mathcal{B}_i)$. The block $\mathcal{R}|_{\mathbf{n}'\mathbf{n}_i}$ is a combination of products of blocks $C_{kl}|_{\mathbf{n}'_{kl}\mathbf{n}_{kl}}$. For each k, l

$$\begin{aligned} R(C_{kl}, \mathbf{n}'_{kl}, \mathbf{n}_{kl}) &= L(C_{kl}) + |\mathbf{n}'_{kl}| + |\mathbf{n}_{kl}| \\ &\leq L(C_{kl}) + \left(|\mathbf{n}'| + \sum_{i < l} L(C_{ki}) \right) + \left(|\mathbf{n}_i| + \sum_{i > l} L(C_{ki}) \right) \\ &\leq L(\mathcal{R}) + |\mathbf{n}'| + |\mathbf{n}_i| < L(A) + L(\mathcal{B}) + |\mathbf{n}'| + |\mathbf{n}_i| \\ &= L(A) + |\mathbf{n}'| + |\mathbf{n}| = R(A, \mathbf{n}, \mathbf{n}'). \end{aligned} \quad (\text{C.2})$$

The block $(\mathcal{B}_i A)|_{\mathbf{n}'\mathbf{n}}$ is calculated as a product of $\mathcal{B}_i|_{\mathbf{n}'\mathbf{n}'_i}$ and $A|_{\mathbf{n}'_i\mathbf{n}}$ where $\mathbf{n}'_i = \mathbf{n}' - \hat{\mathbf{n}}_i$ and $\hat{\mathbf{n}}_i$ is the creation label of \mathcal{B}_i . The brick \mathcal{B}_i contains only creation operators, so $|\mathbf{n}'_i| = |\mathbf{n}'| - |\hat{\mathbf{n}}_i|$ and $L(\mathcal{B}_i) = |\hat{\mathbf{n}}_i|$. Recursion levels of these blocks are

$$\begin{aligned} R(\mathcal{B}_i, \mathbf{n}', \mathbf{n}'_i) &= L(\mathcal{B}_i) + |\mathbf{n}'| + |\mathbf{n}'_i| = L(\mathcal{B}_i) + 2|\mathbf{n}'| - |\hat{\mathbf{n}}_i| = 2|\mathbf{n}'| < R(A, \mathbf{n}', \mathbf{n}), \\ R(A, \mathbf{n}'_i, \mathbf{n}) &= L(A) + |\mathbf{n}'_i| + |\mathbf{n}| = L(A) + |\mathbf{n}'| + |\mathbf{n}| - L(\mathcal{B}_i) < R(A, \mathbf{n}', \mathbf{n}). \end{aligned} \quad (\text{C.3})$$

We have shown that each element in the block matrix (3.29) has recursion level smaller than $R(A, \mathbf{n}', \mathbf{n})$.

It remains to calculate the recursion levels of block in the Gramm matrix. The product of two bricks $\mathcal{B}_i^\dagger \mathcal{B}_j$ transformed into its maximally annihilating form is $\mathcal{B}_j \mathcal{B}_i^\dagger + \mathcal{R}'$. The block $\mathcal{B}_i^\dagger \mathcal{B}_j|_{\mathbf{n}_i \mathbf{n}_j}$ is a sum of $\mathcal{B}_j \mathcal{B}_i^\dagger|_{\mathbf{n}_i \mathbf{n}_j} = \mathcal{B}_j|_{\mathbf{n}_i \mathbf{n}_{ij}} \times \mathcal{B}_i^\dagger|_{\mathbf{n}_{ij} \mathbf{n}_j}$ and $\mathcal{R}'|_{\mathbf{n}_i \mathbf{n}_j}$. Here, $\mathbf{n}_{ij} \equiv \mathbf{n} - \hat{\mathbf{n}}_i - \hat{\mathbf{n}}_j$ and we know that $|\mathbf{n}_{ij}| = |\mathbf{n}| - |\hat{\mathbf{n}}_i| - |\hat{\mathbf{n}}_j| = |\mathbf{n}| - L(\mathcal{B}_i) - L(\mathcal{B}_j)$. Recursion levels of these three blocks are following

$$\begin{aligned} R(\mathcal{B}_j, \mathbf{n}_i, \mathbf{n}_{ij}) &= 2|\mathbf{n}| - 2L(\mathcal{B}_i) \leq R(A, \mathbf{n}', \mathbf{n}) - 2L(\mathcal{B}_i), \\ R(\mathcal{B}_i^\dagger, \mathbf{n}_{ij}, \mathbf{n}_j) &= 2|\mathbf{n}| - 2L(\mathcal{B}_j) \leq R(A, \mathbf{n}', \mathbf{n}) - 2L(\mathcal{B}_j), \\ R(\mathcal{R}', \mathbf{n}_i, \mathbf{n}_j) &= L(\mathcal{R}') + |\mathbf{n}_i| + |\mathbf{n}_j| < L(\mathcal{B}_i) + L(\mathcal{B}_j) + |\mathbf{n}_i| + |\mathbf{n}_j| \\ &= 2|\mathbf{n}| \leq R(A, \mathbf{n}', \mathbf{n}) - 2L(\mathcal{B}_j). \end{aligned} \quad (\text{C.4})$$

We have shown that the recursion levels of all blocks that we need to construct $A|_{\mathbf{n}'\mathbf{n}}$ are smaller than the recursion level of the block itself. It was assumed that $|\mathbf{n}| \neq 0$. If $|\mathbf{n}|$ is zero, then the block is calculated in the sector containing only the empty state. Since we know that the first component of annihilation rank of A is positive, it annihilates Fock vacuum and the block vanishes. The recursion level is always nonnegative and it is zero only for identity operator in the Fock vacuum state. Therefore, one needs only a finite number of recursive steps to construct a given block. In order to construct $A|_{\mathbf{n}'\mathbf{n}}$ one needs at most $R(A, \mathbf{n}', \mathbf{n})$ steps.

Appendix D

Construction of zero angular momentum functions

In 7.2 we constructed the probability density $\rho(\mathbf{x})$. Given an angular momentum multiplet $|\phi^m\rangle$ with total angular momentum j we constructed a wavefunction $\phi_{\boldsymbol{\chi}}^m(\mathbf{x})$, where $\boldsymbol{\chi}$ labels occupation numbers of fermions. Then the probability distribution is given by

$$\begin{aligned}\rho(\mathbf{x}) &= \sum_{m\boldsymbol{\chi}} |\phi_{\boldsymbol{\chi}}^m(\mathbf{x})|^2 \\ &= \sum_{m\boldsymbol{\chi}} \langle \mathbf{x}\boldsymbol{\chi} | \phi^m \rangle \langle \phi^m | \mathbf{x}\boldsymbol{\chi} \rangle\end{aligned}\tag{D.1}$$

$\rho(\mathbf{x})$ is gauge and rotationally invariant. Invariance under gauge transformation is obvious since the wavefunction $\phi_{\boldsymbol{\chi}}^m(\mathbf{x})$ is gauge invariant. Here we prove invariance under rotations, i.e.

$$L^2 \rho(\mathbf{x}) = 0,\tag{D.2}$$

where $L_i = \epsilon_{ijk} x_j p_k^a$ is an orbital momentum operator.

First, we introduce some useful notation. The symbol $\boldsymbol{\chi}$ has $2(N^2 - 1)$ components χ_{α}^a . In a sector with n_F fermions there are n_F components of $\boldsymbol{\chi}$ which have value 1 and the other elements are zeros. $\boldsymbol{\chi}$ can be alternatively written as a pair $(\mathbf{a}, \boldsymbol{\alpha})$ where $\mathbf{a} = (a_1, \dots, a_{n_F})$, $\boldsymbol{\alpha} = (\alpha_1, \dots, \alpha_{n_F})$ are color and spinor indices for which $\chi_{\alpha_i}^{a_i} = 1$. The range of indices is $a_i = 1, \dots, 8$, $\alpha_i = \pm \frac{1}{2}$. We assume that pairs (a_i, α_i) are ordered in some way. Then the wavefunction of $|\phi^m\rangle$ can be written as $\langle \mathbf{x}\mathbf{a}\boldsymbol{\alpha} | \phi^m \rangle$.

Complex conjugation of the wavefunction can be transformed by using properties of time reversal operation

$$\begin{aligned}\langle \phi^m | \mathbf{x}\mathbf{a}\boldsymbol{\alpha} \rangle &= {}_T \langle \mathbf{x}\mathbf{a}\boldsymbol{\alpha} | \phi^m \rangle_T, \\ |\phi^m \rangle_T &= (-1)^m |\phi^{-m} \rangle, \\ |\mathbf{x}\mathbf{a}\boldsymbol{\alpha} \rangle_T &= (-1)^{m_{\boldsymbol{\alpha}}} |\mathbf{x}\mathbf{a} - \boldsymbol{\alpha} \rangle.\end{aligned}\tag{D.3}$$

where $m_{\boldsymbol{\alpha}} = \sum_i \alpha_i$. Then, the probability density $\rho(\mathbf{x})$ can be expressed as

$$\rho(\mathbf{x}) \equiv \sum_{\mathbf{a}\boldsymbol{\alpha}m} |\langle \mathbf{x}\mathbf{a}\boldsymbol{\alpha} | \phi^m \rangle|^2 = \sum_{\mathbf{a}\boldsymbol{\alpha}m} (-1)^{m+m_{\boldsymbol{\alpha}}} \langle \mathbf{x}\mathbf{a}\boldsymbol{\alpha} | \phi^m \rangle \langle \mathbf{x}\mathbf{a} - \boldsymbol{\alpha} | \phi^{-m} \rangle.\tag{D.4}$$

APPENDIX D. CONSTRUCTION OF ZERO ANGULAR MOMENTUM FUNCTIONS

The orbital angular momentum operator can be written as

$$L^2 = L_3^2 + \frac{1}{2}L_-L_+ + \frac{1}{2}L_+L_-, \quad (\text{D.5})$$

where $L_\pm = L_1 \pm iL_2$. From now on indices i, j will take values $\{+, -, 3\}$. The angular momentum L_i is a differential operator and it satisfies the Leibniz rule. For any two different states $|\psi_1\rangle$ and $|\psi_2\rangle$ there is

$$\begin{aligned} L_i(\langle \mathbf{x}|\psi_1\rangle \langle \mathbf{x}|\psi_2\rangle) &= (L_i \langle \mathbf{x}|\psi_1\rangle) \langle \mathbf{x}|\psi_2\rangle + \langle \mathbf{x}|\psi_1\rangle (L_i \langle \mathbf{x}|\psi_2\rangle) \\ &= \langle \mathbf{x}|L_i|\psi_1\rangle \langle \mathbf{x}|\psi_2\rangle + \langle \mathbf{x}|\psi_1\rangle \langle \mathbf{x}|L_i|\psi_2\rangle. \end{aligned} \quad (\text{D.6})$$

Relation (D.6) applied to (D.4) gives

$$\begin{aligned} L_i L_j \rho(\mathbf{x}) &= \sum_{\alpha\alpha m} (-1)^{m+m_\alpha} \left(\right. \\ &\quad \langle \mathbf{x}\alpha\alpha|L_i L_j|\phi^m\rangle \langle \mathbf{x}\mathbf{a} - \alpha|\phi^{-m}\rangle + \langle \mathbf{x}\alpha\alpha|L_i|\phi^m\rangle \langle \mathbf{x}\mathbf{a} - \alpha|L_j|\phi^{-m}\rangle + \\ &\quad \left. \langle \mathbf{x}\alpha\alpha|L_j|\phi^m\rangle \langle \mathbf{x}\mathbf{a} - \alpha|L_i|j - m\rangle + \langle \mathbf{x}\alpha\alpha|\phi^m\rangle \langle \mathbf{x}\mathbf{a} - \alpha|L_i L_j|\phi^{-m}\rangle \right) \end{aligned} \quad (\text{D.7})$$

We plug the relation between total and orbital angular momentum, $L_i = J_i - S_i$, into (D.7) and gather terms with double J_i , double S_i and mixed.

$$L_i L_j \rho(\mathbf{x}) = \sum_{\alpha\alpha m} (-1)^{m+m_\alpha} ((\mathcal{J}\mathcal{J})_{ij} + (\mathcal{J}\mathcal{S})_{ij} + (\mathcal{S}\mathcal{S})_{ij}). \quad (\text{D.8})$$

The corresponding terms are

$$\begin{aligned} (\mathcal{J}\mathcal{J})_{ij} &= \langle \mathbf{x}\alpha\alpha|J_i J_j|\phi^m\rangle \langle \mathbf{x}\mathbf{a} - \alpha|\phi^{-m}\rangle + \langle \mathbf{x}\alpha\alpha|J_i|\phi^m\rangle \langle \mathbf{x}\mathbf{a} - \alpha|J_j|\phi^{-m}\rangle \\ &\quad + \langle \mathbf{x}\alpha\alpha|J_j|\phi^m\rangle \langle \mathbf{x}\mathbf{a} - \alpha|J_i|\phi^{-m}\rangle + \langle \mathbf{x}\alpha\alpha|\phi^m\rangle \langle \mathbf{x}\mathbf{a} - \alpha|J_i J_j|\phi^{-m}\rangle, \end{aligned} \quad (\text{D.9})$$

$$\begin{aligned} (\mathcal{J}\mathcal{S})_{ij} &= -\langle \mathbf{x}\alpha\alpha|S_i J_j|\phi^m\rangle \langle \mathbf{x}\mathbf{a} - \alpha|\phi^{-m}\rangle - \langle \mathbf{x}\alpha\alpha|J_i S_j|\phi^m\rangle \langle \mathbf{x}\mathbf{a} - \alpha|\phi^{-m}\rangle \\ &\quad - \langle \mathbf{x}\alpha\alpha|S_i|\phi^m\rangle \langle \mathbf{x}\mathbf{a} - \alpha|J_j|\phi^{-m}\rangle - \langle \mathbf{x}\alpha\alpha|J_i|\phi^m\rangle \langle \mathbf{x}\mathbf{a} - \alpha|S_j|\phi^{-m}\rangle \\ &\quad - \langle \mathbf{x}\alpha\alpha|S_j|\phi^m\rangle \langle \mathbf{x}\mathbf{a} - \alpha|J_i|\phi^{-m}\rangle - \langle \mathbf{x}\alpha\alpha|J_j|\phi^m\rangle \langle \mathbf{x}\mathbf{a} - \alpha|S_i|\phi^{-m}\rangle \\ &\quad - \langle \mathbf{x}\alpha\alpha|\phi^m\rangle \langle \mathbf{x}\mathbf{a} - \alpha|S_i J_j|\phi^{-m}\rangle - \langle \mathbf{x}\alpha\alpha|\phi^m\rangle \langle \mathbf{x}\mathbf{a} - \alpha|J_i S_j|\phi^{-m}\rangle, \end{aligned} \quad (\text{D.10})$$

$$\begin{aligned} (\mathcal{S}\mathcal{S})_{ij} &= \langle \mathbf{x}\alpha\alpha|S_i S_j|\phi^m\rangle \langle \mathbf{x}\mathbf{a} - \alpha|\phi^{-m}\rangle + \langle \mathbf{x}\alpha\alpha|S_i|\phi^m\rangle \langle \mathbf{x}\mathbf{a} - \alpha|S_j|\phi^{-m}\rangle \\ &\quad + \langle \mathbf{x}\alpha\alpha|S_j|\phi^m\rangle \langle \mathbf{x}\mathbf{a} - \alpha|S_i|\phi^{-m}\rangle + \langle \mathbf{x}\alpha\alpha|\phi^m\rangle \langle \mathbf{x}\mathbf{a} - \alpha|S_i S_j|\phi^{-m}\rangle. \end{aligned} \quad (\text{D.11})$$

Action of spin operators on kets $|\mathbf{x}\alpha\alpha\rangle$ can be easily read from (2.17)

$$S_3 |\mathbf{x}\alpha\alpha\rangle = \frac{1}{2} \sum_i \alpha_i |\mathbf{x}\alpha\alpha\rangle, \quad (\text{D.12})$$

$$S_+ |\mathbf{x}\alpha\alpha\rangle = \sum_k \delta_{\alpha_k, -1/2} |\mathbf{x}\alpha\alpha_+^k\rangle, \quad (\text{D.13})$$

$$S_- |\mathbf{x}\alpha\alpha\rangle = \sum_k \delta_{\alpha_k, 1/2} |\mathbf{x}\alpha\alpha_-^k\rangle. \quad (\text{D.14})$$

where

$$\alpha_\pm^k = (\alpha_1, \dots, \alpha_k \pm \frac{1}{2}, \dots, \alpha_{n_F}). \quad (\text{D.15})$$

In the following we consider $(\mathcal{J}\mathcal{J})_{ij}$, $(\mathcal{J}\mathcal{S})_{ij}$ and $(\mathcal{S}\mathcal{S})_{ij}$ separately. Moreover, in each case the sum over (i, j) splits into $(i, j) = (3, 3)$ and $(i, j) = (+, -), (-, +)$ and these vanish independently. For clarity, further considerations are organized in paragraphs.

Terms with double J_i .

$$\sum_m (-1)^{m+m\alpha} (\mathcal{J}\mathcal{J})_{33} \quad (\text{D.16})$$

$$= (m^2 + m(-m) + m(-m) + (-m)^2) \langle \mathbf{x}\mathbf{a}\mathbf{\alpha} | \phi^m \rangle \langle \mathbf{x}\mathbf{a} - \mathbf{\alpha} | \phi^{-m} \rangle = 0. \quad (\text{D.17})$$

Before we consider $(\mathcal{J}\mathcal{J})_{ij}$ with $i, j = \pm$, recall that

$$J_{\pm} |j, m\rangle = \sqrt{j(j+1) - m(m \pm 1)} |j, m \pm 1\rangle. \quad (\text{D.18})$$

$$\begin{aligned} & (\mathcal{J}\mathcal{J})_{-+} + (\mathcal{J}\mathcal{J})_{+-} \\ &= \sum_m (-1)^m \left(\right. \\ & \quad \frac{1}{2} (j(j+1) - m(m-1) + j(j+1) - m(m+1)) \langle \mathbf{x}\mathbf{a}\mathbf{\alpha} | \phi^m \rangle \langle \mathbf{x}\mathbf{a} - \mathbf{\alpha} | \phi^{-m} \rangle \\ & \quad + (j(j+1) - m(m+1)) \langle \mathbf{x}\mathbf{a}\mathbf{\alpha} | \phi^{m+1} \rangle \langle \mathbf{x}\mathbf{a} - \mathbf{\alpha} | \phi^{-(m+1)} \rangle \\ & \quad + (j(j+1) - m(m-1)) \langle \mathbf{x}\mathbf{a}\mathbf{\alpha} | \phi^{m-1} \rangle \langle \mathbf{x}\mathbf{a} - \mathbf{\alpha} | \phi^{-(m-1)} \rangle \\ & \quad \left. + \frac{1}{2} (j(j+1) - m(m+1) + j(j+1) - m(m-1)) \langle \mathbf{x}\mathbf{a}\mathbf{\alpha} | jm \rangle \langle \mathbf{x}\mathbf{a} - \mathbf{\alpha} | \phi^{-m} \rangle \right) \\ &= \sum_m (-1)^m \left(\right. \\ & \quad 2(j(j+1) - m^2) \langle \mathbf{x}\mathbf{a}\mathbf{\alpha} | \phi^m \rangle \langle \mathbf{x}\mathbf{a} - \mathbf{\alpha} | \phi^{-m} \rangle \\ & \quad + (j(j+1) - m(m+1)) \langle \mathbf{x}\mathbf{a}\mathbf{\alpha} | \phi^{m+1} \rangle \langle \mathbf{x}\mathbf{a} - \mathbf{\alpha} | \phi^{-(m+1)} \rangle \\ & \quad \left. + (j(j+1) - m(m-1)) \langle \mathbf{x}\mathbf{a}\mathbf{\alpha} | \phi^{m-1} \rangle \langle \mathbf{x}\mathbf{a} - \mathbf{\alpha} | \phi^{-(m-1)} \rangle \right) \\ &= \sum_m (-1)^m \left(\right. \\ & \quad 2(j(j+1) - m^2) \langle \mathbf{x}\mathbf{a}\mathbf{\alpha} | \phi^m \rangle \langle \mathbf{x}\mathbf{a} - \mathbf{\alpha} | \phi^{-m} \rangle \\ & \quad - (j(j+1) - (m-1)m) \langle \mathbf{x}\mathbf{a}\mathbf{\alpha} | \phi^m \rangle \langle \mathbf{x}\mathbf{a} - \mathbf{\alpha} | \phi^{-m} \rangle \\ & \quad \left. - (j(j+1) - (m+1)m) \langle \mathbf{x}\mathbf{a}\mathbf{\alpha} | \phi^m \rangle \langle \mathbf{x}\mathbf{a} - \mathbf{\alpha} | \phi^{-m} \rangle \right) \\ &= 0. \end{aligned} \quad (\text{D.19})$$

In the third equality terms with the same m were gathered, hence additional minus sign from $(-1)^m$.

Mixed terms. Note that $[J_3, S_3] = 0$.

$$\begin{aligned} (\mathcal{J}\mathcal{S})_{33} &= -m \langle \mathbf{x}\mathbf{a}\mathbf{\alpha} | S_3 | \phi^m \rangle \langle \mathbf{x}\mathbf{a} - \mathbf{\alpha} | \phi^{-m} \rangle - m \langle \mathbf{x}\mathbf{a}\mathbf{\alpha} | S_3 | \phi^m \rangle \langle \mathbf{x}\mathbf{a} - \mathbf{\alpha} | \phi^{-m} \rangle \\ & \quad + m \langle \mathbf{x}\mathbf{a}\mathbf{\alpha} | S_3 | \phi^m \rangle \langle \mathbf{x}\mathbf{a} - \mathbf{\alpha} | \phi^{-m} \rangle - m \langle \mathbf{x}\mathbf{a}\mathbf{\alpha} | \phi^m \rangle \langle \mathbf{x}\mathbf{a} - \mathbf{\alpha} | S_3 | \phi^{-m} \rangle \\ & \quad + m \langle \mathbf{x}\mathbf{a}\mathbf{\alpha} | S_3 | \phi^m \rangle \langle \mathbf{x}\mathbf{a} - \mathbf{\alpha} | \phi^{-m} \rangle - m \langle \mathbf{x}\mathbf{a}\mathbf{\alpha} | \phi^m \rangle \langle \mathbf{x}\mathbf{a} - \mathbf{\alpha} | S_3 | \phi^{-m} \rangle \\ & \quad + m \langle \mathbf{x}\mathbf{a}\mathbf{\alpha} | \phi^m \rangle \langle \mathbf{x}\mathbf{a} - \mathbf{\alpha} | S_3 | \phi^{-m} \rangle + m \langle \mathbf{x}\mathbf{a}\mathbf{\alpha} | \phi^m \rangle \langle \mathbf{x}\mathbf{a} - \mathbf{\alpha} | S_3 | \phi^{-m} \rangle \\ &= 0 \end{aligned} \quad (\text{D.20})$$

For $(i, j) = (+-), (-, +)$ in all brackets of the form $\langle \mathbf{x}\mathbf{a}\mathbf{\alpha} | J_i S_j | \psi \rangle$ we would like to move S_j to the left and use (D.12). Therefore, we need commutators of S_j with J_i . The required

relation is

$$\begin{aligned}
J_+S_- + J_-S_+ &= S_-J_+ + [J_+, S_-] + S_+J_- + [J_-, S_+] \\
&= S_-J_+ + [S_+, S_-] + S_+J_- + [S_-, S_+] \\
&= S_-J_+ + S_+J_-.
\end{aligned} \tag{D.21}$$

$$\begin{aligned}
&\frac{1}{2} \sum_m (-1)^m ((\mathcal{J}\mathcal{S})_{-+} + (\mathcal{J}\mathcal{S})_{+-}) \\
&= \sum_m (-1)^m \left(-\sqrt{j(j+1) - m(m+1)} \langle \mathbf{x}\mathbf{a}\mathbf{\alpha} | S_- | \phi^{m+1} \rangle \langle \mathbf{x}\mathbf{a} - \mathbf{\alpha} | \phi^{-m} \rangle \right. \\
&\quad - \sqrt{j(j+1) - m(m-1)} \langle \mathbf{x}\mathbf{a}\mathbf{\alpha} | S_+ | \phi^{m-1} \rangle \langle \mathbf{x}\mathbf{a} - \mathbf{\alpha} | \phi^{-m} \rangle \\
&\quad - \sqrt{j(j+1) - m(m-1)} \langle \mathbf{x}\mathbf{a}\mathbf{\alpha} | S_- | \phi^m \rangle \langle \mathbf{x}\mathbf{a} - \mathbf{\alpha} | \phi^{-(m-1)} \rangle \\
&\quad - \sqrt{j(j+1) - m(m+1)} \langle \mathbf{x}\mathbf{a}\mathbf{\alpha} | S_+ | \phi^m \rangle \langle \mathbf{x}\mathbf{a} - \mathbf{\alpha} | \phi^{-(m+1)} \rangle \\
&\quad - \sqrt{j(j+1) - m(m+1)} \langle \mathbf{x}\mathbf{a}\mathbf{\alpha} | \phi^{m+1} \rangle \langle \mathbf{x}\mathbf{a} - \mathbf{\alpha} | S_- | \phi^{-m} \rangle \\
&\quad - \sqrt{j(j+1) - m(m-1)} \langle \mathbf{x}\mathbf{a}\mathbf{\alpha} | \phi^{m-1} \rangle \langle \mathbf{x}\mathbf{a} - \mathbf{\alpha} | S_+ | \phi^{-m} \rangle \\
&\quad - \sqrt{j(j+1) - m(m-1)} \langle \mathbf{x}\mathbf{a}\mathbf{\alpha} | \phi^m \rangle \langle \mathbf{x}\mathbf{a} - \mathbf{\alpha} | S_- | \phi^{-(m-1)} \rangle \\
&\quad \left. - \sqrt{j(j+1) - m(m+1)} \langle \mathbf{x}\mathbf{a}\mathbf{\alpha} | \phi^m \rangle \langle \mathbf{x}\mathbf{a} - \mathbf{\alpha} | S_+ | \phi^{-(m+1)} \rangle \right) \\
&= \sum_m (-1)^m \left(+\sqrt{j(j+1) - m(m-1)} \langle \mathbf{x}\mathbf{a}\mathbf{\alpha} | S_- | \phi^m \rangle \langle \mathbf{x}\mathbf{a} - \mathbf{\alpha} | \phi^{-(m-1)} \rangle \right. \\
&\quad + \sqrt{j(j+1) - m(m+1)} \langle \mathbf{x}\mathbf{a}\mathbf{\alpha} | S_+ | \phi^m \rangle \langle \mathbf{x}\mathbf{a} - \mathbf{\alpha} | \phi^{-(m+1)} \rangle \\
&\quad - \sqrt{j(j+1) - m(m-1)} \langle \mathbf{x}\mathbf{a}\mathbf{\alpha} | S_- | \phi^m \rangle \langle \mathbf{x}\mathbf{a} - \mathbf{\alpha} | \phi^{-(m-1)} \rangle \\
&\quad - \sqrt{j(j+1) - m(m+1)} \langle \mathbf{x}\mathbf{a}\mathbf{\alpha} | S_+ | \phi^m \rangle \langle \mathbf{x}\mathbf{a} - \mathbf{\alpha} | \phi^{-(m+1)} \rangle \\
&\quad + \sqrt{j(j+1) - m(m-1)} \langle \mathbf{x}\mathbf{a}\mathbf{\alpha} | \phi^m \rangle \langle \mathbf{x}\mathbf{a} - \mathbf{\alpha} | S_- | \phi^{-(m-1)} \rangle \\
&\quad + \sqrt{j(j+1) - m(m+1)} \langle \mathbf{x}\mathbf{a}\mathbf{\alpha} | \phi^m \rangle \langle \mathbf{x}\mathbf{a} - \mathbf{\alpha} | S_+ | \phi^{-(m+1)} \rangle \\
&\quad - \sqrt{j(j+1) - m(m-1)} \langle \mathbf{x}\mathbf{a}\mathbf{\alpha} | \phi^m \rangle \langle \mathbf{x}\mathbf{a} - \mathbf{\alpha} | S_- | \phi^{-(m-1)} \rangle \\
&\quad \left. - \sqrt{j(j+1) - m(m+1)} \langle \mathbf{x}\mathbf{a}\mathbf{\alpha} | \phi^m \rangle \langle \mathbf{x}\mathbf{a} - \mathbf{\alpha} | S_+ | \phi^{-(m+1)} \rangle \right) \\
&= 0.
\end{aligned} \tag{D.22}$$

Terms with double S_i . In $(\mathcal{S}\mathcal{S})_{33}$ each S_3 acts to the left giving a constant m_α or $-m_\alpha$. Therefore,

$$(\mathcal{S}\mathcal{S})_{33} = (m_\alpha^2 - m_\alpha^2 - m_\alpha^2 + (-m_\alpha)^2) \langle \mathbf{x}\mathbf{a}\mathbf{\alpha} | \phi^m \rangle \langle \mathbf{x}\mathbf{a} - \mathbf{\alpha} | \phi^{-m} \rangle = 0 \tag{D.23}$$

Finally,

$$\begin{aligned}
& \sum_{\mathbf{a}\boldsymbol{\alpha}} (-1)^{m_{\boldsymbol{\alpha}}} ((\mathcal{S}\mathcal{S})_{+-} + (\mathcal{S}\mathcal{S})_{-+}) \\
&= \sum_{\mathbf{a}\boldsymbol{\alpha}} (-1)^{m_{\boldsymbol{\alpha}}} \left(\right. \\
&\quad + \frac{1}{2} \langle \mathbf{x}\mathbf{a}\boldsymbol{\alpha} | S_+^\dagger S_-^\dagger | \phi^m \rangle \langle \mathbf{x}\mathbf{a} - \boldsymbol{\alpha} | \phi^{-m} \rangle + \frac{1}{2} \langle \mathbf{x}\mathbf{a}\boldsymbol{\alpha} | S_-^\dagger S_+^\dagger | \phi^m \rangle \langle \mathbf{x}\mathbf{a} - \boldsymbol{\alpha} | \phi^{-m} \rangle \\
&\quad + \frac{1}{2} \langle \mathbf{x}\mathbf{a}\boldsymbol{\alpha} | \phi^m \rangle \langle \mathbf{x}\mathbf{a} - \boldsymbol{\alpha} | S_+^\dagger S_-^\dagger | \phi^{-m} \rangle + \frac{1}{2} \langle \mathbf{x}\mathbf{a}\boldsymbol{\alpha} | \phi^m \rangle \langle \mathbf{x}\mathbf{a} - \boldsymbol{\alpha} | S_-^\dagger S_+^\dagger | \phi^{-m} \rangle \\
&\quad \left. + \langle \mathbf{x}\mathbf{a}\boldsymbol{\alpha} | S_+^\dagger | \phi^m \rangle \langle \mathbf{x}\mathbf{a} - \boldsymbol{\alpha} | S_-^\dagger | \phi^{-m} \rangle + \langle \mathbf{x}\mathbf{a}\boldsymbol{\alpha} | S_-^\dagger | \phi^m \rangle \langle \mathbf{x}\mathbf{a} - \boldsymbol{\alpha} | S_+^\dagger | \phi^{-m} \rangle \right) \\
&= \sum_{\mathbf{a}\boldsymbol{\alpha}} (-1)^{m_{\boldsymbol{\alpha}}} \left(\right. \\
&\quad + \frac{1}{2} \sum_{kl} \langle \mathbf{x}\mathbf{a}(\boldsymbol{\alpha}_+^k)_-^l | \phi^m \rangle \langle \mathbf{x}\mathbf{a} - \boldsymbol{\alpha} | \phi^{-m} \rangle + \frac{1}{2} \sum_{kl} \langle \mathbf{x}\mathbf{a}(\boldsymbol{\alpha}_-^k)_+^l | \phi^m \rangle \langle \mathbf{x}\mathbf{a} - \boldsymbol{\alpha} | \phi^{-m} \rangle \\
&\quad + \frac{1}{2} \sum_{kl} \langle \mathbf{x}\mathbf{a}\boldsymbol{\alpha} | \phi^m \rangle \langle \mathbf{x}\mathbf{a} - (\boldsymbol{\alpha}_-^k)_+^l | \phi^{-m} \rangle + \frac{1}{2} \sum_{kl} \langle \mathbf{x}\mathbf{a}\boldsymbol{\alpha} | \phi^m \rangle \langle \mathbf{x}\mathbf{a} - (\boldsymbol{\alpha}_+^k)_-^l | \phi^{-m} \rangle \\
&\quad + \sum_{kl} \langle \mathbf{x}\mathbf{a}\boldsymbol{\alpha}_+^k | \phi^m \rangle \langle \mathbf{x}\mathbf{a} - (\boldsymbol{\alpha}_+^l)_- | \phi^{-m} \rangle + \sum_{kl} \langle \mathbf{x}\mathbf{a}\boldsymbol{\alpha}_-^k | \phi^m \rangle \langle \mathbf{x}\mathbf{a} - (\boldsymbol{\alpha}_-^l)_+ | \phi^{-m} \rangle \left. \right) \\
&= \sum_{\mathbf{a}\boldsymbol{\alpha}} (-1)^{m_{\boldsymbol{\alpha}}} \left(\right. \\
&\quad + \frac{1}{2} \sum_{kl} \langle \mathbf{x}\mathbf{a}(\boldsymbol{\alpha}_+^k)_-^l | \phi^m \rangle \langle \mathbf{x}\mathbf{a} - \boldsymbol{\alpha} | \phi^{-m} \rangle + \frac{1}{2} \sum_{kl} \langle \mathbf{x}\mathbf{a}(\boldsymbol{\alpha}_-^k)_+^l | \phi^m \rangle \langle \mathbf{x}\mathbf{a} - \boldsymbol{\alpha} | \phi^{-m} \rangle \\
&\quad + \frac{1}{2} \sum_{kl} \langle \mathbf{x}\mathbf{a}(\boldsymbol{\alpha}_+^k)_-^l | \phi^m \rangle \langle \mathbf{x}\mathbf{a} - \boldsymbol{\alpha} | \phi^{-m} \rangle + \frac{1}{2} \sum_{kl} \langle \mathbf{x}\mathbf{a}(\boldsymbol{\alpha}_-^k)_+^l | \phi^m \rangle \langle \mathbf{x}\mathbf{a} - \boldsymbol{\alpha} | \phi^{-m} \rangle \\
&\quad \left. - \sum_{kl} \langle \mathbf{x}\mathbf{a}(\boldsymbol{\alpha}_-^l)_+^k | \phi^m \rangle \langle \mathbf{x}\mathbf{a} - \boldsymbol{\alpha} | \phi^{-m} \rangle - \sum_{kl} \langle \mathbf{x}\mathbf{a}(\boldsymbol{\alpha}_+^l)_-^k | \phi^m \rangle \langle \mathbf{x}\mathbf{a} - \boldsymbol{\alpha} | \phi^{-m} \rangle \right) \\
&= 0.
\end{aligned} \tag{D.24}$$

In the third equality the sum over \mathbf{a} and $\boldsymbol{\alpha}$ was reorganized so that there is an identical bracket $\langle \mathbf{x}\mathbf{a} - \boldsymbol{\alpha} | \phi^{-m} \rangle$ in each term. To this end the variables were changed in the following way. In the third term

$$\boldsymbol{\alpha} \rightarrow \boldsymbol{\alpha}' = (\boldsymbol{\alpha}_+^k)_-^l. \tag{D.25}$$

Then,

$$(\boldsymbol{\alpha}'_+)^k = \boldsymbol{\alpha}, \quad m_{\boldsymbol{\alpha}'} = m_{\boldsymbol{\alpha}}. \tag{D.26}$$

A opposite change was done in the fourth term. In the fifth term

$$\boldsymbol{\alpha} \rightarrow \boldsymbol{\alpha}'' = \boldsymbol{\alpha}_-^l, \tag{D.27}$$

and then

$$\boldsymbol{\alpha}'''_+ = \boldsymbol{\alpha}. \tag{D.28}$$

APPENDIX D. CONSTRUCTION OF ZERO ANGULAR MOMENTUM
FUNCTIONS

An opposite change was performed in the sixth component. The ket $|\mathbf{x}\alpha\alpha''\rangle$ is created by one less operator f_+^\dagger and one more operator f_-^\dagger than $|\mathbf{x}\alpha\alpha\rangle$. Therefore, $m_{\alpha''} = m_\alpha - 1$ and $(-1)^{m_{\alpha''}} = -(-1)^{m_\alpha}$, hence additional minus sign.

We proved than all terms in (D.8) vanish and therefore $L^2\rho(\mathbf{x}) = 0$. The proof is now complete.

Appendix E

Gauge fixing for $SU(3)$

In 7.4.1 we consider gauge fixing for a set of three bosonic variables X_i . Each X_i is a hermitean, traceless 3×3 matrix. The gauge transformation is $X_i \rightarrow UX_iU^\dagger$, where U is an element of $SU(3)$ in the fundamental representation. In 7.4.1 we shown how to completely fix the gauge in the generic case. Gauge fixing can be represented by conditions coordinates x_i^a (cf. (7.22)). There are however certain configurations X_i which have to be addressed separately. This is because in these cases there is come residual gauge freedom left. This freedom leads e.g. to identification of false flat valleys of the potential (c.f. (7.26)). In this appendix all such cases are discussed.

The procedure of gauge fixing is algorithmic. That is, it consists several steps. At each step there is some gauge symmetry available. It is then used to transform X_i so that they satisfy some additional constraints. The gauge freedom at each step depends on particular configuration of X_i . For example, in the first step X_1 is diagonalized. In the generic case it is then invariant under gauge transformation only with $U = \text{diag}(e^{i\phi}, e^{i\psi}, e^{-i\phi-i\psi})$. However, if $X_1 = 0$, then it is invariant under gauge transformation with general $U \in SU(3)$. In Tab. E.1 we introduce notation for residual gauge symmetries which will be used in what follows.

Ⓐ	U – general $SU(3)$ matrix	Ⓔ	$U = \text{diag}(e^{i\phi}, e^{i\phi}, e^{-2i\phi})$
Ⓑ	$U = \begin{pmatrix} U_2 & 0 \\ 0 & (\det U_2)^* \end{pmatrix}$	Ⓕ	$U = \text{diag}(e^{-2i\phi}, e^{i\phi}, e^{i\phi})$
Ⓒ	$U = \begin{pmatrix} (\det U_2)^* & 0 \\ 0 & U_2 \end{pmatrix}$	Ⓖ	$U = \text{diag}(e^{i\phi}, e^{-2i\phi}, e^{i\phi})$
Ⓓ	$U = \text{diag}(e^{i\phi}, e^{i\psi}, e^{-i\phi-i\psi})$		

Table E.1: Notations for residual gauge freedom in midsteps in the procedure of gauge fixing. U_2 stands for a general, $SU(2)$ matrix.

Recall how the gauge is fixed in the generic case. First, one diagonalizes X_1 and sets the diagonal elements in increasing order. The residual gauge freedom is Ⓓ. The diagonal

matrix X_1 is invariant under transformations with such U . The gauge transformation is then used to set two matrix elements $(X_2)_{12}$ and $(X_2)_{23}$ real and positive. This fixes the gauge completely.

In 7.4.1 we considered three basic degenerate cases. They are summarized in Tab. E.2 together with the residual gauge freedom and how one can use it to impose further constraints. There are certainly many more different cases. Nevertheless, there are usually similar to one of the three basic cases.

special case	residual gauge freedom	action
$X_1 = 0$	Ⓐ	use U to diagonalize X_2 and then treat X_3 as X_2 in the generic case
after diagonalization of X_1 two eigenvalues are equal, e.g. $(X_1)_{11} = (X_1)_{22}$	Ⓑ	diagonalize upper-left 2x2 submatrix of X_2 and set $(X_2)_{13}, (X_2)_{23}$ positive
after diagonalization of X_1 matrix element $(X_2)_{12}$ vanishes	Ⓓ	set $(X_2)_{13}$ and $(X_2)_{23}$ positive

Table E.2: The basic degenerate cases in gauge fixing procedure.

Finally, we proceed to describing the full algorithm. At each step X_i obey some constraints. There is a residual gauge symmetry that does not violate these constraints. The residual symmetry depends on both, constraints and particular configuration X_i . The gauge symmetry is then used to perform some action (such as to diagonalize a matrix) so that X_i are subject to stricter constraints. This leaves a smaller symmetry group which is then used in next step. Different residual gauge symmetries allow for different sets of actions. In each case an action with highest priority is chosen. The list of possible actions is

1. diagonalize X_i ,
2. diagonalize a 2×2 upper-left or lower-right submatrix of X_i ,
3. set an off-diagonal matrix element to zero; $(X_i)_{12}$ has priority over $(X_i)_{23}$ and $(X_i)_{23}$ has priority over $(X_i)_{13}$,
4. set an off-diagonal matrix element positive, $(X_i)_{12}$ has priority over $(X_i)_{23}$ and $(X_i)_{23}$ has priority over $(X_i)_{13}$.

First action has highest priority and the last has lowest. Each action concerns only one of the three matrices X_i . We say that X_1 has always priority over X_2 and X_2 has priority over X_3 . That is, if the same action is possible for X_1 and X_2 then it is done for X_1 . By diagonalization we mean diagonalization with setting eigenvalues on the diagonal in increasing order.

The full procedure of gauge fixing is presented in a flowchart, Figs E.1 and E.2. Interpretation of the flowchart is following. The pink rectangle is the first step. Rectangles represent new constraints that are imposed on matrices X_i . These conditions can be always fulfilled by performing an action on X_i which is allowed by the residual symmetry group. Each diamond represents a question. If the condition in a diamond node is fulfilled, then there is a degeneracy and the 'yes' arrow has to be followed. Otherwise, one has to follow the 'no' arrow. The blue triangle in Fig. E.1 means that one should

move to the triangle in Fig. E.2. Some arrows have additional symbols, $\textcircled{A}, \dots, \textcircled{G}$. These denote the residual gauge transformations at given stage. For brevity we use $X = X_1, Y = X_2, Z = X_3$. Moreover, 'diagonalize UL of M' means: 'diagonalize 2×2 submatrix in the upper-left corner of M'. Similarly, LR stands for 'the lower-right submatrix'.

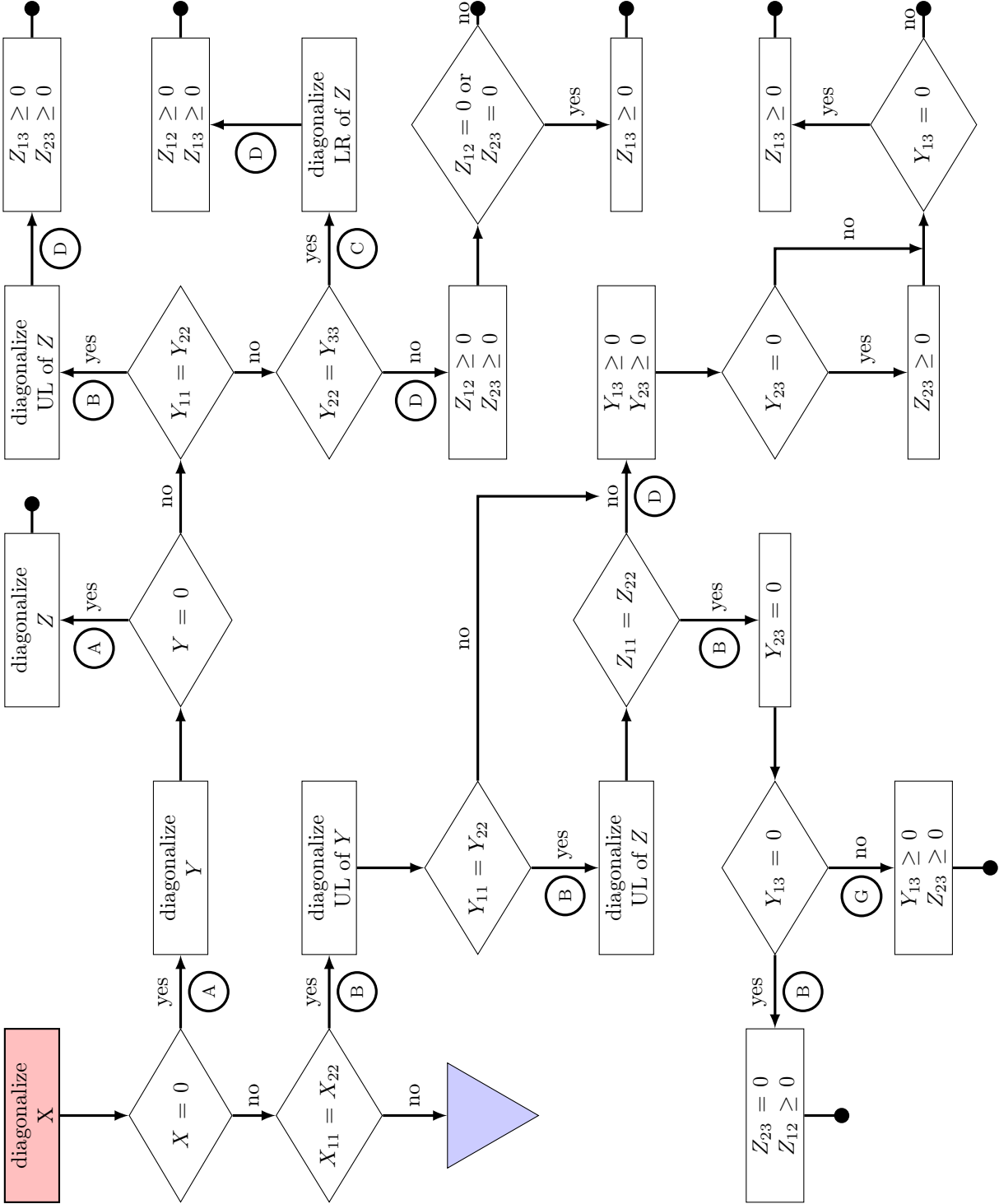


Figure E.1: Flowchart of procedure of fixing the gauge, part 1.

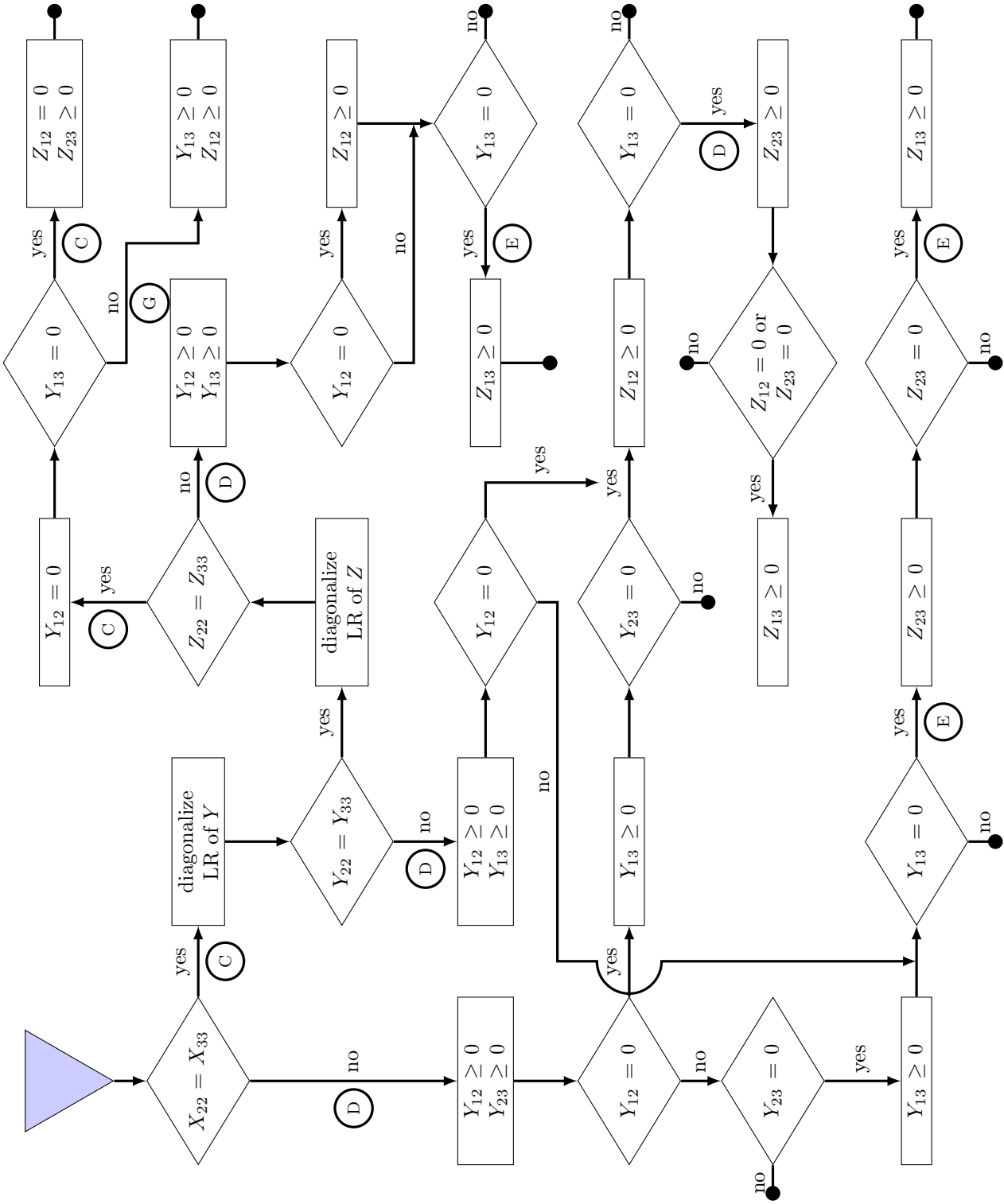


Figure E.2: Flowchart of procedure of fixing the gauge, part2.

Bibliography

- [1] S. Weinberg. Implications of dynamical symmetry breaking. *Phys.Rev.*, D13:974–996, 1976.
- [2] S. Dimopoulos and S. Raby. Supercolor. *Nucl.Phys.*, B192:353, 1981.
- [3] S. Dimopoulos, S. Raby, and Frank Wilczek. Supersymmetry and the scale of unification. *Phys.Rev.*, D24:1681–1683, 1981.
- [4] J. R. Ellis, J.S. Hagelin, D. V. Nanopoulos, K. A. Olive, and M. Srednicki. Supersymmetric relics from the Big Bang. *Nucl.Phys.*, B238:453–476, 1984.
- [5] S. Ferrara and B. Zumino. Supergauge invariant Yang-Mills theories. *Nucl.Phys.*, B79:413, 1974.
- [6] L. Brink, J. H. Schwarz, and J. Scherk. Supersymmetric Yang-Mills theories. *Nucl.Phys.*, B121:77, 1977.
- [7] M. Claudson and M. B. Halpern. Supersymmetric ground state wave functions. *Nucl.Phys.*, B250:689, 1985.
- [8] S. Samuel. Solutions of extended supersymmetric matrix models for arbitrary gauge groups. *Phys.Lett.*, B411:268–273, 1997, hep-th/9705167.
- [9] J. Hoppe. Quantum theory of a massless relativistic surface and a two-dimensional bound state problem. *unpublished*, <http://hdl.handle.net/1721.1/15717>.
- [10] E. Bergshoeff, E. Sezgin, and P.K. Townsend. Supermembranes and eleven-dimensional supergravity. *Phys.Lett.*, B189:75–78, 1987.
- [11] B. de Wit, J. Hoppe, and H. Nicolai. On the quantum mechanics of supermembranes. *Nucl.Phys.*, B305:545, 1988.
- [12] B. de Wit, M. Luscher, and H. Nicolai. The supermembrane is unstable. *Nucl.Phys.*, B320:135, 1989.
- [13] H. Nicolai and R. Helling. Supermembranes and M(atr)ix theory. 1998, hep-th/9809103.
- [14] T. Banks, W. Fischler, S.H. Shenker, and L. Susskind. M theory as a matrix model: A Conjecture. *Phys.Rev.*, D55:5112–5128, 1997, hep-th/9610043.
- [15] John B. Kogut and Leonard Susskind. The Parton picture of elementary particles. *Phys.Rept.*, 8:75–172, 1973.
- [16] G. W. Moore, N. Nekrasov, and S. Shatashvili. D particle bound states and generalized instantons. *Commun.Math.Phys.*, 209:77–95, 2000, hep-th/9803265.

- [17] M. Staudacher. Bulk Witten indices and the number of normalizable ground states in supersymmetric quantum mechanics of orthogonal, symplectic and exceptional groups. *Phys.Lett.*, B488:194–198, 2000, hep-th/0006234.
- [18] T. Fischbacher. Bulk Witten indices from $D = 10$ Yang-Mills integrals. *Nucl.Phys.*, B694:525–535, 2004, hep-th/0312262.
- [19] W. Taylor. M(atrrix) theory: Matrix quantum mechanics as a fundamental theory. *Rev.Mod.Phys.*, 73:419–462, 2001, hep-th/0101126.
- [20] Katrin Becker and Melanie Becker. A two loop test of M(atrrix) theory. *Nucl.Phys.*, B506:48–60, 1997, hep-th/9705091.
- [21] M. Porrati and A. Rozenberg. Bound states at threshold in supersymmetric quantum mechanics. *Nucl.Phys.*, B515:184–202, 1998, hep-th/9708119.
- [22] U. H. Danielsson, G. Ferretti, and B. Sundborg. D particle dynamics and bound states. *Int.J.Mod.Phys.*, A11:5463–5478, 1996, hep-th/9603081.
- [23] M.B. Halpern and C. Schwartz. Asymptotic search for ground states of $SU(2)$ matrix theory. *Int.J.Mod.Phys.*, A13:4367–4408, 1998, hep-th/9712133.
- [24] S. Catterall and T. Wiseman. Black hole thermodynamics from simulations of lattice Yang-Mills theory. *Phys.Rev.*, D78:041502, 2008, 0803.4273.
- [25] S. Catterall and T. Wiseman. Extracting black hole physics from the lattice. *JHEP*, 1004:077, 2010, 0909.4947.
- [26] K. N. Anagnostopoulos, M. Hanada, J. Nishimura, and S. Takeuchi. Monte Carlo studies of supersymmetric matrix quantum mechanics with sixteen supercharges at finite temperature. *Phys.Rev.Lett.*, 100:021601, 2008, 0707.4454.
- [27] M. Hanada, Y. Hyakutake, G. Ishiki, and J. Nishimura. Holographic description of quantum black hole on a computer. 2013, 1311.5607.
- [28] M. Hanada, J. Nishimura, and S. Takeuchi. Non-lattice simulation for supersymmetric gauge theories in one dimension. *Phys.Rev.Lett.*, 99:161602, 2007, 0706.1647.
- [29] J.D. Bjorken. *Elements of Quantum Chromodynamics*. 1979.
- [30] M. Luscher. Some analytic results concerning the mass spectrum of Yang-Mills gauge theories on a torus. *Nucl.Phys.*, B219:233–261, 1983.
- [31] M. Luscher and G. Munster. Weak coupling expansion of the low lying energy values in the $SU(2)$ gauge theory on a torus. *Nucl.Phys.*, B232:445, 1984.
- [32] P. Weisz and V. Ziemann. Weak coupling expansions of the low lying energy values in $SU(3)$ gauge theory on a torus. *Nucl.Phys.*, B284:157, 1987.
- [33] V. Ziemann. *Qualitative Untersuchung des niedrig liegenden Spektrums reiner Yang-Mills Theorien im endlichen Volumen mit besonderer Berücksichtigung von $SU(3)$* . PhD thesis, Universität Hamburg, June 1986.
- [34] J. Koller and P. van Baal. A rigorous nonperturbative result for the glueball mass and electric flux energy in a finite volume. *Nucl.Phys.*, B273:387, 1986.

-
- [35] J. Koller and P. van Baal. A nonperturbative analysis in finite volume gauge theory. *Nucl.Phys.*, B302:1, 1988.
- [36] R.A. Janik and J. Wosiek. Towards the matrix model of M theory on a lattice. *Acta Phys.Polon.*, B32:2143–2154, 2001, hep-th/0003121.
- [37] J. Wosiek. Spectra of supersymmetric Yang-Mills quantum mechanics. *Nucl.Phys.*, B644:85–112, 2002, hep-th/0203116.
- [38] M. Campostrini and J. Wosiek. High precision study of the structure of D=4 supersymmetric Yang-Mills quantum mechanics. *Nucl.Phys.*, B703:454–498, 2004, hep-th/0407021.
- [39] M. Trzetrzelewski. Large N behavior of two dimensional supersymmetric Yang-Mills quantum mechanics. *J.Math.Phys.*, 48:012302, 2007, hep-th/0608147.
- [40] P. Korcyl. Exact solutions to D=2 Supersymmetric Yang-Mills Quantum Mechanics with SU(3) gauge group. *Acta Phys.Polon.Supp.*, 2:623, 2009, 0911.2152.
- [41] P. Korcyl. Solutions of D=2 supersymmetric Yang-Mills quantum mechanics with SU(N) gauge group. *J.Math.Phys.*, 52:052105, 2011, 1101.0591.
- [42] P. van Baal. The Witten index beyond the adiabatic approximation. 2001, hep-th/0112072.
- [43] J. Kotanski. Energy spectrum and wave-functions of four-dimensional Supersymmetric Yang-Mills Quantum Mechanics for very high cut-offs. *Acta Phys.Polon.*, B37:2813–2838, 2006, hep-th/0607012.
- [44] Jan Kotanski. Virial theorem for four-dimensional supersymmetric Yang-Mills quantum mechanics with SU(2) gauge group. *Acta Phys.Polon.*, B37:3659–3666, 2006, hep-th/0610091.
- [45] M. Trzetrzelewski. The Number of gauge singlets in supersymmetric Yang-Mills quantum mechanics. *Phys.Rev.*, D76:085012, 2007, 0708.2946.
- [46] C. Itzykson and J.B. Zuber. *Quantum Field Theory*. McGraw-Hill, 1980.
- [47] S. Weinberg. *The quantum theory of fields. Vol. 3: Supersymmetry*. Cambridge University Press, 2000.
- [48] S.M. Dancoff. Nonadiabatic meson theory of nuclear forces. *Phys.Rev.*, 78:382–385, 1950.
- [49] M. Trzetrzelewski and J. Wosiek. Quantum systems in a cut Fock space. *Acta Phys.Polon.*, B35:1615–1624, 2004, hep-th/0308007.
- [50] Z. Ambrozinski and J. Wosiek. Resumming not summable perturbative series. *Acta Phys.Polon.*, B44(1):49–58, 2013.
- [51] Z. Ambrozinski. Tunneling in cosine potential with periodic boundary conditions. *Acta Phys.Polon.*, B44:1261–1272, 2013, arXiv: 1303.0708.
- [52] M. Trzetrzelewski. Reduction of su(N) loop tensors to trees. *J.Math.Phys.*, 46:103512, 2005, math-ph/0505084.

- [53] M. Bresan, C. Procesi, and S. Spenko. Quasi-identities on matrices and the Cayley-Hamilton polynomial. arXiv: 1212.4597.
- [54] A.J. Macfarlane, A. Sudbery, and P. Weisz. Explicit representations of chiral invariant lagrangian theories of hadron dynamics. *Proc.Roy.Soc.Lond.*, 314:217–250, 1970.
- [55] P. Di Francesco, P. Mathieu, and D. Senechal. *Conformal field theory*. Springer-Verlag New York, Inc.
- [56] M. Hamermesh. *Teoria grup w zastosowaniu do zagadnień fizycznych*. Państwowe Wydawnictwo Naukowe, 1968.
- [57] J.M. Drouffe and C. Itzykson. Lattice gauge fields. *Phys.Rept.*, 38:133–175, 1978.
- [58] H. Weyl. *The Theory of Groups and Quantum Mechanics*. Methuen & Co. Ltd, 1931.
- [59] M. Trzetrzelewski. Quantum mechanics in a cut Fock space. *Acta Phys.Polon.*, B35:2393–2416, 2004, hep-th/0407059.
- [60] B. Simon. Some quantum operators with discrete spectrum but classically continuous spectrum. *Annals Phys.*, 146:209–220, 1983.
- [61] P. Korcyl. Classical trajectories and quantum supersymmetry. *Phys.Rev.*, D74:115012, 2006, hep-th/0610105.
- [62] J. Wess and J. Bagger. *Supersymmetry and supergravity*. Princeton University Press, 1983.
- [63] P. Salomonson and J.W. van Holten. Fermionic coordinates and supersymmetry in quantum mechanics. *Nucl.Phys.*, B196:509, 1982.
- [64] J. Goldstone and R. Jackiw. Unconstrained temporal gauge for Yang-Mills theory. *Phys.Lett.*, B74:81, 1978.
- [65] G.K. Savvidy. Yang-Mills Quantum Mechanics. *Phys.Lett.*, B159:325, 1985.
- [66] J. J. Sakurai. *Modern Quantum Mechanics*. Addison-Wesley Publishing Company, 1994.